APPLICATIONS OF ELECTROCHEMILUMINESCENCE DETECTION ON MICROFABRICATED DEVICES
Doctoral Dissertation

Anna-Maria Spehar-Délèze

Helsinki University of Technology
Department of Chemical Technology
Laboratory of Inorganic and Analytical Chemistry

APPLICATIONS OF ELECTROCHEMILUMINESCENCE DETECTION ON MICROFABRICATED DEVICES
Doctoral Dissertation

Anna-Maria Spehar-Délèze

Dissertation for the degree of Doctor of Philosophy to be presented with due permission of the Department of Chemical Technology for public examination and debate in Auditorium E at Helsinki University of Technology (Espoo, Finland) on the 6th of October, 2006, at 12 noon.

Helsinki University of Technology
Department of Chemical Technology
Laboratory of Inorganic and Analytical Chemistry

Teknillinen korkeakoulu
Kemian tekniikan osasto
Epäorgaanisen ja analyyttisen kemian laboratorio

HELSINKI UNIVERSITY OF TECHNOLOGY P.O. BOX 1000, FI-02015 TKK http://www.tkk.fi	ABSTRACT OF DOCTORAL DISSERTATION

Author	Anna-Maria Spehar-Délèze

Name of the dissertation

Applications of electrochemiluminescence detection on microfabricated devices

Date of manuscript	Date of the dissertation	6. October 2006
☑ Monograph	☐ Article dissertation (summary + original articles)	

Department	Chemical Technology
Laboratory	Inorganic and Analytical Chemistry
Field of research	Analytical Chemistry
Opponent(s)	Prof. Ari Ivaska
Supervisor	Prof. Sakari Kulmala
(Instructor)	

Abstract

The aim of this thesis was to investigate bioanalytical applications of electrochemiluminescence (ECL), which refers to the generation of light at the surface of an electrode. Two types of ECL detection were studied: anodic ECL and cathodic hot electron-induced ECL (HECL). In anodic ECL light is generated at traditional electrode materials, such as noble metal or carbon, while in cathodic HECL thin insulating film-coated electrodes are used, and light generation is initiated by tunnel emission of hot, energetic electrons. Both types of ECL provide high spatial control.

ECL applications for hybridization assays were investigated. Short 15-base oligonucleotide probes were immobilized on gold and oxide-coated silicon and aluminum electrodes. Hybridization with complementary targets was detected by ECL. Results showed that the oligonucleotides were successfully immobilized and high surface probe density was achieved. Labeled targets were detected at subnanomolar concentration levels. Two base pair mismatches were successfully discriminated.

A homogeneous hybridization assay where hybridization was detected by quenching of anodic ECL of a Ru(II) label by another luminophore (Cy5) was performed on thin film carbon electrodes. The quenching efficiency was 78% when the distance between the label moieties was short (<2 nm).

Also, an immunoassay on double barrier aluminum/aluminum oxide electrodes with Tb(III) chelate as the HECL label was performed.

A microfluidic system was fabricated in poly(dimethylsiloxane) (PDMS) and glass with integrated carbon fiber and platinum electrodes, and tested for direct ECL detection of guanosine. The magnitude of electroosmotic flow (EOF) in PDMS microchannels was determined using the current monitoring method. Results revealed that the origin of the surface charge in PDMS is the same as in silica, but its amount is considerably lower.

Keywords	electrochemiluminescence, hot electron, DNA hybridization, immunoassay, microfabrication		
ISBN (printed)	951-22-8383-2	ISSN (printed)	1795-2239
ISBN (pdf)	951-22-8384-0	ISSN (pdf)	1795-4584
ISBN (others)		Number of pages	160
Publisher	Picaset Oy		
Print distribution	Anna-Maria Spehar-Délèze		
☑ The dissertation can be read at http://lib.tkk.fi/Diss/			

Abstract

The aim of this thesis was to investigate bioanalytical applications of electrochemiluminescence (ECL), which refers to the generation of light at the surface of an electrode. Two types of ECL detection were studied: anodic ECL and cathodic hot electron-induced ECL (HECL). In anodic ECL light is generated at traditional electrode materials, such as noble metal or carbon, while in cathodic HECL thin insulating film-coated electrodes are used, and light generation is initiated by tunnel emission of hot, energetic electrons. Both types of ECL provide high spatial control.

ECL applications for hybridization assays were investigated. Short 15-base oligonucleotide probes were immobilized on gold and oxide-coated silicon and aluminum electrodes. Hybridization with complementary targets was detected by ECL. Results showed that the oligonucleotides were successfully immobilized and high surface probe density was achieved. Labeled targets were detected at subnanomolar concentration levels. Two base pair mismatches were successfully discriminated.

A homogeneous hybridization assay where hybridization was detected by quenching of anodic ECL of a $Ru(bpy)_3^{2+}$ label by another luminophore (Cy5) was performed on thin film carbon electrodes. The quenching efficiency was 78% when the distance between the label moieties was short ($\leq$ 2 nm). Also, an immunoassay on double barrier aluminum/aluminum oxide electrodes with Tb(III) chelate as the HECL label was performed.

A microfluidic system was fabricated in poly(dimethylsiloxane) (PDMS) and glass with integrated carbon fiber and platinum electrodes, and tested for direct ECL detection of guanosine. The magnitude of electroosmotic flow (EOF) in PDMS microchannels was determined using the current monitoring method. Results revealed that the origin of the surface charge in PDMS is the same as in silica, but its amount is considerably lower.

Preface

The research for this thesis was done in a collaboration between the Laboratory of Inorganic and Analytical Chemistry of Helsinki University of Technology and the Institute of Microtechnology (IMT) in Neuchâtel, Switzerland. Most of the work was carried out during the years 2001-2005.

First of all, I wish to thank Prof. Sakari Kulmala for offering me a position as doctoral student in his research team. I truly appreciate his encouragement, supervision, enthusiasm to discover new areas of chemistry and the freedom he gave me to test my own ideas. He also has great organizational skills, which allowed wide scientific collaboration in the form of the Chemsem graduate school. Several summer schools with excellent scientific and social programs were set up and run as a result of his organizational efforts.

In particular I remember travels with Markus Håkansson, Annika Nyman and Jane (Qinhong) Jiang. It was a pleasure not only to work but simply to enjoy time with you. Philip Canty, Johanna Suomi, Kaisa Lehmus, Miia Kotiranta, Satu Ek, Sirje Liukko, and Johanna Johansson are thanked for their help and friendship. Matti Lehtimäki helped with Latex.

Everybody in the Laboratory of Inorganic and Analytical Chemistry contributed to my work with their kindness and the creation of good working atmosphere.

I am most greatful to Prof. Nico de Rooij for allowing me to join his interdisciplinary team in Neuchâtel, where I was able to study microfabrication technologies and microfluidics and their applications in analytical chemistry today.

Many thanks to Prof. Milena Koudelka-Hep for her guidance, time spent on brainstorming, revising my papers, and invaluable discussions. She always displayed great patience and wisdom and helped me greatly in my scientific and

personal development. I am also very grateful to Prof. Sabeth Verpoorte. I started my work at IMT in her microfluidics team, and I was most impressed by her creative, motivating and intelligent way to lead a very interdisciplinary research group. Sander Koster taught me all practical aspects of my work and was of invaluable assistance at the beginning of my stay at IMT.

The technical staff of IMT - Gianni Mondin, Nicole Hegelbach-Guye, Sylvain Jeanneret, Edith Millotte, and Sylviane Pochon - are thanked for the great job they did and for their friendliness and patience. All of you at IMT were extremely welcoming and I thank everyone of you. Special thanks go to Alexandra Homsy, Andreas Kuoni, Anpan Han, Arash Dodge, Ben Chui, Danick Briand, Gian-Luca Lettieri, Giovanni Egidi, Jan Lichtenberg, Laura Ceriotti, Luca Berdondini, Olivier Guenat, Peter van der Wal, Severin Waldis, Silvia Generelli, Teru Akiyama, Tobias Kraus, Kaspar Suter, and Vincent Linder. You in particular have contributed to my personal learning and helped to make the time at IMT enjoyable.

My thanks also to Timo Ala-Kleme and the Labmaster team in Turku.

Finally, I wish to thank my family members in Croatia, Finland, Switzerland, and the United States for their help, love, and understanding. Although you are scattered around the world, your support and encouragement have been most important. Last but not least, I thank my dear husband, Frédéric, for his endless love and support during these long and busy years.

Contents

Abbreviations and symbols

APTES   aminopropyltriethoxysilane

BHF   buffered hydrofluoric acid

CE   capillary electrophoresis

CE-EC   capillary electrophoresis integrated with electrochemical detection

CL   chemiluminescence

CT   complementary target

CTAB   cetyltrimethylammonium bromide

CV   cyclic voltammogram

CVD   chemical vapor deposition

DC   direct current

DMF   N,N-dimethylformamide

DMSO   dimethylsulfoxide

DNA   deoxyribonucleic acid

e_{aq}^- hydrated electron

ECL   electrochemiluminescence

EDA   N-(2-aminoethyl)-3-aminopropyltrimethoxysilane

EDC   1-(3-(dimethylamino)propyl)-3-ethylcarbodiimide hydrochloride

EOF   electroosmotic flow

FIA   flow injection analysis

HDMS   hexamethyldisilazane

HECL   hot electron-induced electrochemiluminescence

HPLC   high performance liquid chromatography

hTSH   human thyroid stimulating hormone

ID   internal diameter

LIF   laser-induced fluorescence

LPCVD   low pressure chemical vapor deposition

LRET   luminescence resonance energy transfer

16-MHA   16-mercaptohexadecanoic acid

MST   microsystem technology

3-MPA	3-mercaptopropanoic acid
MT	mismatched target
NASBA	nucleic acid sequence based amplification
NHS	N-hydroxysuccinimide
NT	noncomplementary target
PCR	polymerase chain reaction
PDC	1,4-phenylene diisothiocyanate
PDMS	poly(dimethylsiloxane)
PECVD	plasma enhanced chemical vapor deposition
PMT	photomultiplier tube
RCL	radiochemiluminescence
RhB	rhodamine B
RIE	reactive ion etch
RuHex	ruthenium(III) hexaamine
SAM	self-assembled monolayer
SCE	standard calomel electrode
SDS	sodium dodecyl sulfate
SNP	single-nucleotide polymorphism
TAMRA	succinimidyl ester of 5-(and 6-)carboxytetramethylrhodamine
TAS	total analysis system
TPA	n-tripropylamine
TR	time resolved

1. Scope and outline of the thesis

1.1 Motivation and background

Electrochemiluminescence, or electrogenerated chemiluminescence (ECL), is light generated at the surface and in close proximity of an electrode. The main motivation of this work was to investigate and further develop analytical methods based on ECL detection. Two types of ECL were investigated: anodic ECL of Ru(II) complexes, in which light is generated on traditional electrode materials, such as a noble metal or carbon, and cathodic hot electron-induced ECL (HECL), in which light generation is induced by electron tunneling from thin insulating film-coated electrodes. Both types of ECL provide high spatial control, which makes ECL an interesting detection method for analytical microsystems. Current trends in bioanalytical chemistry are miniaturization and integration of different functionalities on a single chip. The advantages of miniaturized systems are reduced reagent consumption, increased reaction rates, portability, and parallelization. The applicability of anodic ECL and cathodic HECL for bioassay detection was investigated as part of this research. Electrokinetic properties of poly(dimethylsiloxane) (PDMS) and coupling of anodic ECL detection into microfluidic systems were studied.

1.2 Organization of the thesis

Chapter 2 provides an introduction to anodic ECL and cathodic HECL, as well as to their state-of-the-art applications in bioaffinity assays. As well a short introduction to microfabrication technology is provided, with emphasis on technology needed for realization of analytical microsystems.

Chapter 3 describes a heterogeneous hybridization assay on gold electrodes. Short 15-base DNA strands were conjugated with a synthesized electrochemilumines-

cent label, bis(2,2'-bipyridine)-5-isothiocyanato-1,10-phenanthroline ruthenium(II) at the amino-modified 5' end. Gold electrodes were derivatized with the 15-base oligonucleotide probes via 1-(3-(dimethylamino)propyl)-3-ethylcarbo-diimide hydrochloride (EDC) / N-hydroxysuccinimide (NHS) cross-linking reaction and hybridized with Ru(II) chelate-labeled strands. Two types of self-assembled monolayers were utilized for the immobilization reaction, namely 3-mercapto-propanoic acid (3-MPA) and 16-mercaptohexadecanoic acid (16-MHA). Longer thiols were more stable at the high electrode potentials needed for the ECL generation. The system was sensitive down to one fmol of labeled complementary strand, detected in 30 μL of buffer. Mismatch discrimination was achieved both passively by washing and actively by application of negative electrode potential on electrodes prior to detection. Active denaturing leads to better results, however. Two base pair mismatches were discriminated at room temperature.

Chapter 4 describes cathodic HECL of rhodamine B and the application of rhodamine derivative for heterogeneous hybridization assay on oxide-coated aluminum and silicon electrodes. Thin oxide film-coated aluminum and silicon electrodes were modified with an aminosilane layer and derivatized with short, 15-base oligonucleotide probes via diisothiocyanate coupling. Target oligonucleotides were conjugated with tetramethylrhodamine (TAMRA) dye at their amino-modified 5' end, and hybridization was detected as HECL of TAMRA. Preliminary results indicated sensitivity down to subnanomolar level and low nonspecific adsorption. The detectability of rhodamine dyes was better on oxide-coated silicon than on oxide-coated aluminum electrodes, and two base pair mismatched hybrids were successfully discriminated. The experimental results are useful for the design of disposable electrochemiluminescent DNA biosensors.

Chapter 5 reports an HECL-based hybridization assay on oxide-coated silicon electrodes, using bis(2,2'-bipyridine)-5- isothiocyanato-1,10-phenanthroline ruthenium(II)-labeled oligonucleotide strands as HECL luminophores.

An immunoassay based on HECL detection of Tb(III) chelate-labels on double

barrier $Al/Al_2O_3/Al/Al_2O_3$ electrodes is presented in Chapter 6. Primary capturing antibodies were physically adsorbed on electrodes and immunoreaction was detected using Tb(III) chelate-labeled complementary antibodies. The detectability was improved with respect to single barrier Al/Al_2O_3 electrodes.

Chapter 7 reports a homogeneous ECL quenching-based hybridization assay. Short oligonucleotide probes were labeled with electrochemiluminescent bis(2,2'-bipyridine)-4'-methyl-4-carboxybipyridine-ruthenium N-succinimidyl ester-bis(hexafluorophosphate) ruthenium (Ru(II)) and a complementary strand was labeled with photoluminescent Cy5 dye. Upon hybridization of the complementary strands, the ECL of the Ru label was quenched 78%. The ECL results were compared with photoluminescence results. Under the experimental conditions employed it appears that luminescence resonance energy transfer (LRET) occurs when Ru(II)-label is photoexcited, but not when it is excited via ECL.

The possibilities and challenges of integration of ECL detection with microfluidic systems fabricated in poly(dimethylsiloxane) (PDMS) are considered in Chapter 8. This chapter consists of two parts: a description of a microfluidic system fabricated in Pyrex and PDMS with integrated carbon-fiber and platinum electrodes for anodic ECL detection, and a determination of EOF in PDMS microchannels by current monitoring method.

A summary of the work is presented in Chapter 9. The main characteristics of the various methods are noted, together with the advantages and disadvantages of each. The outlook for future is suggested.

1.3 Author's contribution

Writing of this thesis has been done solely by the author. All the work described in Chapters 3 and 5 was done by the author. This included planning of the experiments, microfabrication of the devices, carrying out of the experimental work,

and interpretation of the results under the supervision of Prof. Milena Koudelka and Prof. Sakari Kulmala. The first part of the work described in Chapter 4, the investigation of the HECL properties of a rhodamine dye, was planned and performed with other members of the HECL team at HUT, mainly Qinhong Jiang, who carried out most of the experimental work. The work recounted in the second part of Chapter 4, the hybridization assay, was planned by the author who also carried out most of the experimental work, under the supervision of Prof. Sakari Kulmala. The experimental work described in Chapter 6 was done under the supervision of Prof. Sakari Kulmala by the author together with Markus Håkansson and other collaborators. All the experimental work described in Chapter 7 was performed by the author, while the planning and interpretation of the results was done together with Dr. Sander Koster and Prof. Milena Koudelka. The planning of experiment, microfabrication of the devices, measurements, and results related to ECL detection of guanosine, as reported in Chapter 8, were performed by the author alone. The investigation of the electrokinetic properties of PDMS/PDMS and PDMS/glass microchannels was part of a collaboration project between the research team of Dr. Elisabeth Verpoorte at IMT, and Prof. Wolfgang Thormann from the University of Berne, Switzerland. The experiment was planned by Prof. Thormann. All measurements were performed solely by the author, while the results were interpreted by the author together with Dr. Sander Koster, Dr. Verpoorte, and Prof. Thormann.

2. Introduction

This chapter provides an introduction to electrochemiluminescence (ECL), its relation to other types of luminescence, and its state-of-the-art applications in bioanalysis. As the present trends in chemistry are miniaturization and the integration of different functionalities on a single chip, an introduction is given to the microfabrication technology used for realization of analytical microsystems.

2.1 Electrochemiluminescence (ECL)

2.1.1 Generation of luminescence

Luminescence is defined here as an emission of light from compounds in the excited state. Depending on the nature of the process that leads to the excited state of a luminophore (a luminescent molecule), it is usual to distinguish between photoluminescence, chemiluminescence (CL), and electrochemiluminescence (ECL). In photoluminescence, a luminophore excited by absorption of photons of certain energy releases light by emitting photons of lower energy than the photons absorbed. Photoluminescence methods can be further classified into fluorescence and phosphorescence. Lifetimes of fluorescent luminophores are in the order of 10^{-10}- 10^{-6} s, while those of phosphorescent luminophores range from 10^{-6} to 10^{-3} s. Fluorescence occurs from the excited singlet state of the luminophore, which means it has the same spin multiplicity as the ground state. Phosphorescence occurs from the excited triplet state, and the luminophore has a different spin multiplicity state from the ground state.[1]

Chemiluminescence (CL) is a process where luminescence is generated by chemical reactions. The most widely used CL luminophore is luminol (5-amino-2,3-dihydro-1,4-phthalazinedione), which emits light at 425 nm in the presence of a suitable coreactant and a catalyst. The coreactant is usually a nonluminescent

compound with which the luminophore has to react in order to reach the excited state. Chemiluminescent detection methods are widely used in clinical assays owing to the very low detection limits (down to sub-attomole level), short assay times, and the broad range of analytes.[2] CL detection is usually targeted at nonbound substances that can freely diffuse in solution and is less suitable for the detection of surface-bound analytes. However, the sensitivity of CL for microarray applications has been enhanced using three-dimensional microchannels for DNA hybridization detection.[3] Short DNA capturing strands were immobilized on microchannels of radius 5 μm and volume 39 pL and hybridized with horseradish peroxidase-labeled target strands.

Electrochemiluminescence, or electrogenerated chemiluminescence (ECL), can be described as CL produced directly or indirectly as a result of electrochemical reaction or a reaction sequence, and utilized in detection it can be classified as a spectroelectrochemical method. ECL detection has numerous applications and is regularly reviewed.[4–7] Compared with CL, it has many advantages: spatial control, as the ECL active species are generated at the surface of an electrode upon application of suitable potential; higher selectivity, introduced by control of the electrode potential; and generation of ECL from certain luminophores not known to generate traditional CL. ECL can be divided into several subclasses on the basis of the ECL generation mechanism. Two types of ECL are discussed here: anodic ECL and cathodic HECL. Both types can be described as coreactant ECL, which means that the ECL of the luminophore is generated by the applied potential in the presence of a coreactant. A coreactant is defined as a species that upon oxidation or reduction produces an intermediate that reacts with an electrochemiluminescent luminophore to produce an excited state.

2.1.2 Anodic ECL

Anodic ECL is generated on traditional electrode materials, such as noble metals or carbon, using the conventional electrochemical set up consisting of working,

counter and reference electrodes. Although many different luminophores, including luminol[8,9] and various metal chelates of ruthenium, osmium, and other transition metals have been investigated for ECL applications,[7,10–12] the most widely used ECL luminophore is $Ru(bpy)_3^{2+}$. The preference to $Ru(bpy)_3^{2+}$ is due to its capability to generate ECL at room temperature, in aqueous buffer solutions, and in the presence of dissolved oxygen and other impurities. Since its discovery in 1959 by Paris and Brandt,[13] it has found numerous applications, such as detection of amines and amino acids,[14–16] codeine,[17] lidocaine[18] and DNA.[19] It has also been used as a label in bioassays. Most ECL-based assays rely on a reaction between $Ru(bpy)_3^{2+}$ and TPA [TPA = tri-n-propylamine, $(CH_3CH_2CH_2)_3N$] as a coreactant, since this reaction gives the highest ECL efficiency of all known coreactant ECL systems.[20] The mechanism of the reaction has been extensively studied and several routes leading to the generation of the excited state of $Ru(bpy)_3^{2+}$ have been proposed.[21] One of the routes is presented in reactions 2.1 - 2.4.

$$Ru(bpy)_3^{2+} \rightarrow Ru(bpy)_3^{3+} + e^- \tag{2.1}$$

$$TPA - e^- \rightarrow TPA^{\cdot+} \rightarrow TPA^{\cdot} + H^+ \tag{2.2}$$

$$Ru(bpy)_3^{3+} + TPA^{\cdot} \rightarrow Ru(bpy)_3^{2+*} + products \tag{2.3}$$

$$Ru(bpy)_3^{2+*} \rightarrow Ru(bpy)_3^{2+} + h\nu \tag{2.4}$$
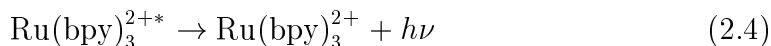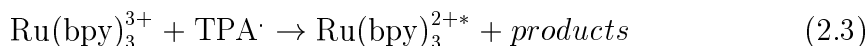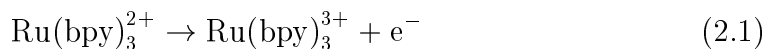
First, $Ru(bpy)_3^{2+}$ is oxidized at the electrode (reaction 2.1). The coreactant, TPA, upon being oxidized either heterogeneously on the electrode or homogeneously by $Ru(bpy)_3^{3+}$ rapidly loses a proton forming a $TPA^{\cdot}$ radical (reaction 2.2). The reaction between the newly formed radical and the ruthenium complex leads to a formation of the excited species, $Ru(bpy)_3^{2+*}$, which emits light in a broad band centered at 620 nm.[7] A particular advantage of the system described is that $Ru(bpy)_3^{3+}$ is regenerated during the ECL process, allowing a single $Ru(bpy)_3^{2+*}$ species to participate in many ECL generation cycles, with consequent signal amplification.

Several compounds can be determined by quenching of ECL. Phenolic compounds (e.g. epinephrine,[22] phenol, catechol and hydroquinones[23]) are reported to effectively quench $Ru(bpy)_3^{2+}$ and TPA induced ECL. The proposed mechanism is the formation of an intermediate at the electrode surface. The quenching of ECL is solution dependent, high quenching occurring in aqueous solutions and little or no quenching in acetonitrile.

While $Ru(bpy)_3^{2+}$ is by far the most commonly used ruthenium complex in ECL-based analytical applications, some other ruthenium complexes are known to be electrochemiluminescent. $Ru(phen)_3^{2+}$, for example, exhibits high ECL intensity at least in the presence of codeine,[17] TPA,[24] or oxalic acid[25] as coreactant. A ruthenium derivative with two bipyridine and one phenanthroline ligand used for codeine determination was observed to generate 2.5-times higher intensity of ECL compared with $Ru(bpy)_3^{2+}$.[17]

Anodic ECL has been exploited as a detector in flow injection analysis (FIA),[17,26] high performance liquid chromatography (HPLC),[15] capillary electrophoresis (CE),[18,27–29] and microchip CE.[24,30,31] Implementation of the ECL detection after CE separation is challenging due to the need for decoupling of the detection electric field from the high voltage separation field. Decoupling has been successfully achieved in end-column detection mode, by placing the detection electrode at some distance from the capillary end, a method most notably developed by the group of Erkang Wang.[28,30] In this approach the analytes are separated in the separation channel and separation buffer, while $Ru(bpy)_3^{2+}$ is present in excess at the detection end only. In one approach, a platinum working electrode 300 μm in diameter was placed 75 μm after the CE separation column, and lidocaine was detected in urine samples with detection limit of 2.0 x 10^{-8} mol/L.[18] In a PDMS-fabricated μCE chip, ECL detection was achieved by using a transparent indium tin oxide working electrode in the end-column mode. The system achieved detection limits of 1.2 μM for proline, which was used as a model analyte.[30] In a different approach, the high electric separation field was used to induce detection potential at a floating, U-shaped electrode placed inside the separation

microchannel.[24] The separation field induced sufficient potential difference across the electrode to oxidize $Ru(bpy)_3^{2+}$ and TPA at the one end of the electrode and to cause ECL generation. This method was used for indirect detection of three amino acids. Another approach been described where microfluidic systems relied on anodic ECL as a photonic reporter for redox reactions.[32] Two-channel and multichannel microfluidic sensors based on this principle have been developed.[33,34]

2.1.3 Cathodic HECL

HECL is generated by a reaction sequence induced by tunnel emission of hot electrons through a thin insulating film-coated electrode into an electrolyte solution upon cathodic polarization. Figure 2.1 shows a schematic representation of HECL on an oxide-coated n-Si electrode.

Upon thermalization and solvation, these electrons become hydrated (e_{aq}^-). Hot or hydrated electrons are capable of reducing compounds that are not electroactive in aqueous solutions on noble metal electrodes. Suitable electrode materials for HECL generation are silicon, magnesium and aluminum coated with thin insulating films,[35,36] and aluminum-doped zinc oxide coated with Y_2O_3.[37] Silicon electrodes are usually heavily n^+ or p^+ doped to increase conductivity. The set up for HECL is considerably simpler than that for anodic ECL as a reference electrode is not necessary.

Many common photoluminescent and chemiluminescent labels generate HECL. Examples include luminol and its derivatives,[38,39] $Ru(bpy)_3^{2+}$,[40,41] SYBR (R) Green I,[42] coumarine dyes,[43] rhodamine B,[44] and lanthanide(III) chelates.[45,46] The most sensitive HECL luminophores discovered are terbium labels, which can be detected down to sub-picomolar concentration. The distinct advantage of cathodic HECL over anodic ECL is that various luminophores with different optical and redox properties can be excited simultaneously.[38,47] Following reactions have

9
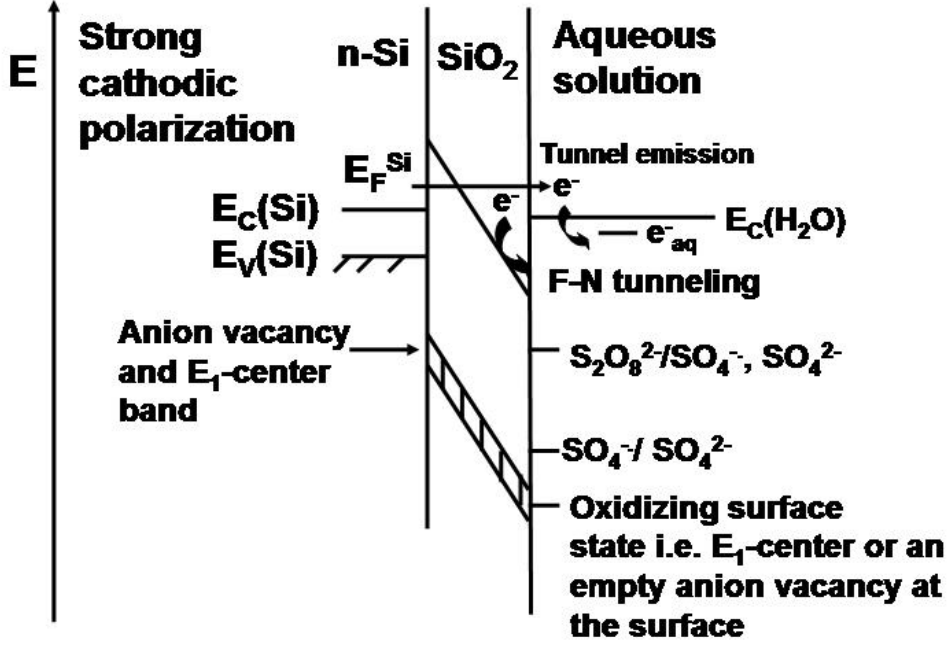
Figure 2.1: Schematic representation of hot electron injection during cathodic high-amplitude pulse-polarization on oxide-coated n-Si. Hot electrons of energy equal to the source energy are tunneled through thin oxide films, <5 nm, while in the case of thicker oxides charge transfer occurs *via* Fowler-Nordheim tunneling.

been proposed to lead to the formation of the excited Ru(bpy)_3^{2+*} species:[40,41]

$$e_{aq}^- + \text{S}_2\text{O}_8^{2-} \rightarrow \text{SO}_4^{\cdot-} + \text{SO}_4^{2-} \tag{2.5}$$

$$\text{Ru(bpy)}_3^{2+} + e_{aq}^- \rightarrow \text{Ru(bpy)}_3^+ \tag{2.6}$$

$$\text{Ru(bpy)}_3^+ + \text{SO}_4^{\cdot-} \rightarrow \text{Ru(bpy)}_3^{2+*} + \text{SO}_4^{2-} \tag{2.7}$$

$$\text{Ru(bpy)}_3^{2+} + \text{SO}_4^{\cdot-} \rightarrow \text{Ru(bpy)}_3^{3+} + \text{SO}_4^{2-} \tag{2.8}$$

$$\text{Ru(bpy)}_3^{3+} + e_{aq}^- \rightarrow \text{Ru(bpy)}_3^{2+*} \tag{2.9}$$

10
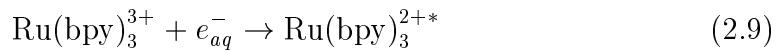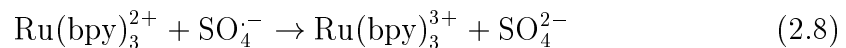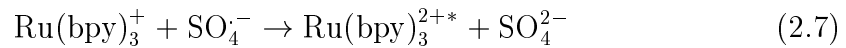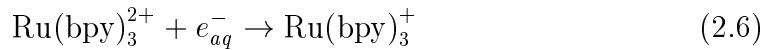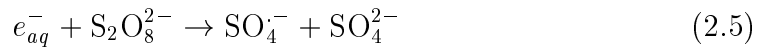
The excited species formed at the end is the same as in reaction 2.4. In the reactions 2.5-2.9, coreactant is $S_2O_8^{2-}$, which upon reduction by hot or hydrated electrons forms highly oxidizing radicals. An HECL-based application has been reported for detection of organic compounds in aqueous solutions in a flowing stream using oxide-coated aluminum electrode.[48]

2.2 Bioaffinity assays

2.2.1 Basic principles of bioaffinity assays

Two types of bioaffinity assays are considered, namely, immunoassays and DNA hybridization assays. Immunoassay technology has been in use over 40 years.[49] Radioimmunoassays were developed by Yalow and Berson,[50] who reported the first use of antibodies for clinical assays in a competitive radioimmunoassay of insulin in the 1960s. DNA hybridization assays in turn, have been intensively investigated only during the last decade, due to the progress in genomic research. Completion of the human genome sequence has shown that the number of protein-coding human genes is 30 000-40 000, only twice the number in a worm or fly.[51,52] Changes or deletions of one nucleobase in a natural DNA sequence, so-called single-nucleotide polymorphisms (SNPs), are quite frequent in the human genome, occurring at a rate of about one per thousand nucleotides.[53] DNA microarray technology allows simultaneous analysis of the entire human genome on a small surface. Two types of DNA microarrays are currently in use: cDNA microarrays and oligonucleotide microarrays.[54] In cDNA arrays, each immobilized strand corresponds to a unique gene and is 200-500 nucleotides long, while oligonucleotide microarrays and DNA biosensors use short, 15-50 base long DNA strands (oligonucleotides).[55] Latter format is gaining popularity due to its simplicity and the higher sensitivity for SNP detection.

Immunoassays and DNA hybridization assays have many similarities, since both are based on a unique biorecognition process, however, antibodies contain numer-

ous amino and carboxylic acid groups and can be readily physically adsorbed on unmodified surfaces by combination of electrostatic and hydrophobic interactions. Immobilization of oligonucleotides, in contrast, requires addition of a functional group during synthesis that allows their coupling to a surface in a controlled manner. The most common modifiers are amino and thiol groups. A surface used for immobilization of oligonucleotides should be flat, homogeneous, and thermally and chemically stable, and a reproducible surface treatment that allows high density immobilization of DNA strands and offers low background must be feasible. In addition, the achievement of massively parallel assays requires compatibility with microfabrication technologies. Oligonucleotide microarrays can be produced either by *in situ* synthesis of oligonucleotides on a solid support or by immobilization of conventionally synthesized oligonucleotides on a prepared active microarray. Different types of activated glass plates are commercially available. The common requirements for a microarray are high chemical resistance against solvents, mechanical stability, and, normally low intrinsic fluorescence since fluorescence detection is the most common detection method. Important parameters for successful hybridization are the amount of DNA probe attached to the surface, probe length, and accessibility of the targets to the probes. Probes should not be too close to the surface in order to allow easy access of targets. The spacer should be at least 40 atoms long and should not contain charged groups.[56] A critical factor in DNA microarrays is the concentration of the probes available for hybridization.

The first large-scale manufacturing of microarrays was done by Affymetrix (http://www.affymetrix.com) using photolithographic technology similar to that used in the production of computer chips. The present format of the GeneChip array uses photolithographic methods and phosphoramidite chemistry for *in situ* synthesis of 500 000 different oligonucleotide sequences of 25 bases on a 1.28 x 1.28 cm^2 chip, each element being 18 x 18 μm in size.[57]

Most present bioassays rely on fluorescence detection; however, electrochemical and ECL detection methods are of great interest due to the relatively simple

instrumentation, high sensitivity, low-cost, and easy miniaturization.[58–60] Electrochemical DNA biosensors are being developed as alternatives to conventional DNA microarrays.[61] Characteristic for all types of biosensors is that they incorporate a biologically active layer for biorecognition directly interfaced to a signal transducer, which converts the physical parameter into a measurable analytical signal. Most electrochemical DNA biosensors are based on carbon and gold electrodes.[59] DNA biosensors are potentially useful for the detection of chemically induced DNA damage and detection of the microorganisms through the hybridization of species-specific sequences of DNA.[62]

2.2.2 Applications of ECL in bioaffinity assays

Anodic ECL of the $Ru(bpy)_3^{2+}$ label has been used in immunoassays and DNA assays for over a decade.[63–65] In bioassay applications analyte or its receptor is labeled with $Ru(bpy)_3^{2+}$ -based derivative and ECL is detected in the presence of TPA as coreactant. Commercial technology utilizes paramagnetic beads as solid support for the immobilization of capturing biomolecules. Upon biorecognition reaction with labeled target biomolecules, the beads are passed into a flow cell, where a magnet captures the beads on the surface of an electrode. The beads are washed to remove any unattached $Ru(bpy)_3^{2+}$ label and the TPA-containing buffer is pumped into a flow cell. ECL of the labeled analytes is generated by application of a suitable potential and the emitted light is recorded with a photomultiplier tube (PMT). The beads are then washed away, and the flow cell is cleaned and prepared for the next sample. The detection limit of the bead-based ECL system is in attomolar range.[7]

The commercial bead-based ECL method is widely used for detection of polymerase chain reaction (PCR) amplified DNA fragments.[63,66,67] Highly sensitive methods are needed for the detection of PCR products in order to reduce the number of amplification cycles, as a greater number of amplification cycles causes wider variation. The bead-based PCR-ECL system has been utilized for the

detection of various genes from viruses in human blood and serum[66,68] and measurement of the DNA helicase activity of *Escherichia coli* DNA.[69] Recently, ECL has been used for the detection of heat shock proteins from *oocysts* using nucleic acid sequence based amplification (NASBA) of mRNA. NASBA is an isothermal technique that specifically amplifies RNA molecules for the detection. The amplification and detection of 10 mRNA molecules has been reported.[70] The drawback of the beads is that they are opaque, which causes signal loss from the side of the beads not seen by a PMT. This issue has been addressed by Hsueh *et al.*,[64] who fabricated a flow-through microcell from silicon and glass for the ECL quantification of DNA. The ECL signal of the bead-immobilized $Ru(bpy)_3^{2+}$-labeled DNA strands was generated on the interdigitated platinum thin-film electrodes and the ECL signal was measured using a silicon PIN photodiode. The detection limit was 40 fmol in a volume of 150 μl.

Despite the great potential of ECL only a few examples of assays where a capturing DNA strand or antibody is directly immobilized on an electrode surface are reported.[65,71,72] Miao and Bard[65] performed on gold electrodes an oligonucleotide hybridization assay using 23-base oligonucleotides and an immunoassay using C-reactive protein. The ECL intensity of the hybridization with a noncomplementary strand resulted in a signal that was 10% of the signal of the complementary strand, most probably due to the nonspecific adsorption. Bertolino *et al.*[71] fabricated a silicon-based ECL chip with interdigitated gold electrodes and integrated photodiode. The system was used for hybridization detection and was able to discriminate 25% mismatched strands. Firrao[72] compared several electrode materials for detection of $Ru(bpy)_3^{2+}$-labeled DNA strands, and found glassy carbon to be the best in terms of sensitivity. Detection limit of 10 pmol for hybridized complementary strand was obtained.

Heterogeneous immunoassays on oxide-coated aluminum and silicon electrodes with HECL as detection method have been reported.[40,73–75] Capturing antibodies were physically adsorbed on oxide-coated aluminum[40,73,74] and silicon[75] electrodes, and the biorecognition reaction was detected using receptors labeled with

HECL luminophore. Detection of PCR amplified DNA strands using SYBR R
Green I as HECL luminophore has been reported.[42]

2.3 Microsystem technology (MST)

The main trends in analytical chemistry today are miniaturization and integra-
tion. Whereas in traditional chemistry sample preparation, separation, detection,
and other processes related to sample treatment are performed in separate steps
and usually require volumes on the order of milliliters, microfabrication technol-
ogy has enabled integration of two or more of these steps in a single chip and
reduction of volumes to sub-microliter range. Several terms are used for chemical
and biochemical microsystems: micro total analysis system (μTAS),[76] microsys-
tem technology (MST), lab-on-a-chip (LOC) and biomicroelectromechanical sys-
tems (bioMEMS). Generally, the term μTAS is used for systems that incorporate
electrokinetically actuated sample separation and detection on chip.[77] The first
instrument on a microchip was an integrated gas chromatograph.[78] This initiated
the application of micromachining technology to construction of chemical analy-
sis devices. The aim in analytical microsystems is to integrate fluidic, electronic
and mechanical components on a single chip or substrate. Application of MST
is highly promising in fields of medicine and biology, particularly in regard to
diagnostic systems for body fluids.[79]

The heart of a chemical microsystem is the microfluidics, the handling of very
small amounts of fluids in a controlled manner. In any miniaturization it is impor-
tant to understand scaling of different phenomena, since miniaturized components
are not simply smaller counterparts of the macroscopic world. Consequences of
miniaturization include increased surface-to-volume ratio and omnipresence of the
laminar flow. Two types of flow are common in microfluidic systems: pressure-
driven flow and electrically actuated flow. Pressure-driven flow is based on pres-
sure difference ΔP between channel openings according to the equation

$$Q = \Delta P / R \qquad\qquad (2.10)$$

where Q is volumetric flow rate and R is the fluidic resistance. Fluidic resistance depends on the geometry of the channel. For circular channels, flow rate depends on radius of the capillary to the power of four. Reynolds number 2300 is used to differentiate between laminar and turbulent flow. In microchips the Reynolds number is smaller than one. Due to the omnipresence of laminar flow, sample mixing occurs only due to lateral diffusion. The smaller the radius of the channel is, the higher is the pressure needed to pump the liquid through the channel. Electrokinetic pumping takes advantage of the surface charge of the microchannel for moving the sample and separating different components. The requirement is that the inner wall of the microchannel is charged.

The most successfully miniaturized chemical method to date is capillary electrophoresis (CE), and CE is separation method mostly used in microanalysis due to its high efficiency, low reagent consumption and fast separation times. Traditional CE is done in fused silica capillaries 20 - 100 cm long and 20 - 100 μm in diameter. Due to the ionization of the capillary wall silanol groups at suitable pH, the inner wall becomes covered with negative surface charge, and a double layer is formed by attachment of positive ions to the wall. When an electric field is applied over the capillary, the movable cationic outer layer starts to move toward the cathode, dragging analytes in a plug. This electroosmotic flow (EOF) or bulk flow acts as a pumping mechanism to propel all molecules (cationic, neutral, and anionic) toward the detector, with separation ultimately being determined by differences in the electrophoretic migration of the individual analytes. As electrophoretic migration occurs, all analytes are swept toward the detector by bulk flow. The main advantage of CE is the uniform sample plug, which allows sharp peaks.

If the EOF is adequate but not too strong, the respective electrophoretic mo-

bilities of the analytes lead to the formation of discrete zones by the time they reach the detector. If the EOF is slow, diffusion of the analyte zones could result in substantial band broadening and, under conditions of very low EOF, some of the analytes may not reach the detector within a reasonable analysis time. If the EOF is too fast, on the other hand, components of the mixture may not have adequate on-capillary time for separation to occur. Electroosmotic mobility depends on viscosity of the liquid, its dielectric constant and zeta potential of the inner capillary wall. Zeta potential, in turn, depends on surface charge on the capillary wall, pH, and ionic strength of the electrolyte. An increase of ionic strength decreases the double wall of the capillary, thus decreasing the EOF and increasing the separation time. An advantage of increasing ionic strength is reduced analyte-wall interactions. The electrophoretic mobility is determined by size and charge of the analytes. Anions move electrophoretically toward the anode, cations toward the cathode. The EOF is generally stronger than electrophoretic mobility, so the net flow is toward the cathod, and consequently, the elution order is cations, neutral analytes and anions. The high surface to volume ratio of capillaries with these dimensions allow very efficient dissipation of Joule heat generated from large applied fields (typically used values range from 500 to 1000 V/cm).

The typical buffer concentration in CE ranges from 10 to 100 mM. The use of moderately high ionic strength buffers is desirable for suppression of ion-exchange effects between the charged analyte ions and the ionized silanol groups on the capillary wall. However, the Joule heat associated with high ionic strength (over 100 mM) may overcome the capillary thermostating capability of the system at higher applied voltages. Excessive Joule heating can have undesirable effects on both resolution and analyte stability.

CE microchips typically have a 1 cm long sample introduction channel and a 4 cm long separation channel, while width and height values depend on the fabrication material. Early CE microchips were fabricated in glass, where the channel geometry is semicircular due to the limitations in microfabrication technologies. Thus

typical width ranges from 40 to 80 μm and height is in the range from 10-20 μm. Silicon and polymer microchips allow more flexible geometry, and the used width and height values are in the same range (30-60 μm). The most common detection method at present is laser-induced fluorescence (LIF). The small injection plugs, high electric fields, and short separation channel lengths produce separation times on the order of seconds or minutes. LIF requires an external excitation source, which limits miniaturization possibilities.

Electrochemical detection methods are relatively simple and inexpensive, and they are suitable for a broad range of analytes due to the variety of electrode materials and electrochemical processes that can be exploited for detection. The technologies for thin film deposition and fabrication are well-developed, and electrodes are of small dimensions, which allows the fabrication of detectors with minimal dead volume. The signal from an electrode is easier to register than a LIF signal. Despite these attractive properties, a CE microchip with an integrated electrochemical detector (CE-EC) has found few commercial applications to date, and is mainly utilized in research laboratories. The main challenge for an EC-CE system is its sensitivity to electrical noise and the need for decoupling of the measurement electrodes from the high voltage electric field needed for electrophoretic separation.

MST plays a particularly important role in the field of DNA analysis, and produced the most extensively integrated analytical chips have been developed for this purpose. Various PCR-based microfluidic devices, fabricated in silicon or polymeric materials with integrated fluidic connections, heating modules and in some cases detection electrodes, have been reported.[80,81] Kajiyama *et al.*[82] reported a thermal gradient DNA chip fabricated in silicon with p-n junction heaters for local hybridization temperature control, which improved mismatch discrimination efficiency. Liu *et al.*[83] reported an automated miniaturized device for hybridization and gene expression analysis, which combined a semiconductor-based microarray with microfluidic elements. The device allowed *in situ* synthesis of probe oligonucleotides, as well as automated hybridization and labeling steps

18

on-chip. A PDMS microfluidic chip for DNA hybridization has been reported.[84] In this approach a PDMS microchannel was coated with photobiotin, which was activated by exposure to UV light (254/366 nm) through a photomask in order to achieve localized immobilization. Upon photoexposure the nonactivated biotin was washed away and the activated biotin was incubated with avidin to allow immobilization of biotin-labeled oligonucleotides. Several immunoassays in microfluidic systems have been reported.[85] Traditional microtiter-based immunoassays are highly sensitive and reliable; however, long incubation times, on the order of hours or even days, are common. Microfluidic immunoassay and hybridization assay formats offer rapid reaction times on the order of minutes.

2.3.1   Basic processes in microfabrication

The fabrication of microsystem involves following main steps: photomask design, cleaning of wafers, photolithography, deposition, and etching.[86–89] The first step of the process, photomask design, can be done using a suitable software program, such as AutoCAD, Expert, or, for relatively simple structures, CleWin. The photomask consists of opaque and transparent areas, which define the desired structures. Two types of photomasks are common: (i) hard masks made of a chromium layer on a quartz plate (resolution down to 1 μm) and (ii) high-resolution printed transparencies attached to a quartz plate (pixel resolution 7 μm), which represents a considerably cheaper solution.

Many of the processes used for fabrication of analytical microsystems have been developed for the microelectronics industry. The need of for an extremely clean environment requires that the fabrication is performed in clean rooms, where laminar flow in hoods prevents the transport of dust and air mixing. Clean rooms are classified according to the purity, type 1000 signifying an environment containing less than 1000 particles larger than 0.5 μm each per cubic foot.[90] For comparison, the air of a normal office contains as many as 50 million particles of that size in one cubic meter. People are the main source of contamination, and

protective clothing must be worn.

2.3.2 Wafer cleaning

The processes needed for actual device microfabrication in a clean room are schematically illustrated in Figure 2.2. The first step is to properly clean the substrates, or wafers. Wet cleaning using acid, base and solvent cleanings are the main cleaning methods. The most common wet clean method, known as *RCA-clean* because it was invented at RCA Laboratories, consists of a sequence of different wet cleans effective in removing of different types of contamination.[88] A typical cleaning sequence consist of dipping silicon wafers in a hot bath composed of mixture of concentrated ammonium hydroxide and hydrogen peroxide for 10-20 min, followed by rinsing with water. The mixture of peroxide and hydroxide causes simultaneous oxidation and etching of the silicon surface, which allows efficient removal of organic contamination. Wafers are then placed into a hot bath consisting of a hot mixture of hydrochloric acid and hydrogen peroxide for 10-20 min, which efficiently removes metal particle contamination. A silicon surface is covered with a native thin oxide, and this oxide is usually removed during the standard cleaning by etching in hydrofluoric acid (HF). This step can be performed between the previously described steps or after them. HF cleaning leaves the surface hydrophobic with H-termination, which greatly reduces oxidation of the silicon surface.

At the Institute of Microtechnology (IMT), Neuchâtel, the standard process for cleaning of silicon wafers involves cleaning in hot mixture of concentrated sulfuric acid and hydrogen peroxide for 10 min to remove organic residues. This is followed by rinsing with water, etching of native silicon dioxide for 1 min in buffered hydrofluoric solution (BHF), rinsing with water, soaking for 10 min in a fuming nitric acid for 10 min to reoxidize the silicon surface, and finally, rinsing with water. Pyrex wafers are cleaned with organic solvents such as acetone and isopropanol to remove organic residues, rinsed with water, dried, and then placed
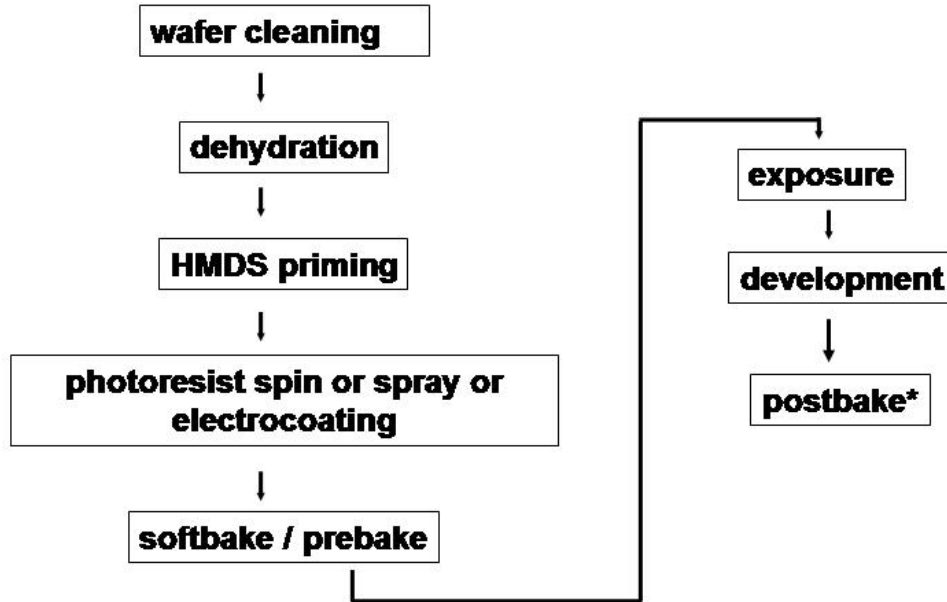
Figure 2.2: Schema of photolithography processes used for device fabrication in clean room. The processes marked with * are not always performed.

for 10 min in concentrated nitric acid.

2.3.3   Photolithography

Photolithography involves three main steps: application of a photoresist (a photosensitive polymer), optical exposure to print an image of the mask onto the photoresist, and development in a developer solution to dissolve nonpolymerized photoresist and render visible the latent image. Before a photoresist can be applied to a wafer, wafers must be dehydrated in an oven at 120 ℃. To improve the adhesion of the photoresist on the wafer, hexamethyldisilazane (HDMS) priming is performed for 15 minutes in vapor phase, at room temperature and atmospheric pressure. Then the photoresist is spun on the wafer, held in position on a rotating table (spinner) by a vacuum chuck. Rotation of the spinner spins the photoresist

homogeneously on the wafer. The thickness of the layer depends on the viscosity of the photoresist and of the rotation speed of the spinner, faster rotation leading to a thinner photoresist layer. After spinning the photoresist layer is prebaked to evaporate most of the solvents, typically for 1 min baking on a hot plate heated to 100 ℃. After the prebake the image is transferred onto the wafer through optical exposure. Photoresist is then developed in a development solution. The remaining photoresist is postbaked at 125 ℃ for 30 min in order to harden it and to remove residual solvents.

The photoresist can be positive or negative, which leads to a different behavior upon exposure. Upon exposure with a suitable light source, the photoactive compound of a positive photoresist undergoes a photochemical reaction that changes its molecular structure and converts it in a soluble acid species, which is then dissolved in an alkaline developer. In negative photoresists, the polymer typically undergoes crosslinking upon light exposure and becomes insoluble, while the non-exposed part is dissolved in developer. Positive photoresists are more widely used than negative. However, the most commonly used negative photoresist, SU-8, is gaining popularity as a material for device fabrication due to its chemical resistance and reliability.[26,91] It is suitable for the fabrication of thick layers and structures with high aspect ratio (>10:1).

Theoretical size of the features that can be created with a particular photoresist depends on the wavelength of the exposure light, thickness of the photoresist layer, and the distance between the photoresist layer and the mask. The expression for the smallest mask feature, called the minimum linewidth, is given by[89]

$$w_{min} = \frac{3}{2}\sqrt{\lambda\left(s + z\right)} \qquad (2.11)$$

where w_{min} is the minimum linewidth, s is the gap between the mask and the photoresist surface, λ is the wavelength of the exposing radiation, and z is the thickness of the photoresist. The most common light source is a mercury spec-

tral lamp and wavelength of 365 nm.[89] Photolithography can be performed in contact or proximity mode. In the contact mode, the mask is in contact with the photoresist layer, and s is 0. The disadvantage of the contact mode is that the photoresist can leave residues on the mask. In the proximity mode, there is a distance between the mask and the photoresist layer. This minimizes defects that result from the contact between the mask and photoresist but decreases resolution. A transparency mask is never completely planar due to the difficulty of attaching it completely flat to a quartz mask, and proximity mode is usually used. In a typical fabrication process where a transparency mask is used, the mask is brought within 25-100 μm of the resist surface. For the case of proximity printing the equation 2.11 can be rewritten as:

$$w_{min} = \frac{3}{2}\sqrt{\lambda * s} \qquad (2.12)$$

The energy of the exposure depends on the type of the used photoresist and the thickness desired.

2.3.4 Deposition of thin films

Various thin films are used in microfabrication. One of the features that makes silicon the most useful material of the microelectronics industry is its ability to grow a thin layer of silicon dioxide. At ambient environment, the silicon surface is covered with an oxide layer about 1-2 nm thick. This native oxide is usually stripped away in hydrofluoric acid in wafer preparation stage as described above. In IMT, the surface is homogeneously oxidized in hot nitric acid before oxidation. High-quality silicon dioxide can be obtained by oxidizing silicon in water vapor or in dry oxygen at elevated temperature (850-1200 ℃).[89]

$$\text{Si} + \text{O}_2 \overset{850-1200\,°\text{C}}{\rightarrow} \text{SiO}_2(dry) \qquad (2.13)$$

23

$$\text{Si} + 2\text{H}_2\text{O} \overset{850-1200\,^{\circ}\text{C}}{\rightarrow} \text{SiO}_2 + 2\text{H}_2 (wet) \tag{2.14}$$
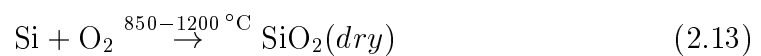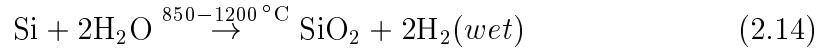
Dry oxidation in pure oxygen at high temperature produces a better quality oxide than steam oxidation, but the oxide growth occurs considerably slower. Thermal oxidation of silicon generates compressive stress in the silicon dioxide due to mismatch between the coefficient of thermal expansion of silicon and silicon dioxide. Thus, thermally grown oxide films thicker than one micrometer can cause bowing of the underlying substrate.[86]

Chemical vapor deposition (CVD) allows deposition of silicon dioxide, silicon nitride, and polysilicon films. The CVD process allows deposition of thicker silicon dioxide layers in shorter time and at lower temperature than can be produced thermally. However, the electrical and mechanical qualities of CVD oxide are inferior to those of thermally grown oxide. Silicon nitride can be deposited by low-pressure CVD (LPCVD), which operates at relatively high temperatures (500-800 ℃) or by plasma-enhanced CVD (PECVD), which operates at lower temperatures (typically 300 ℃).[89] LPCVD produces stoichiometric silicon nitride (Si_3N_4), while PECVD generates nonstoichiometric silicon nitride (Si_xN_y). Silicon nitride is commonly used in MST because of its excellent chemical, electrical, optical, and mechanical properties. Although SiO_2 is an excellent dielectric, it shows poorer passivating characteristics than silicon nitride in aqueous media and it is also relatively permeable to alkali ions.[86] LPCVD-produced Si_3N_4 films are of high quality and are practically free from pinholes. PECVD Si_xN_y is the typical encapsulating material used for the final passivation of devices, as a moisture barrier and to prevent sodium diffusion. Although it is very similar to LPCVD Si_3N_4, passivation is poorer and layers must be thicker, typically 400 nm instead of 200 nm.

2.3.5 Fabrication of thin film electrodes

The most commonly used metals for electrode fabrication in analytical microsystems are noble metals, aluminum, and silver.[89] Noble metals are deposited as thin films by electron gun evaporation. The source material is placed in a crucible and heated by e-beam under high *vacuum* conditions. Vapor phase is generated when the vapor pressure of the metal exceeds that of the environment. The surface of the substrate is kept cooler, and when the vapor of the metal comes in touch with the substrate, it condenses by nucleation mechanism and a thin film grows on the substrate. The poor adhesion of noble metals to dielectrics means that a seed layer must be deposited first, usually chromium or titanium for gold, and titanium or tantalum for platinum-group metals. Typically, 10 - 20 nm of a seed metal layer is deposited prior to a 100-nm -thick layer of noble metal.[89]

Patterning of the metal electrodes can be performed by wet etching, if a suitable etchant exists, or by lift-off (see Figure 2.3). There are no good wet etchants for platinum-group metals, but gold can be etched with a mixture of KI and I_2. An advantage of lift-off is that the same mask can be utilized for fabrication of platinum-group and gold electrodes. For microanalytical devices it may be important that metals are deposited on an insulating surface in order to avoid short-circuits. Therefore, before metal deposition silicon surfaces are passivated by thermal oxidation of silicon up to a thickness of 100 nm, after which a layer of 200 nm of LPCVD Si_3N_4 is deposited. Direct deposition of LPCVD Si_3N_4 is not desirable, as it would lead to high stress on the surface. This passivation layer also prevents diffusion of metal into silicon.[89]

In a typical process used at IMT for metal electrode fabrication, a positive photoresist (usually AZ 1518) is spun on a silicon or Pyrex wafer at thickness of 1 - 1.5 μm. If the electrodes are to be fabricated on nonplanar surface, e.g. channels have been already etched, the photoresist layer must be spun thicker, or it can be sprayed instead of spun. If the wafer containing electrodes is afterwards to be bonded to glass, it is important to have a completely flat surface. This can
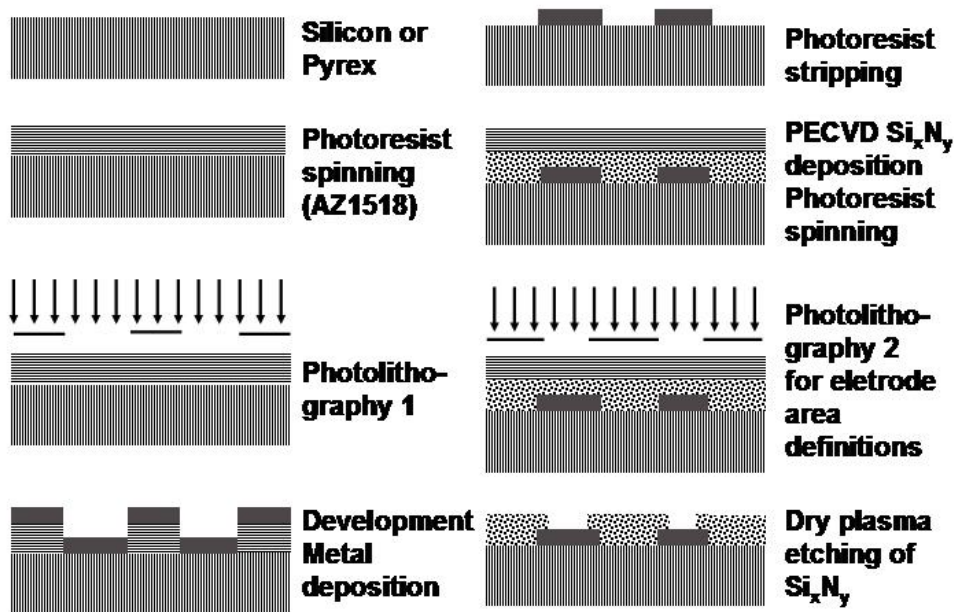
Figure 2.3: Lift-off process for fabrication of electrodes and the electrode surface area defined by plasma opening of deposited thin PECVD Si_xN_y layer.

be achieved on glass wafer by etching the openings for the electrodes in buffered hydrofluoric acid (BHF) solution before metal deposition. A postbake is not performed when lift-off is the next process step, as this would evaporate solvents and make photoresist removal more difficult. After lift-off of the photoresist, a layer of PECVD Si_xN_y is deposited on the wafer and opened by plasma-etching on suitable areas to define the active surface area of the electrode.

2.3.6 Etching

Critical to any microtechnology process sequence is the ability to selectively remove materials with high selectivity and resolution. The etching process can be classified as wet or dry depending on whether it is done in an aqueous solution or by plasma.[88] Etching can also be isotropic or anisotropic. Isotropic etching

means that the vertical and lateral etch rates are the same. In this case, the resulting structures are hemispherical and more than twice as wide as deep because of the initial opening in the etch mask. Material that is to be anisotropically wet etched must be of crystalline structure. Silicon has three distinct crystalline planes: <100>, <110>, and <111>. Silicon can be isotropically etched in a solution composed of hydrofluoric acid, nitric acid and acetic acid and anisotropically etched in 40% potassium hydroxide (KOH) heated to 80 ℃. The anisotropic wet etching of silicon in potassium hydroxide is explained by the fast etch rate of the <100> planes with respect to the <111> planes. The etch angle of the <100> and <111> planes is always 54.74°. Another anisotropic wet etchant for silicon is tetramethylammonium hydroxide, which is gaining popularity because it is relatively easy to handle, fully compatible with electronic fabrication, and masking is easier.[88]

The only chemical capable of dissolving silicon dioxide and thus glass is hydrofluoric acid (HF). The dissolution of glass is based on a reaction of the acid with silica, as follows:

$$SiO_2 + 4HF \rightarrow SiF_4 + 2H_2O \qquad (2.15)$$

$$SiF_4 + 2HF \rightarrow H_2SiF_6 \qquad (2.16)$$

H_2SiF_6 is a water-soluble product. Glass does not have crystalline structure, and is therefore always wet etched isotropically.[89] For deep glass structures, 49% solution of HF, which has an etch rate approximately of 10 μm/min, or 20% HF which has an etch rate of approximately 1 μm/min, are used. Commercially available silicon dioxide and glass etching solutions contain hydrofluoric acid buffered with ammonium fluoride (NH_4F) and are sold as buffered hydrofluoric acid (BHF). Conventional BHFs consist of mixtures of 40% NH_4F and 50% HF. Depending on the individual application, the compositions vary from almost pure 40% NH_4F solutions to less concentrated HF-solutions with 13% HF and about 30% of NH_4F. The etch rates of these solutions vary from 1.3 nm/min to 342 nm/min.

Preparation of the mask for etching is of great importance, since the mask determines the structural accuracy of the later device structures. A good mask must both very well adhere to the wafer and have excellent resistance to the etching solution. In the ideal case,a photoresist can be used as a mask. Photoresist masks show low defect density, are relatively cheap, and offer manifold property variations due to the wide variety of polymeric materials available. The risk of photoresist lift-off during the etching process must be considered. Pure HF solution exhibits strong penetration into the glass-photoresist interface and destroys the mask quickly, while BHF solutions are less aggressive. Thus, photoresist masks can be used when shallow structures in glass are desired, while etching of deeper structures requires a hard mask. Examples of common hard masks for etching processes are silicon dioxide, silicon nitride, polysilicon and chromium. Polysilicon is used as an etching mask for glass at IMT. In a typical process, a 200-nm-thick LPCVD polysilicon layer is deposited and photoresist is spun on it. After photolithography, the exposed polysilicon is opened with reactive ion etch (RIE). Polysilicon is a sufficiently protective layer against 20% and 50%HF. After the channels are sufficiently etched, polysilicon is etched in 40% KOH at 60 ℃. The dissolution process is fast taking only 5-10 min. The LPCVD polysilicon process is compatible with standard lithographical processes and no underetching, except that isotropically induced, is generated. Widely used etch masks for silicon are silicon nitride and silicon dioxide.[88,89]

The terms dry etching, plasma etching, and reactive ion etching (RIE) are used synonymously. RIE is done in a vacuum chamber with reactive gases excited by RF fields. The glow discharge generates active species that react with the surface and produce volatile compounds. RIE is very suitable for etching of silicon nitrides, which can be wet etched only in boiling phosphoric acid. RIE can be used for isotropic or anisotropic etching depending on the gases and etched material. In the case of silicon, RIE is typically used for fabrication of vertical or near vertical sidewalls. Silicon is easily etched by halogens, as the reaction products - silicon fluorides, chlorides, and bromides - are volatile at room temperature.[88] Deep RIE can be used for fabrication of deep vertical walls in silicon.

2.3.7 Bonding

Bonding together of different materials is very important in the fabrication of microchips. Pyrex is the most widely used glass in microtechnology, because of its thermal stability and compatibility with silicon. Anodic bonding of Pyrex glass and silicon is widely practised because the easily movable sodium ions make an extraordinary strength of the bond.[87] Two glass wafers can be bonded by fusion bonding. Surface flatness and purity are critical for successful fusion bonding, as particles and surface roughness will undermine the bond strength. Two Pyrex wafers can be fusion bonded at 650 ℃. Thin film deposition and structuring of active metal electrodes is a mature and well-controlled process. A disadvantage of glass is that it can be etched only isotropically as it does lack crystalline structure. As noted above, successful bonding of two glass plates requires complete planarity, a particular challenge in the bonding electrode-containing plate to glass. In this case, the glass should be etched so that the deposited electrodes do not protrude above the surface, which might lead to conformational problems, e. g.such as deposition of metal at edges and metal wings. PDMS is easily reversibly or irreversibly bonded to itself or to a glass wafer. Owing to the elasticity of PDMS and its facility for conformational change, it can adapt to small roughnesses on the wafer, such as metal electrodes.

2.3.8 Microfabrication in polymers

The need for transparency, electrical isolation, biocompatibility, and resistivity to alkaline solutions has pushed the development of glass and polymer fabrication methods. The work on capillary electrophoresis on chip initially focused on microfabrication on glass and quartz due to the mature fabrication technology available for these materials and their chemical similarity to fused silica.[92–94] Glass is an electronic insulator, chemically stable and transparent, facilitating optical detection, and glass chips have found wide use. Micromachining is expensive, however, and requires clean room facilities. Additionally, glass is easily broken

and relatively expensive. The disadvantages of glass microchips have led to the investigation of alternative substrate materials, particularly polymers.[95] Polymer materials suitable for fabrication of CE chips need to satisfy several conditions: they need to support electroosmotic flow, be electrical isolators and allow good heat dissipation. Most widely investigated polymeric materials are poly(methyl methacrylate) (PMMA), polyimide, polyethylene, polycarbonate, poly-ethylene tere-phthalate glycol and poly(dimethylsiloxane) (PDMS).

Poly(dimethylsiloxane) (PDMS) is an elastomeric material, which has gained much popularity in the fabrication of microfluidic systems. Its advantages include low cost, rapid microfabrication by replica molding, optical transparency in visible range down to 280 nm, nontoxicity, and easy reversible sealing to a number of materials, including glass, another PDMS slide, silicon, and silicon nitride.[77,96] Irreversible bonding can be achieved upon plasma oxidation of slides to be bonded. The slides are oxidized during 6 s at room temperature, and they have to be aligned together in the next few minutes. Figure 2.4 shows the fabrication of a PDMS channel using a master fabricated with a negative photoresist SU-8.

In a typical fabrication procedure, prepolymeric liquid material is carefully mixed with a curing agent in ratio 10:1 and degassed in a dessicator. The degassed liquid mixture is poured on a master and left to polymerize during 3-4 hours at 65 ℃. The same master can be used for the fabrication of a practically unlimited number of PDMS chips. Microfluidic channels and reservoirs are easily fabricated in PDMS. The master can be fabricated in silicon or SU-8. A significant disadvantage of PDMS is its hydrophobicity, which causes high adsorption and absorption of biomolecules on its surface and into the bulk of PDMS, and difficulty in filling the channels with aqueous solutions.
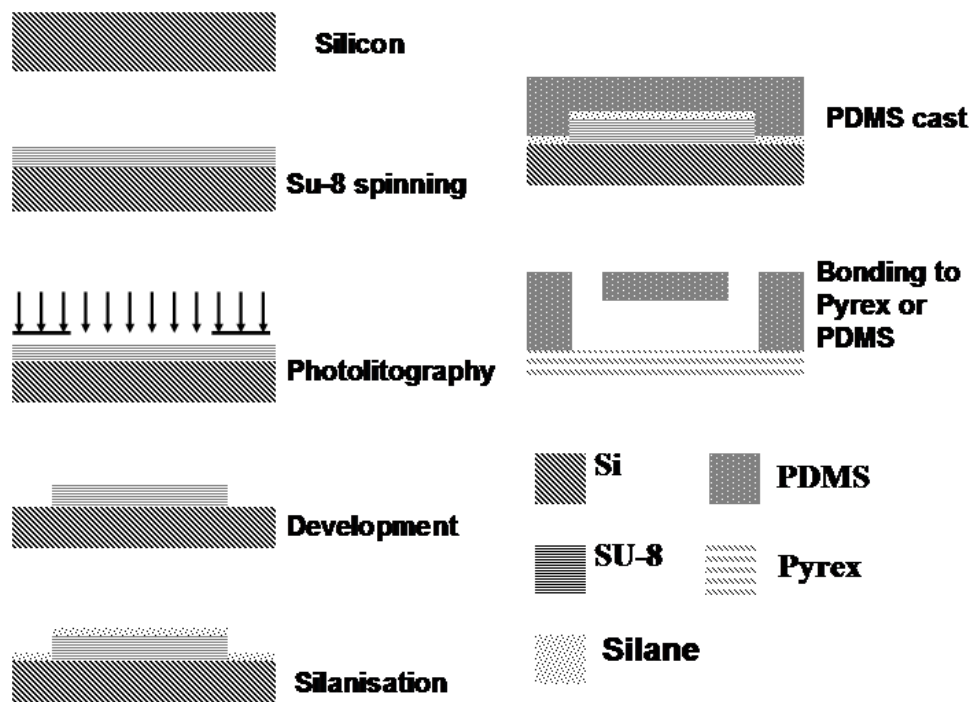
Figure 2.4: Rapid prototyping of PDMS structures using a master fabricated with SU-8 negative photoresist.

References

1. Ingle, J. D., Crouch, S. R., Spectrochemical analysis, Prentice Hall 1988, pp. 325–351.

2. Kricka, L. J., Clinical applications of chemiluminescence, *Anal. Chim. Acta* **500** (2003) 279–286.

3. Cheek, B. J., Steel, A. B., Torres, M. P., Yu, Y.-Y., Yang, H., Chemiluminescence detection for hybridization assays on the flow-through chip, a three-dimensional microchannel biochip, *Anal. Chem.* **73** (2001) 5777–5783.

4. Knight, A., A review of recent trends in analytical application of electrogenerated chemiluminescence, *Trends Anal. Chem.* **18** (1999) 47–62.

5. Fahnrich, K. A., Pravda, M., Guilbault, G. C., Recent applications of electrogenerated chemiluminescence in chemical analysis, *Talanta* **54** (2001) 531–559.

6. Kulmala, S., Suomi, J., Current status of modern analytical luminescence methods, *Anal. Chim. Acta* **500** (2003) 21–69.

7. Richter, M., Electrochemiluminescence ECL, *Chem. Rev.* **104** (2004) 3003–3036.

8. Wilson, R., Akhavan-Tafti, H., DeSilva, R., Schaap, A. P., Comparison between acridan ester, luminol, and ruthenium chelate electrochemiluminescence, *Electroanalysis* **13** (2001) 1083–1092.

9. Marquette, C. A., Leca, B. D., Blum, L. J., Electrogenerated chemiluminescence of luminol for oxidase-based fibre-optic biosensors, *Luminescence* **16** (2001) 159–165.

10. McCord, P., Bard, A., Part 54. Electrogenerated chemiluminescence of ruthenium(II) 4,4-diphenyl-2,2-bipyridine and ruthenium(II) 4,7-diphenyl-1,10-

phenanthroline systems in aqueous and acetonitrile solutions, *Electroanal. Chem.* **318** (1991) 91–99.

11. Kapturkiewicz, A., Electrogenerated chemiluminescence from the tris(4,7-diphenyl-1,10-phenanthroline)ruthenium(II) complex, *Chem. Phys. Lett.* **236** (1995) 389–394.

12. Walworth, J., Brewer, K. J., Richter, M. M., Enhanced electrochemiluminescence from $Os(phen)_2(dppene)^{2+}$ (phen =1,10- phenanthroline and dppene = bis(diphenylphosphino)ethene) in the presence of triton X-100 (polyethylene glycol tert-octylphenyl ether), *Anal. Chim. Acta* **503** (2004) 241–245.

13. Paris, J. P., Brandt, W. W., Charge transfer luminescence of a ruthenium(II) chelate, *J. Am. Chem. Soc.* **81** (1959) 5001.

14. Jackson, W. A., Bobbitt, D. R., Chemiluminescent detection of amino acids using in situ generated $Ru(bpy)_3^{3+}$, *Anal. Chim. Acta* **285** (1994) 309–320.

15. Skotty, D. R., Lee, W.-Y., Nieman, T. A., Determination of dansyl amino acids and oxalate by HPLC with electrogenerated chemiluminescence detection using tris(2,2-bipyridyl)ruthenium(II) in the mobile phase, *Anal. Chem.* **68** (1996) 1530–1535.

16. Yin, X.-B., Dong, S., Wang, E., Anal. applications of the electrochemiluminescence of tris(2,2'-bipyridyl)ruthenium and its derivatives, *Trends Anal. Chem.* **23** (2004) 432–441.

17. Michel, P. E., Fiaccabrino, G. C., de Rooij, N. F., Koudelka-Hep, M., Integrated sensor for continuous flow electrochemiluminescent measurements of codeine with different ruthenium complexes, *Anal. Chim. Acta* **392** (1999) 95–103.

18. Cao, W., Liu, J., Yang, X., Wang, E., New technique for capillary electrophoresis directly coupled with end-column electrochemiluminescence detection, *Electrophoresis* **23** (2002) 3683–3691.

19. Dennany, L., Foster, J., Rusling, J., Simultaneous direct electrochemilumines-cence and catalytic direct voltammetry detection of DNA in ultrathin films, *J. Am. Chem. Soc.* **125** (2003) 5123–5128.

20. Leland, J. K., Powell, M. J., Electrogenerated chemiluminescence – an oxidative-reduction type ECL reaction sequence using tripropyl amine, *J. Electrochem. Society* **137** (1990) 3127–3131.

21. Miao, W., Choi, J.-P., Bard, A. J., Electrogenerated electrochemilu-minescence 69: The tris(2,2'-bipyridine)ruthenium(II) (Ru(bpy)$_3^{2+}$)/tri-n-propylamine (TPrA) system revisited-A new route involving TPrA$^{+\cdot}$ cation radicals, *J. Am. Chem. Soc.* **124** (2002) 14478–14485.

22. Li, F., Cui, H., Lin, X.-Q., Determination of adrenaline by using inhibited Ru(bpy)$_3^{2+}$ electrochemiluminescence, *Anal. Chim. Acta* **471** (2002) 187–194.

23. McCall, J., Alexander, C., Richter, M. M., Quenching of electrogenerated chemiluminescence by phenols, hydroquinons, catechols and benzoquinones, *Anal. Chem.* **71** (1999) 2523–2527.

24. Arora, A., Eijkel, J. C. T., Morf, W. E., Manz, A., A wireless electrochemilu-minescence detector applied to direct and indirect detection for electrophore-sis on a microfabricated glass device, *Anal. Chem.* **73** (2001) 3282–3288.

25. Kuwabara, T., Noda, T., Ohtake, H., Toyama, S., Ikariyama, Y., Classifica-tion of DNA binding mode of antitumor and antiviral agents by the electro-chemiluminescence of ruthenium complex, *Anal. Biochem.* **314** (2003) 30–37.

26. L'Hostis, E., Michel, P. E., Fiaccabrino, G. C., Strike, D. J., de Rooij, N. F., Koudelka-Hep, M., Microreactor and electrochemical detectors fabricated us-ing Si and SU-8, *Sens. Actuators B* **64** (2000) 156–162.

27. Chiang, M.-T., Whang, C.-W., Tris(2,2-bipyridyl)ruthenium(III)-based elec-trochemiluminescence detector with indium tin oxide working electrode for capillary electrophoresis, *J. Chromatogr. A* **934** (2001) 59–66.

28. Cao, W., Jia, J., Yang, X., Dong, S., Wang, E., Capillary electrophoresis with solid-state electrochemiluminescence detector, *Electrophoresis* **23** (2002) 3692–3698.

29. Yan, J., Yang, X., Wang, E., Fabrication of a poly(dimethylsiloxane)-based electrochemiluminescence detection cell for capillary electrophoresis, *Anal. Chem.* **77** (2005) 5385–5388.

30. Qiu, H., Yan, J., Sun, X., Liu, J., Cao, W., Yang, X., Wang, E., Microchip capillary electrophoresis with an integrated indium tin oxide electrode-based electrochemiluminescence detector., *Anal. Chem.* **75** (2003) 5435–5440.

31. Yan, J., Yang, X., Wang, E., Electrogenerated chemiluminescence on microfluidic chips, *Anal. Bioanal. Chem.* **381** (2005) 48–50.

32. Zhan, W., Alvarez, J., Crooks, R. M., Electrochemical sensing in microfluidic system using electrogenerated chemiluminescence as a photonic reporter of a redox reactions, *J. Am. Chem. Soc.* **124** (2002) 13265–13270.

33. Zhan, W., Alvarez, J., Crooks, R. M., A multichannel microfluidic sensor that detects anodic redox reactions indirectly using anodic electrogenerated chemiluminescence, *Anal. Chem.* **75** (2003) 313–318.

34. Zhan, W., Alvarez, J., Crooks, R. M., A two-channel microfluidic system sensor that uses anodic electrogenerated chemiluminescence as a photonic reporter of cathodic redox reactions, *Anal. Chem.* **75** (2003) 313–318.

35. Kulmala, S., *Electrogenerated lanthanide(III)luminescence at oxide-covered aluminum electrodes in aqueous solutions and closely related studies*, Ph.D. thesis, University of Turku (1995).

36. Ala-Kleme, T., *Hot electron-induced electrogenerated chemiluminescence*, Ph.D. thesis, University of Turku (2002).

37. Hakansson, M., Helin, M., Putkonen, M., Jiang, Q., Kotiranta, M., Suomi, J., Ala-Kleme, T., Kulmala, S., Electrochemiluminescence of Tb(III) chelates

at optically transparent tunnel emission electrodes fabricated by atomic layer deposition, *Anal. Chim. Acta* **541** (2005) 137–141.

38. Kulmala, S., Ala-Kleme, T., Papkovsky, A. K. D., Loikas, K., Cathodic electrogenerated chemiluminescence of luminol at disposable oxide-covered aluminum electrodes, *Anal. Chem.* **70** (1998) 1112–1118.

39. Suomi, J., Hakansson, M., Jiang, Q., Kotiranta, M., Helin, M., Niskanen, A., Kulmala, S., Time-resolved detection of electrochemiluminescence of luminol, *Anal. Chim. Acta* **541** (2005) 167–169.

40. Ala-Kleme, T., Kulmala, S., Vare, L., Juhala, P., Helin, M., Hot electron-induced electrogenerated chemiluminescence of Ru(bpy)$_3^{2+}$ chelate at oxide-covered aluminum electrodes, *Anal. Chem.* **71** (1999) 5538–5543.

41. Jiang, Q., Suomi, J., Hakansson, M., Niskanen, A. J., Kotiranta, M., Kulmala, S., Cathodic electrogenerated chemiluminescence of Ru(bpy)$_3^{2+}$ chelate at oxide-coated silicon electrodes, *Anal. Chim. Acta* **541** (2005) 157–163.

42. Laakso, P., Anttila, H., Kairisto, V., Eskola, J., Kulmala, S., Ala-Kleme, T., Hot electron-induced electrogenerated chemiluminescence of SYBR (R) Green I, *Anal. Chim. Acta* **541** (2005) 83–87.

43. Helin, M., Jiang, Q., Ketamo, H., Hakansson, M., Spehar, A.-M., Kulmala, S., Ala-Kleme, T., Electrochemiluminescence of coumarin derivatives induced by injection of hot electrons into aqueous electrolyte solution, *Electrochim. Acta* **51** (2005) 725–730.

44. Jiang, Q., Spehar, A.-M., Hakansson, M., Suomi, J., Ala-Kleme, T., Kulmala, S., Hot electron-induced cathodic electrochemiluminescence of rhodamine B at disposable oxide-coated aluminium electrodes, *Electrochim. Acta* **51** (2006) 2706–2714.

45. Kulmala, S., Ala-Kleme, T., Latva, M., Loikas, K., Takalo, H., Hot electron-induced electrogenerated chemiluminescence of rare earth(III) chelates at oxide-covered aluminum electrodes, *J. Fluorescence* **8** (1998) 59–65.

46. Jiang, Q., Hakansson, M., Spehar, A.-M., Ahonen, J., Ala-Kleme, T., Kulmala, S., Hot electron-induced time-resolved electrogenerated chemiluminescence of a europium(III) label in fully aqueous solutions, *Anal. Chim. Acta* **558** (2006) 302–309.

47. Ala-Kleme, T., Kulmala, S., Latva, M., Generation of free radicals and electrochemiluminescence at pulse-polarized oxide-covered silicon electrodes in aqueous solutions, *Acta Chim. Scandinavica* **51** (1997) 541–546.

48. Haapakka, K., Lipiainen, J., Instrumentally simple flow detector for the determination of traces of electroluminescent compounds in aqueous solutions, *Anal. Chim. Acta* **233** (1990) 199–206.

49. Hemmila, I. A., *Applications of fluorescence in immunoassays*, Wiley-Interscience 1991.

50. Yalow, R., Berson, S. A., Immunoassay of endogenous plasma insulin in man, *J. Clin. Investigation* **39** (1960) 1157–1175.

51. Lander, E. S., Linton, L. M., Birren, B., Nusbaum, C., Zody, M. C., Baldwin, J., Devon, K., Dewar, K., Doyle, M., FitzHugh, W., Funke, R., Gage, D., et al., Initial sequencing and analysis of the human genome, *Nature* **409** (2001) 860–921.

52. Venter, J. C., Adams, M. D., Myers, E. W., Li, P. W., Mural, R. J., Sutton, G. G., Smith, H. O., Yandell, M., Evans, C. A., Holt, R. A., Gocayne, J. D., Amanatides, P., et al., The sequence of human genome, *Science* **291** (2001) 1303–1351.

53. Kolchinsky, A., Mirzabekov, A., Analysis of SNPs and other genomic variations using gel-based chips, *Human Mutation* **19** (2002) 343–360.

54. Dharmadi, Y., Gonzales, R., DNA microarrays: experimental issues, data analysis and application to bacterial systems, *Biotechnol. Progress* **20** (2004) 1309–1324.

55. Gooding, J. J., Electrochemical DNA hybridization biosensors, *Electroanalysis* **14** (2002) 1149–1156.

56. LeBerre, V., Trevisiol, E., Dagkessamanskaia, A., Sokol, S., Caminade, A.-M., Majoral, J. P., Meunier, B., Francois, J., Dendrimeric coating of glass slides for sensitive DNA microarrays analysis, *Nucleic Acids Research* **31** (2003) 1–8.

57. Barrett, J. C., Kawasaki, E. S., Microarrays: the use of oligonucleotides and cDNA for the analysis of gene expression, *DDT* **8** (2003) 134–141.

58. Wang, J., Nanoparticle-based electrochemical DNA detection, *Anal. Chim. Acta* **500** (2003) 247–257.

59. Lucarelli, F., Marrazza, G., Turner, A. F., Mascini, M., Carbon and gold electrodes as electrochemical transducers for DNA hybridisation sensors, *Biosens. Bioelectron.* **19** (2004) 515–530.

60. Liepold, P., Wieder, H., Hillebrandt, H., Friebel, A., Hartwich, G., DNA-arrays with electrical detection: A label-free low cost technology for routine use in life sciences and diagnostics, *Bioelectrochem.* **67** (2005) 143–150.

61. Vercoutere, W., Biosensors for DNA sequence detection, *Curr. Opin. Chem. Biol.* **6** (2002) 816–822.

62. Rogers, K. G., Mascini, M., Biosensors for analytical monitoring, *U.S. Environmetal Protection Agency* (2005) www.epa.gov/cgi–bin/epaprintolonly.cgi, 03.11.2005.

63. Blackburn, G. F., Shah, H. P., Kenten, J. H., Leland, J., Kamin, R. A., Link, J., Peterman, J., Powell, M. J., Shah, A., Talley, D. B., Tyagi, S. K., Wilkins, E., Wu, T. G., Massey, R. J., Electrochemiluminescence detection for development of immunoassays and DNA probe assays for clinical diagnostics, *Clin. Chem.* **37** (1991) 1534–1539.

64. Hsueh, Y.-T., Collins, S., Smith, R. L., DNA quantitation with an electrochemiluminescence microcell, *Sens. Actuators B* **49** (1998) 1–4.

65. Miao, W., Bard, A. J., Electrogenerated electrochemiluminescence determination of immobilised DNA and C-reactive protein on Au(111) gold electrodes using tris(2,2')bipyridyl ruthenium(II) labels, *Anal. Chem.* **75** (2003) 5825–5834.

66. Boom, R., Sol, C., Gerrits, Y., Boer, M. D., van Dillen, D. P. W., Highly sensitive assay for detection and quantitation of human cytomegalovirus DNA in serum and plasma by PCR and electrochemiluminescence, *J. Clin. Microbiol.* **37** (1999) 1489–147.

67. Bruno, J., Kiel, J. L., In vitro selection of DNA aptamers to anthrax spores with electrochemiluminescence detection, *Biosens. Bioelectron.* **14** (1999) 457–464.

68. de Jong, M. D., Weel, G. F., Schuurman, T., van Dillen, P. M. E. W., Boom, R., Quantitation of Varicella-Zoster virus DNA in whole blood, plasma, and serum by PCR and electrochemiluminescence, *J. Clin. Microbiol.* **38** (2000) 2568–2573.

69. Zhang, L. T., Schwartz, G., O'Donnel, M., Harrison, R. K., Development of a novel helicase assay using electrochemiluminescence, *Anal. Biochem.* **293** (2001) 31–37.

70. Baeumner, A. J., Humiston, M. C., Montagna, R. A., Durst, R. A., Detection of viable oocysts of Cryptosporidium parvum following nucleic acid sequence based amplification, *Anal. Chem.* **73** (2001) 31176–1180.

71. Bertolino, C., MacSweeney, M., Tobin, J., O'Neill, B., Sheehan, M. M., Coluccia, S., Berney, H., A monolithic silicon based integrated signal generation and detection system for monitoring DNA hybridization, *Biosens. Bioelectron.* **21** (2005) 565–573.

72. Firrao, G., Detection of DNA/DNA hybridization by electrogenerated chemiluminescence, *Int. J. Environ. Anal. Chem.* **85** (2005) 609–612.

73. Kankare, J., Haapakka, K., Kulmala, S., Nanto, V., Eskola, J., Takalo, H., Immunoassay by time-resolved electrogenerated luminescence, *Anal. Chim. Acta* **266** (1992) 205–212.

74. Kulmala, S., Hakansson, M., Spehar, A.-M., Nyman, A., Kankare, J., Loikas, K., Ala-Kleme, T., Eskola, J., Homogeneous and heterogeneous electrochemiluminoimmunoassays of hTSH at disposable oxide-covered aluminum electrodes, *Anal. Chim. Acta* **458** (2002) 271–280.

75. Helin, M., Vare, L., Hakansson, M., Canty, P., Hedman, H. P., Heikkila, L., Ala-Kleme, T., Kankare, J., Kulmala, S., Electrochemiluminoimmunoassay of hTSH at disposable oxide-coated n-silicon electrodes, *J. Electroanal. Chem.* **524** (2002) 176–183.

76. Manz, A., Graber, N., Widmer, H. M., Miniaturized total chemical analysis systems: A novel concept for chemical sensing, *Sens. Actuators B* **1** (1990) 244–248.

77. Duffy, D. C., McDonald, J. C., Shueller, O. J. A., Whitesides, G. M., Rapid prototyping of microfluidic systems in poly(dimethylsiloxane), *Anal. Chem.* **70** (1998) 4974–4984.

78. Terry, S. C., Jerman, J. H., Angel, J. B., A gas chromatographic air analyzer fabricated on a silicon wafer, *IEEE Trans. Electron. Devices* **26** (1979) 1880–1886.

79. Dario, P., Carrozza, M. C., Benvenuto, A., Menciassi, A., Micro-systems in biomedical applications, *J. Microsystems Microeng.* **10** (2000) 235–244.

80. Erickson, D., Li, D., Integrated microfluidic devices, *Anal. Chim. Acta* **507** (2004) 11–26.

81. Kim, J. A., Lee, J. Y., Seong, S., Cha, S. H., Lee, S. H., Kim, J. J., Park, T. H., Fabrication and characterization of PDMS-glass hybrid continuous-flow PCR chip, *Biochem. Eng. J.* **29** (2006) 91–97.

82. Kajiyama, T., Miyahara, Y., Kricka, L. J., Wilding, P., Graves, D. J., Surrey, S., Fortina, P., Genotyping on a themal gradient DNA chip, *Methods* **13** (2003) 467–475.

83. Liu, R. H., Nguyen, T., Schwarzkopf, K., Fuji, H. S., Petrova, A., Siuda, T., Peyvan, K., Bizak, M., Danley, D., McShea, A., Fully integrated miniature device for automated gene expression DNA-microarray processing, *Anal. Chem.* **78** (2006) 1980–1986.

84. Shamansky, L. M., Davis, C. B., Stuart, J. K., Kuhr, W. G., Immobilization and detection of DNA on microfluidic chips, *Talanta* **55** (2001) 909–918.

85. Guijt, R. M., Baltussen, E., van Dedem, G. W. K., Use of bioaffinity interactions in electrokinetically controlled assays on microfabricated devices, *Electrophoresis* **23** (2002) 823–835.

86. Madou, M., *Fundamentals of microfabrication: the science of miniaturisation*, CRC Press, Boca Raton, Florida 1997.

87. Maluf, N., *An introduction to microelectromechanical systems engineering*, Artech House 2000.

88. Franssila, S., *Introduction to microfabrication*, John Wiley & sons 2004.

89. Jorgensen, A. M., Mogensen, K. B., in Microsystem engineering of lab-on-a-chip devices, Wiley-VCH 2004, pp. 117–160.

90. Petersen, D., Telleman, P., in Microsystem engineering of lab-on-a-chip devices, Wiley-VCH 2004, pp. 9–12.

91. El-Ali, J., Perch-Nielsen, I. R., Poulsen, C. R., Bang, D. D., Telleman, P., Wolff, A., Simulations and experimental validation of a SU-8 based PCR thermocycler chip with integrated heaters and temperature sensor, *Sens. Actuators A* **110** (2004) 3–10.

92. Manz, A., Harrison, D., Verpoorte, E., Fettiger, J., Paulus, A., Pauli, H., Widmer, H., Planar chips technology for miniaturization and integration of

separation techniques into monitoring systems - capillary electrophoresis on a chip, *J. Chromatogr.* **593** (1992) 253–258.

93. Harrison, D., Manz, A., Fan, Z., Ludi, H., Widmer, H., Capillary electrophoresis and sample injection systems integrated on a planar glass chip, *Anal. Chem.* **64** (1992) 1926–1932.

94. Harrison, D., Fluri, K., Seiler, K., Fan, Z., Effenhauser, C., Manz, A., Micromachining a miniaturized capillary electrophoresis-based chemical analysis system on a chip, *Science* **261** (1993) 895–897.

95. Becker, H., Locascio, L. E., Polymer microfluidic devices, *Talanta* **56** (2002) 267–287.

96. McDonald, J. C., Duffy, D. C., Anderson, J. R., Chiu, D. T., Wu, H., Schueller, O. J. A., Whitesides, G. M., Fabrication of microfluidic systems in poly(dimethylsiloxane), *Electrophoresis* **21** (2000) 27–40.

3. Hybridization assay on gold electrodes

This chapter describes a hybridization assay utilizing anodic ECL of a synthesized ruthenium label composed of two bipyridine ligands and one phenanthroline ligand for hybridization detection.[1] Probes were immobilized on microfabricated gold electrodes and hybridization was detected using ECL emission of a Ru(II)-labeled oligonucleotide target. An electric field was used for mismatch discrimination.

3.1   Introduction

The most common electrode materials used in electrochemical biosensors are carbon and gold.[2] Carbon is generally considered an excellent material for electrochemical detection of biomolecules because it is less prone to fouling and has a relatively wide potential window in aqueous solutions. However, microfabrication of glassy carbon is still at an early stage of development compared with that of noble metals. In addition, the immobilization properties vary with the different carbon types.

Immobilization of DNA strands on gold can be readily accomplished by incorporation of a functional mercapto group on an oligonucleotide during synthesis. This process is tedious, however, because the modification of DNA is complicated and the yield of mercapto-containing DNA is low.[3,4] Another common way to immobilize biomolecules on gold is via mercapto-carboxylic acids, which in the presence of carbodiimides can form amide bond with an amino group present in a biomolecule. The most common carbodiimide is 1-(3-(dimethylamino)propyl)-3-ethylcarbodiimide hydrochloride (EDC), which is widely used for the conjugation of biological substances. It catalyzes the formation of amide bonds between carboxylic acids or phosphates and amines by activating carboxyl or phosphate group to form an O-acylisourea derivative, which then rapidly reacts with pri-

mary amines.[5] Covalent immobilization of amino-modified oligonucleotides and proteins is achieved in this way. N-Hydroxysuccinimide (NHS) is frequently added to the EDC solution, resulting in the formation of an intermediate active ester, which then reacts with amine. Thus the final product is the same, but the intermediate is more stable and the reaction yield is usually higher.[5]

Theoretical calculations have shown that the electrostatic surface effects can influence immobilization and hybridization kinetics of DNA strands, as well as the stability of the formed duplex.[6] In practice, it has been shown that, hybridization kinetics of long DNA strands (157-864 bases) with short probes immobilized on indium tin oxide electrodes was considerably faster upon application of low voltage of 200 mV between the electrodes.[7] A positive potential of +300 mV *vs.* Ag/AgCl has been reported to increase immobilization kinetics of thiolated oligonucleotides on gold electrodes,[8–10] while negative potential of -300 mV *vs.* Ag/AgCl was reported to cause denaturing of hybridized mismatched strand while leaving complementary duplexes intact.[9] Common to the above mentioned examples is that the applied electric field is so low that only non-Faradaic currents are induced. In an approach described by Sosnowski *et al.*[11] electric current pulses were applied on hybridized strands. Single base mismatch discrimination was achieved in DNA duplexes over length of 6 to 27 nucleotides. In order to protect DNA from unwanted electrochemical side reactions that electric current might induce, such as local pH change and possible radical formation, the immobilization was performed on a 1 μm thick agarose gel layer previously deposited on the electrodes.

3.2 Experimental section

3.2.1 Chemicals and materials

The 15-base oligonucleotides having C_6 linker and amino-modification at the 5' end were purchased from MicroSynth, Switzerland. An oligonucleotide probe of

sequence 5'-NH$_2$ - TTGCTAAGGATCATT-3' was used. Targets were a complementary target, 5'-NH$_2$ - AATGATCCTTAGCAA-3' and a mismatched target, 5'-NH$_2$ - AATGAT**T**CT**G**AGCAA-3', with two base mismatches (indicated in bold). Sodium dihydrogen phosphate monohydrate, disodium hydrogen phosphate dihydrate, sodium tetraborate decahydrate, potassium chloride, tris(hydroxymethyl) aminomethane (Tris), dimethylsulfoxide (DMSO), dimethylformamide (DMF), magnesium chloride hexahydrate, sodium dodecyl sulfate (SDS), cetyltrimethylammonium bromide (CTAB), glycine (mixture of L- and D-isomers), n-tripropyl-amine (TPA), 3-mercaptopropanoic acid (3-MPA), 16-mercaptohexadecanoic acid (16-MHA), 90%, 1-ethyl-3-(3-dimethylaminopropyl) carbodiimide hydrochloride (EDC), N-hydroxysuccinimide (NHS), 1-methylimidazole, hexamineruthenium(III) chloride (RuHex), thiophosgene, calcium carbonate, and ammonium hexafluorophosphate were all acquired from Sigma-Aldrich, Switzerland. Ruthenium trichloride, 99%, 2,2'-bipyridyl, lithium chloride, tin dichloride dihydrate, 5-amino-1,10-phenanthroline were obtained from Acros, Switzerland and ethanol (0.2% H$_2$O) from Merck, Switzerland. AZ 1518 photoresist was product of Clariant, and Dow Corning poly(dimethylsiloxane) (PDMS) kit Sylgard 184 was from Distrelec, Switzerland.

3.2.2 Synthesis of Ru(II)-1 and Ru(II)-2

Bis(2,2'-bipyridine)-5-amino-1,10-phenanthroline ruthenium (II) (Ru(II)-**1**) was synthesized according to previously published procedures.[12–14] Briefly, bipyridine and tri-chlororuthenium were heated and refluxed during three hours in DMF. After solvent evaporation, the mixture was crystallized at 0 ℃ with acetone, refluxed with water-ethanol solution, and treated with lithium chloride. The resulting compound was refluxed with 5-amino-1,10 phenanthroline in the ethanol-water solution for 3 hours. After ethanol was evaporated hexafluorophosphate ammonium salt was added. The resulting yellow Ru(II)-**1** compound was purified with column chromatography. Finally, the amino group of Ru(II)-**1** was converted to the active isothiocyanato group of Ru(II)-**2** compound with thiophosgene in the presence of calcium carbonate and dry acetone.

3.2.3 Ruthenium labeling of oligonucleotides

Oligonucleotides were labeled according to a slightly modified procedure of Molecular probes.[15] Briefly, prior to labeling, oligonucleotides were purified by chloroform extraction and precipitated with ethanol. Then amino-modified oligonucleotides were dissolved in 100 mM tetraborate buffer, pH 8.5, to obtain a concentration of 250 μM. Ru(II)-**2** was dissolved in a small volume of DMSO and added to the oligonucleotide solution at 30-fold excess concentration with respect to the oligonucleotides. This mixture was gently shaken in the dark during six hours. Labeled oligonucleotides were precipitated by addition of 3 M NaCl and cold absolute ethanol in a volume ratio of 0.1:2.5 with respect to the oligonucleotide solution. The mixture was kept 30 min at -20 ℃ and then centrifuged 30 min at 12 000 rpm. The supernatant was removed and the pellet was rinsed twice with cold 70% ethanol. Labeled oligonucleotides were allowed to dry in air for 10 min, and stored at -20 ℃ until use.

3.2.4 Instrumentation and methods

The concentrations of probe and labeled oligonucleotides were determined by UV-VIS measurements, performed in 50 mM tetraborate buffer, pH 7.8, using a Hewlett-Packard 8453 spectrophotometer. The cyclic voltammograms were recorded using an Autolab PGSTAT12 (Eco chemi) potentiostat in three-electrode mode against a silver pseudoreference electrode on chip made by placing a droplet of silver conductive glue on a gold electrode.[16] Cyclic voltammograms were measured in 10 mM tris buffer, pH 7.0, sweeping potential first in the negative direction. The ECL potential was generated with a PAR 273 potentiostat and the signal was recorded with a PMT tube (Hamamatsu H5701-50, Switzerland) through an optical filter with a bandwidth 600 $\pm$ 80 nm, which was controlled with a lab-written Labview program collecting data points at a frequency of 8 Hz. A voltage of -950 V was supplied to the PMT using a lab-built high-voltage power supply. ECL measurements were performed in 300 mM phosphate buffer,

pH 7.8, containing 100 mM TPA and 0.1% SDS. The ECL signal was generated by stepping the potential from 0 to 1.15 V for a pulse period of 300 ms and stepping back to 0 V. Denaturing experiments using electric field were done in 30 mM phosphate buffer, pH 7.0. All measurements were performed at room temperature.

3.2.5   Preparation of oligonucleotide-modified gold electrodes

Gold electrodes were microfabricated by a lift-off process on Pyrex or silicon wafers as described in Chapter 2, and the electrode surface area was defined by PECVD Si_xN_y opening. The diameters of the working electrodes were 100 μm, 300 μm, and 500 μm, respectively. While all three working electrodes were used for preliminary experiments and optimization, all results reported in this chapter were obtained on the 500 μm electrode. A reservoir was made by pinching a hole of a diameter around 3 mm in a PDMS layer, which was then reversibly sealed about electrodes. Figure 3.1 shows a prepared gold chip with three working electrodes, an integrated silver pseudoreference electrode, and a counter electrode.

Before immobilization, the electrodes were cleaned in 30% sulfuric acid containing 5% hydrogen peroxide for 10 min, rinsed with copious amounts of water and dried under a stream of nitrogen. Self-assembled monolayers of 3-MPA and 16-MHA thiols were formed during one hour from 1 mM solution prepared in absolute ethanol. After soaking in thiol solution, the electrodes were cleaned with ethanol and water and dried in a stream of nitrogen. The amino-modified oligonucleotides were immobilized on SAM covered electrodes via EDC/NHS coupling,[5] which leads to a covalent bond between surface carboxylic acid and amino-terminal of the oligonucleotide. The oligonucleotides were dissolved in 100 mM 1-methylimidazole buffer, pH 7, containing 100 mM of $MgCl_2$ x 6 H_2O into which, prior to immobilization, freshly prepared EDC and NHS were added to obtain concentrations of 100 mM and 75 mM, respectively. Then 10 μL of oligonucleotide solution was carefully pipetted and dispensed on the three working electrodes,
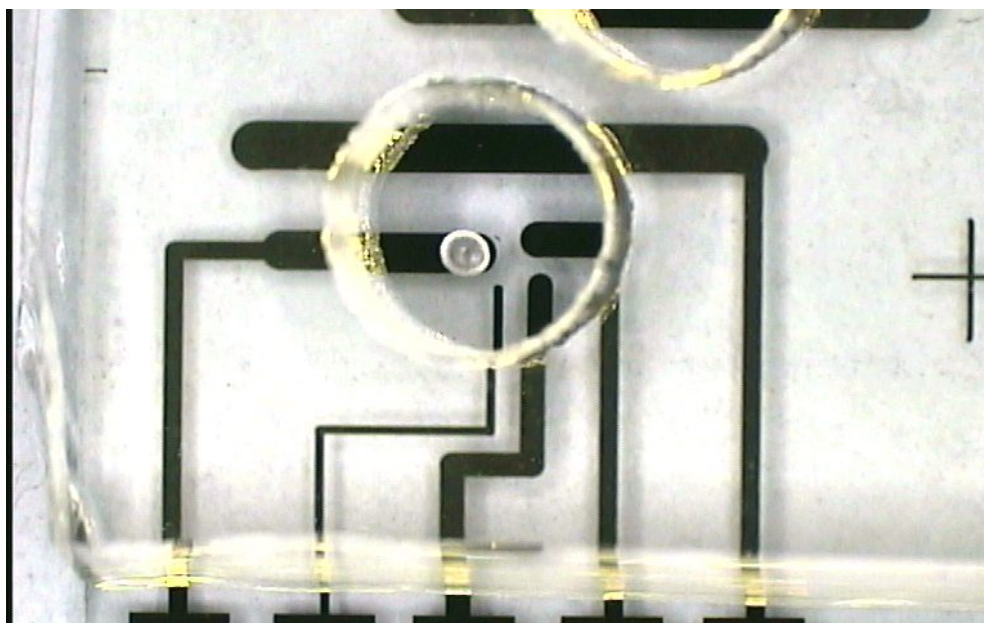
Figure 3.1: Gold chip used for heterogeneous ECL assay. The volume of the PDMS reservoir is about 30 µL. The diameter of the largest electrode is 500 µm, that of the medium 300 µm, and that of the smallest 100 µm. Silver pseudo-reference electrode was made by placing a droplet of silver glue on a gold electrode and curing it at 120 ℃ during two hours (left).

taking care not to cover the reference and counter electrodes, and left for three hours in a humid chamber. Noncovalently attached probes were washed away with ethanol and water and the chips were dried in a nitrogen stream.

3.2.6 Hybridization

After probe immobilization, unreacted EDC/NHS groups were deactivated by treating the electrodes with a 30 mM phosphate buffer containing 10 mM glycine and 0.2% SDS for 30 min. Then the surface was blocked by treatment with 35 µg/mL of single stranded calf thymus DNA for 10 min. Labeled complementary and mismatched strands were dispensed on working electrode and allowed to be incubated for two hours. Hybridization was performed in 30 mM phosphate buffer, pH 7.5, containing 100 mM $MgCl_2$ x 6 H_2O.

3.3 Results and discussion

3.3.1 Spectroscopic properties of the labeled compounds

Figure 3.2 shows the UV/VIS absorption spectra of Ru(II)-**1** solution (a), unlabeled 15-base oligonucleotide (b), and Ru(II)-labeled 15-base oligonuleotide (c) measured in 50 mM tetraborate buffer, pH 7.8. As can be seen in Figure 3.2, the synthesized Ru(II) complex exhibits a metal-to-ligand charge transfer peak (MLCT) at 455 nm, as well as absorption peaks at $\approx$ 285 nm and $\approx$ 249 nm, comparable to the Ru(bpy)$_3^{2+}$ complex.

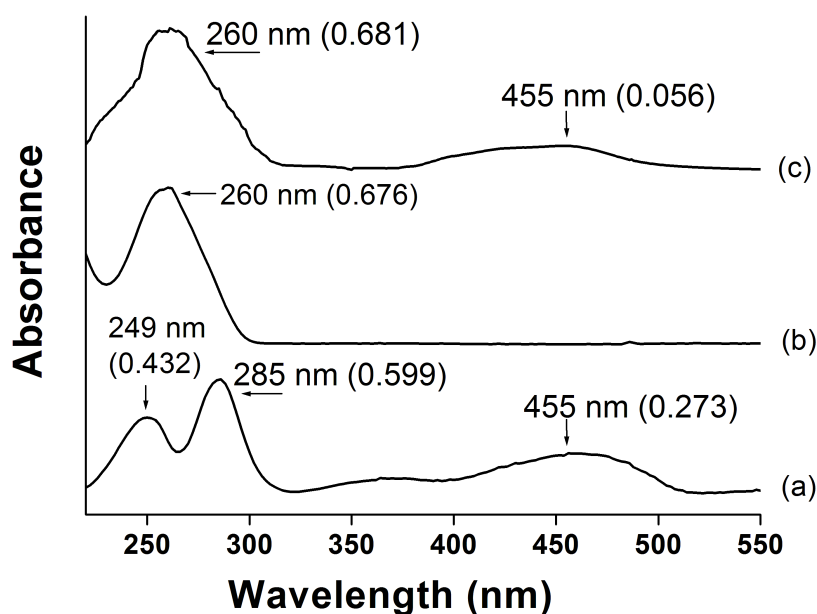**Figure 3.2:** UV-VIS spectra of Ru(II)-**1** complex (a), unlabeled probe (b), and labeled complex (c). Spectra were measured using quartz cuvette with an optical path length of 1 cm in 50 mM tetraborate buffer, pH 7.8.

These absorption peaks could be attributed to LC $\pi \to \pi^*$ transitions and $d \to \pi^*$ transitions, respectively[17]. The concentration of unlabeled probe was determined

49

from the absorbance peak at 260 nm using the absorption coefficient value given by the oligonucleotide provider. The spectrum of the labeled oligonucleotide exhibits a characteristic peak at 260 nm, with Ru(II) peaks at 285 nm and 249 nm overlaid, and a MLCT peak centered at 455 nm. From the absorbance spectra it can be deduced that the labeling efficiency was 100%.

3.3.2 Optimization of ECL conditions

The anodic ECL is highly dependent on pH, applied voltage, and presence and type of surfactants. We first measured the ECL signal in 300 mM phosphate buffer containing 100 mM TPA, pH 7.8, because we previously found this buffer suitable for the Ru(bpy)$_3^{2+}$ ECL generation.[16]
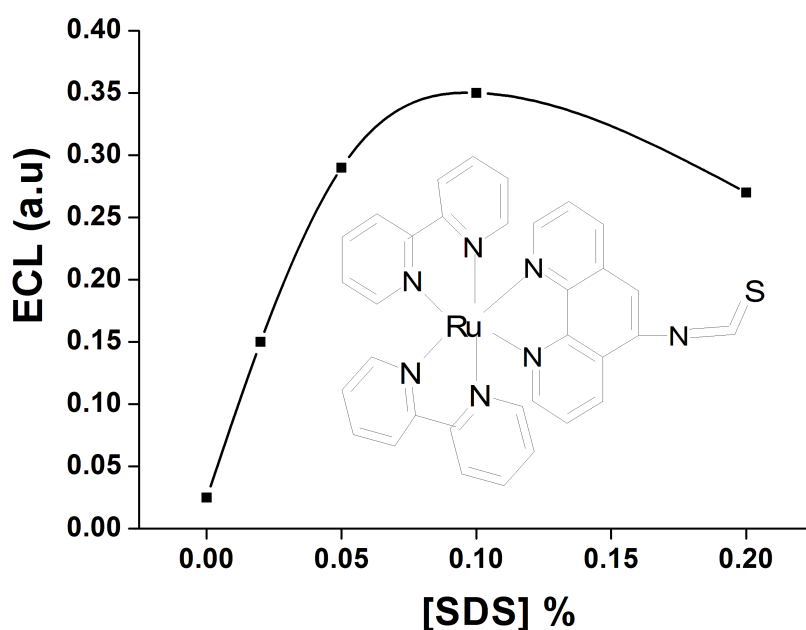

Figure 3.3: ECL efficiency versus concentration of SDS, measured by application of potential of 1.15 V *vs.* Ag pseudoreference electrode during 300 ms. Measurements were performed on the 500 μm diameter electrode. The inset shows the molecular structure of the Ru(II)-**2** label.

The signal was very weak (see Figure 3.3). The influence of surfactants was therefore investigated, the anionic surfactant sodium dodecyl sulfate (SDS)and that of the cationic surfactant cetyltrimethylammonium bromide (CTAB). Addition of SDS strongly increased the ECL intensity, with intensity maximum in the presence of 0.1% SDS, while further increase of the surfactant concentration caused a slight weakening of the signal. CTAB also increased the signal but less than SDS. Further optimization experiments and the measurements on DNA-modified electrodes were therefore done in the presence of 0.1% SDS.
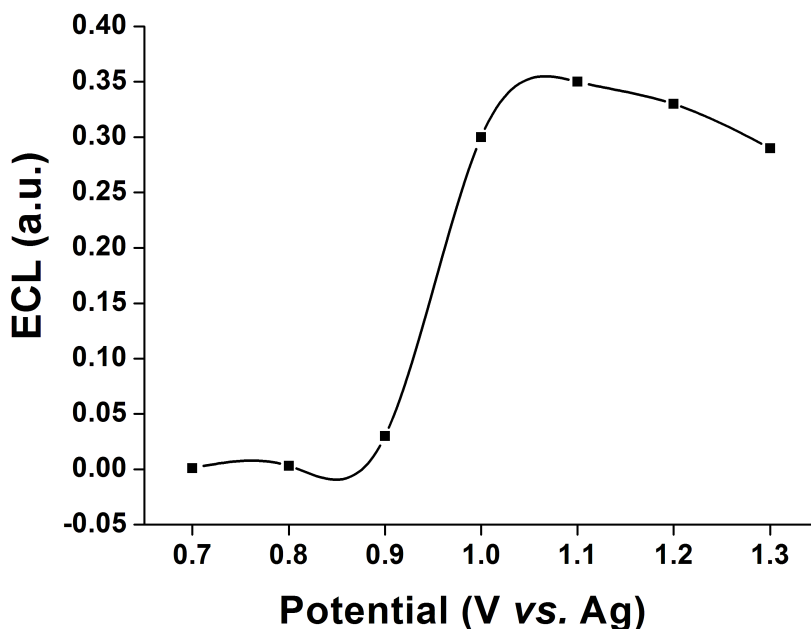
Figure 3.4: ECL intensity as a function of applied potential in the presence 0.1% SDS *vs.* an Ag pseudoreference electrode. Measurement conditions as in Figure 3.3.

The optimal potential for the ECL generation was found by recording a cyclic voltammogram (CV) at 50 mV/s from 0 to 1.3 V. The maximum ECL signal was obtained at 1.15 V *vs.* an Ag pseudoreference electrode integrated on the chip (Figure 3.4). This potential was subsequently used for the ECL detection on DNA-modified electrodes.

3.3.3   Voltammetric characterization of the modified surface

Voltammetry is a common method for the characterization of modified electrodes. RuHex ($Ru(NH_3)_6^{3+}$) binds electrostatically to DNA strands due to the negatively charged phosphate backbone and has previously been used for surface coverage determinations of thiolated oligonucleotides on gold.[18,19] With a view to these studies we chose RuHex for surface characterization. The 3-MPA and 16-MHA SAMs were formed on a series of chips under identical conditions, as is described above in the Experimental section. The presence of Mg^{2+} ions in the immobilization buffer is known to produce more densely packed probe films due to the decreased electrostatic repulsion between adjacent DNA strands.[20] Figure 3.5 shows cyclic voltammograms obtained on unmodified clean gold, 16-MHA thiolated gold, the ester covered gold (EDC/NHS treatment), and DNA-modified gold surface. Voltammograms on two types of monolayers are very similar; there was no detectable difference in monolayer formation or probe immobilization efficiency.

As can be seen in Figure 3.5, voltammograms obtained on unmodified and on ester (EDC/NHS treatment) covered gold are very similar while the reduction peak on the SAM-covered surface is less pronounced and the oxidation and reduction peaks are shifted. The immobilization of DNA strands clearly increases the size of the reduction and oxidation peaks of CV. This is due to the accumulation of RuHex at the electrode surface upon binding to the oligonucleotide strands. As can be noticed, the reduction peak is considerably more pronounced compared to the oxidation peak. Previously RuHex voltammograms have been shown on similarly prepared surface, where the reduction peak of RuHex decreased upon DNA immobilization.[4] A probable explanation for this difference in our and the earlier results is that we immobilized DNA strands with their 5' end, and thus we expect them to be in an upright position. In the other case, amino groups present in the DNA strand were used to achieve immobilization, resulting in a longitudinal positioning of DNA with respect to the surface. No difference in peak splitting was observed upon surface treatment, $\Delta E_p \approx 100$ mV, in all cases. To calculate
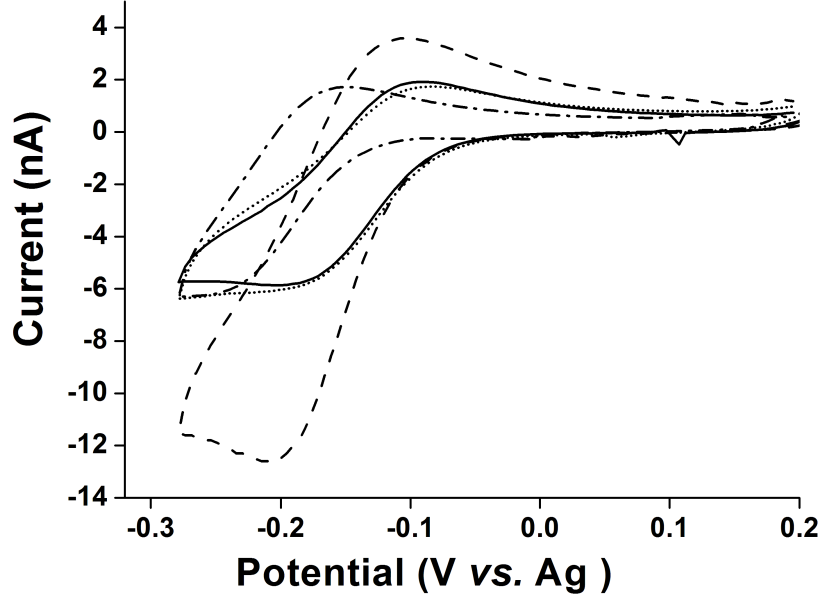
Figure 3.5: Cyclic voltammograms of 20 μM RuHex solution in 10 mM tris buffer pH 7.0, obtained at bare gold electrodes (dash-dot curve), at a 16-MHA modified electrode (solid curve), at a 16-MHA/EDC/NHS modified electrode (dotted curve) and at 16-MHA/EDC/NHS/DNA electrode (dashed curve), treated with 1 μM probe solution. Sweep rate is 50 mV/s.

the surface coverage, we integrated the right-side half of the reduction peak of the oligonucleotide-modified surfaces, subtracted the area of the voltammograms in the absence of DNA, multiplied the resulting area by two, and calculated probe density using the following equations:[19]

$$\Gamma_{Ru} = \frac{Q}{nFA} \tag{3.1}$$

$$\Gamma_{DNA} = \Gamma_{Ru}\frac{z}{m}N_A \tag{3.2}$$

where Γ_{Ru} is the surface saturation of RuHex, Q is charge, n is the number of electrons transferred in the reaction, F is the Faraday constant, A is the electrode

53

surface area, Γ_{DNA} is probe coverage, z is charge of RuHex, m is number of nucleotides in a DNA strand, and N_A is the Avogadro constant. The value obtained for the surface coverage upon treatment with 1 μM probe solution is about 9 x 10^{12} molecules/cm^2 (dashed curve voltammogram in Figure 3.5), which is within typical surface coverage range of DNA probes (10^{11} - 10^{13} molecules/cm^2).[18,21] That our SAM formation and probe immobilization were successful is shown by i) the difference in voltammograms upon surface treatment with mercaptocarboxylic acid and probe solution, ii) the increase in reduction current of RuHex upon surface treatment with increasing concentrations of probe solution, and iii) the stabilization of reductive current at probe concentration of 600 nM and higher. This indicates saturation of available probe binding sites.

3.3.4   ECL on DNA-modified electrodes

Figure 3.6 shows the results of ECL assays obtained on a series of chips modified with different probe concentrations (0, 10 pM, 100 pM, 1 nM, 10 nM, 50 nM, 100 nM, 500 nM and 1 μM) and incubated with a constant concentration (1 μM) of labeled complementary and mismatched target. After the incubation time of two hours, chips were washed with 30 mM phosphate buffer, pH 7.0, containing 0.2% SDS, and heated to about 38 ℃. As can be seen from Figure 3.6, the ECL results obtained on 3-MPA and 16-MHA surfaces were closely similar, only about 10% higher on the 3-MPA surface than the 16-MHA surface. The difference is probably due to the shorter distance between the label moiety and the electrode surface.

The negative controls and the chips derivatized with probe solution of 10 pM generated comparable intensity, indicating that the non-specific adsorption is very low. Evidently the surface treatment and washings were sufficient to prevent non-specific adsorption. In all cases, the ECL intensity peaked at probe concentration of 100 nM. From that we can conclude that the optimal surface coverage and hence, the most efficient hybridization was achieved at this probe concentration.
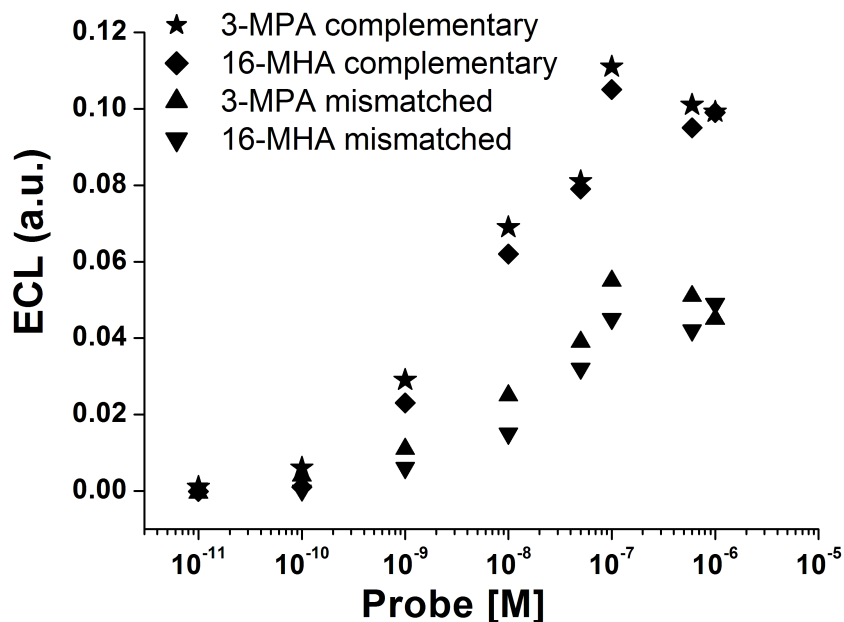
Figure 3.6: ECL calibration curves obtained upon hybridization on 3-MPA and 16-MHA monolayers. ECL was generated by stepping potential from 0 to 1.15 V vs Ag pseudoreference for a pulse period of 300 ms. Signal was recorded using PMT through an optical filter of bandwidth 600 ± 80 nm. Measurement buffer was 300 mM phosphate, 100 mM TPA and 0.1% SDS, pH 7.8.

Peterson *et al.*[8] have shown that at higher probe densities hybridization efficiency decreases due to the steric hindrance and electrostatic repulsion caused by the immobilized probes. Signals obtained from mismatched duplexes were considerably lower (approximately 50%) than those obtained with the complementary duplexes.

Gold-thiol bond is unstable at high voltages, so to minimize thiol desorption we used a short pulse time of 300 ms for the ECL generation. Under these conditions, the oligonucleotides immobilized on the 3-MPA surface gave stronger signals, however, signals obtained from 16-MHA monolayer were more repeatable. One very important difference between the two types of monolayers was found during the course of the work. Longer thiols were more resistant to the high positive poten-

tial needed for the ECL generation, probably because longer alkanethiol chains adsorb better than the shorter ones and are better organized.[22] The optimal potential for ECL generation in our case was 1.15 V *vs.* Ag pseudoreference on a chip. On 16-MHA monolayer the ECL signals could be measured many tens of times, with washing in between without decrease of the signal, demonstrating that the formed monolayer was stable. To be sure, new monolayers were nevertheless formed for all assay experiments for caution. The experiments testing electric field denaturing were performed only on 16-MHA formed SAMs.

3.3.5 Effect of the applied electric field

As can be seen from Figure 3.6, mismatch discrimination was achieved by careful electrode washing. However, we were interested to know whether the selectivity could be improved using an electric field. The possibility to control surface potential of the immobilization platform and thus the processes occurring on the surface is of particular interest when work is done on electrodes, rather than nonconductive surfaces.

A set of DNA chips was incubated with different concentrations of complementary and mismatched Ru(II)-labeled strands and allowed to hybridize in passive conditions during three hours. After washing of the chips with denaturing buffer (30 mM phosphate buffer, pH 7.0), the ECL signal of the electrodes was recorded in the ECL buffer. Denaturing buffer was then placed into the reservoir, and negative potential of -300 mV *vs.* Ag pseudoreference electrode was applied twice, for 150 s each time. The ECL signal was always recorded in ECL buffer. The negative electrode potential of -300 mV *vs.* Ag pseudoreference electrode was used as electrochemical side reactions, such as electrolysis of water or damage to DNA do not take place at this potential.[7,9] This is a very important point, because the distance of the oligonucleotides from the electrode surface is only about 2-3 nm (d(C-C) = 0.14 nm[23]), and electrode potential of -300 mV causes a field gradient on the order of 10^8 V/m. Electrostatic surface conditions do are known
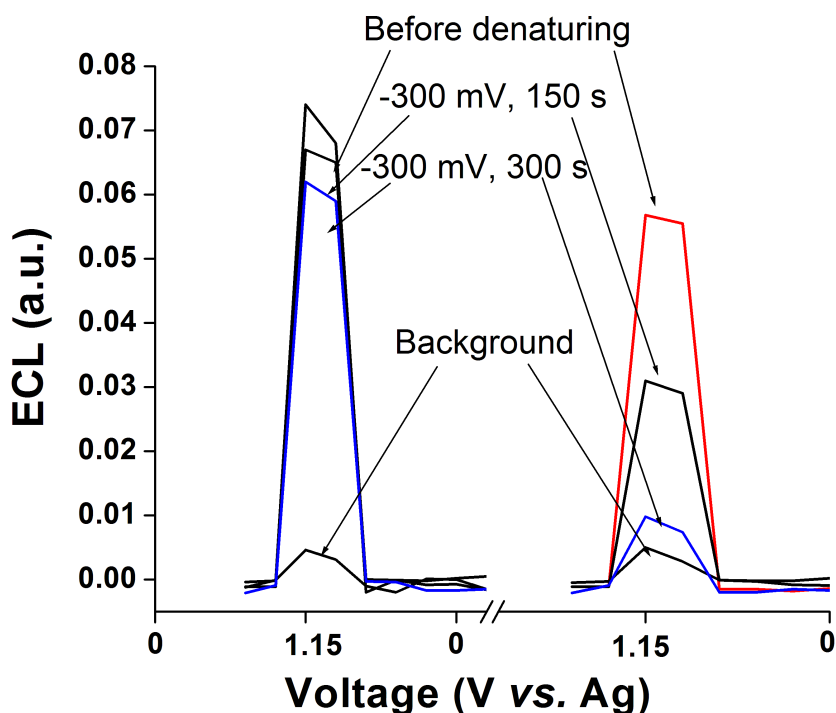
Figure 3.7: ECL signal of complementary duplex (left) and mismatched duplex (right), prior and after application of negative potential on the electrode for indicated time. ECL measurements were done as described in Figure 3.5, while negative electrode potential was applied in denaturing buffer (30 mM phosphate, pH 7.0).

to influence the stability of a formed duplex, and the distance up to which surface conditions do influence surface-bound species strongly depends on ionic strength of the solution.[6] Thus, application of negative electrode potential is expected to destabilize the formed duplex, the mismatched more than the matched, and the effect is expected to be more pronounced in solutions of lower ionic strength. If this is so, it could explain why we did not observe denaturing of the mismatched duplex in the ECL buffer. However, the influence of the surfactant (0.1% SDS) was not investigated and cannot be ruled out.

Figure 3.7 shows electrochemiluminograms obtained using complementary duplexes (left) and mismatched duplexes (right) upon application of negative elec-

trode potential of -300 mV for 150 s. As can be seen, upon application of the potential of -300 mV *vs.* Ag pseudoreference, the ECL signal of the complementary duplex remained unchanged, while the signal of the mismatched strand decreased by approximately 50%. Further application of the negative potential slightly decreased the ECL signal of the complementary strand, while the signal from the mismatched strand decreased close to the background level. The same experiment was performed in the ECL buffer, but no denaturing was observed for either the complementary nor the mismatched duplex.
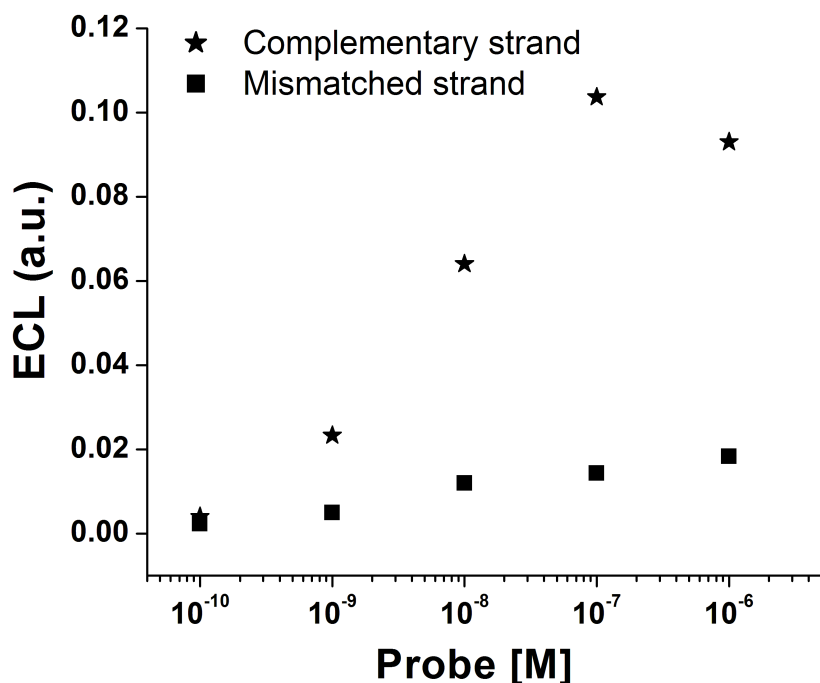
Figure 3.8: Calibration plot on Au-chip measured with immobilized probes using electrical denaturing. Denaturing using negative potential of -300 mV during 300 s caused mismatched target to dehybridize while matched hybrid gave good signal. ECL conditions as in Figure 3.7.

Figure 3.8 presents the calibration curve obtained on DNA-modified electrodes using denaturing voltage of -300 mV for 300 s before the ECL measurement. The results show that, through control of the electrode potential, successful discrimination can be achieved between mismatched and perfect complementary strand.

Comparison of Figures 3.6 and 3.8 reveals that better mismatch discrimination results is obtained by electric field-aided denaturing compared to washing, For example, for concentration of 10 nM of probe solution, the hybridization result for mismatched strand after washing is about 40%, whereas after electrostatic denaturing only about 20% of the complementary strand. A strong appeal the mismatch discrimination achieved by control of the electrode potential at room temperature, as compared with extensive washing, is the relative simplicity of the approach.

3.4   Conclusions

Synthesized ruthenium complex exhibited high ECL intensity in the presence of 0.1% anionic surfactant SDS and potential of 1.15 V *vs.* Ag pseudoreference electrode. Microfabricated gold electrodes were derivatized with 15-mer, 5' amino-modified oligonucleotides using mercaptocarboxylic acid SAM, and EDC/NHS coupling. Two different SAMs, 3-MPA and 16-MHA, were studied. The performance in terms of immobilization was very similar, but the 16-MHA SAM was more stable. Ru(II)-labeled complementary strands were detected down to a picomolar concentration, corresponding to a total amount of one fmol. Two base pair mismatch discrimination was achieved with and without application of an electrode potential; however, mismatched discrimination was considerably better when negative electrode potential of -300 mV *vs.* Ag pseudoreference was applied for 300 s before the ECL detection.

References

1. Spehar-Deleze, A.-M., Schmidt, L., Neier, R., Kulmala, S., de Rooij, N., Koudelka-Hep, M., Electrochemiluminescent hybridization chip with electric field aided mismatch discrimination, *Biosens. Bioelectron.* *doi:10.1016/J.bios.2006.02.013* .

2. Lucarelli, F., Marrazza, G., Turner, A. F., Mascini, M., Carbon and gold electrodes as electrochemical transducers for DNA hybridisation sensors, *Biosens. Bioelectron.* **19** (2004) 515–530.

3. Ge, C., Liao, J., Yu, W., Gu, N., Electric potential control of DNA immobilization on gold electrode, *Biosens. Bioelectron.* **18** (2003) 53–58.

4. Huang, E., Zhou, F., Deng, L., Studies of surface-coverage and orientation of DNA molecules immobilized onto preformed alkanethoil self-assembled monolayers, *Langmuir* **16** (2000) 3272–3280.

5. Hermanson, G. T., Bioconjugate techniques, Academic press 1996, pp. 169–176.

6. Vainrub, A., Pettitt, B. M., Surface electrostatic effects in oligonucleotide microarrays: Control and optimization of binding thermodynamics, *Biopolymers* **68** (2003) 265–270.

7. Su, H.-J., Surrey, S., McKenzie, S. E., Fortina, P., Graves, D. J., Kinetics of heterogeneous hybridization on indium tin oxide surfaces with and without an applied potential, *Electrophoresis* **23** (2002) 1551–1557.

8. Peterson, A. W., Heaton, R. J., Georgiadis, R. M., The effect of surface probe density on DNA hybridization, *Nucleic Acids Research* **29** (2001) 5163–5168.

9. Heaton, R. J., Peterson, A. W., Georgiadis, R. M., Electrostatic surface plasmon resonance: Direct electric field-induced hybridization and denaturation in monolayer nucleic acid films and label-free discrimination of base mismatches, *Proc. Natl. Acad. Sci.* **98** (2001) 3701–3704.

10. Swami, N. S., Chou, C.-F., Terberueggen, R., Two-potential electrochem. probe for study of DNA immobilization, *Langmuir* **21** (2005) 1937–1941.

11. Sosnowski, R. G., Tu, E., Butler, W. F., O'Connell, J. P., Heller, M. J., Rapid determination of single base mismatch mutations in DNA hybrids by direct electric field control, *Proc. Natl. Acad. Sci.* **94** (1997) 1119–1123.

12. Sprintschnik, G., Sprintschnik, H. W., Kirsch, P. P., Whitten, D. G., Photochemical reactions in organized monolayer assembiles. 6. Preparation and photochemical reactivity of surfactant ruthenium(II) complexes in monolayer assembiles and at water-solid interfaces, *J. Am. Chem. Soc.* **99** (1977) 4947–4954.

13. Garcia-Fresnadillo, D., Orellana, G., Interaction of sulfonated ruthenium polypyridine complexes with surfactants probed by luminescence spectroscopy, *Helvetica Chim. Acta* **84** (2001) 2708–2730.

14. Youn, H., Terpetschnig, E., Szmacinski, H., Lakowitz, J. R., Fluorescence energy transfer immunoassay based on a long-lifetime luminescent metal-ligand complex, *Anal. Biochem.* **232** (1995) 24–30.

15. Molecular probes, Eugene, USA, *Amine-reactive probes* (2003), mP00143.

16. Spehar, A.-M., Koster, S., Kulmala, S., Verpoorte, E., de Rooij, N., Koudelka-Hep, M., The quenching of electrochemiluminescence upon oligonucleotide hybridization, *Luminescence* **19** (2004) 287–295.

17. Juris, A., Balzani, V., Barigelletti, F., Campagna, S., Belser, P., von Zelewsky, A., Ru(II) polypyridine complexes: photophysics, photochemistry, electrochemistry and chemiluminescence, *Coord. Chem. Rev.* **84** (1988) 85–277.

18. Steel, A. B., Herne, T. M., Tarlov, M. J., Electrochemical quantification of DNA immobilized on gold, *Anal. Chem.* **70** (1998) 4670–4677.

19. Yu, H.-Z., Luo, C.-Y., Sankar, C. G., Sen, D., Voltammetric procedure for examining DNA-modified surfaces: Quantitation, cationic binding activity and electron–transfer kinetics, *Anal. Chem.* **75** (2003) 3902–3907.

20. Boon, E. M., Salas, J. E., Barton, J. K., An electrical probe of protein-DNA interactions on DNA-modified surfaces, *Nature Biotechnol.* **20** (2002) 282–286.

21. Gooding, J. J., Electrochemical DNA hybridization biosensors, *Electroanalysis* **14** (2002) 1149–1156.

22. Rowe, G. K., Creager, S. E., Chain length and solvent effects on competitive self-assembly of ferrocenylhexanethiol and 1 -alkanethiols onto gold, *Langmuir* **10** (1994) 1186–1192.

23. Sutton, L. E., Table of interatomic distances and configuration in molecules and ions, Chemical Society, London, UK 1965, pp. 1956–1959.

4. HECL of rhodamine and application in hybridization assay

Chapter 4 investigates the mechanism and characteristics of HECL of rhodamine B (RhB) on oxide-coated aluminum electrodes.[1] Upon optimization of the light-generating conditions, a heterogeneous oligonucleotide hybridization assay was performed utilizing oligonucleotides labeled with rhodamine derivative as HECL luminophore.[2] Thin oxide film-coated aluminum and silicon electrodes were used as the immobilization platform.

4.1 Introduction

Rhodamine compounds belong to a group of xanthene dyes and are widely used in analytical chemistry, for example as active medium of dye lasers,[3,4] and in bio-analytical chemistry.[5,6] Rhodamine B is excited by visible light of 560 nm, it has a molar extinction coefficient of 88 000 M^{-1} cm^{-1}, and a photoluminescence (PL) quantum yield close to unity. In chemiluminescence systems, rhodamine dyes are mainly used as sensitizers.[7] TAMRA (tetramethylrhodamine), one of the most common rhodamine derivative, and it is widely used as a label in fluorescence-based bioassays[8] and as an acceptor in luminescence resonance energy transfer based assays.[9]

Radiochemiluminescence (RCL) is one of the least studied forms of luminescence, but some 40 years ago it was observed that RhB produces RCL under steady X-ray irradiation in an aqueous solution.[10,11] Later RCL of RhB was studied using pulse radiolysis with 2 μs, 4-MeV electron pulses.[12] During and after the electron pulse, one-electron reduced and oxidized radical forms of RhB ($RhB_{red}^{\cdot}$ and $RhB_{ox}^{\cdot}$) were observed, produced by the primary species of the radiolysis of water, namely hydrated electrons and hydroxyl radicals. The oxidation of $RhB_{red}^{\cdot}$ by hydroxyl radical and the reduction of $RhB_{ox}^{\cdot}$ by hydrated electron were

assumed to be sources of the excited species RhB*. The excitation by electron pulses appeared to be about a thousand times more efficient than the fluorescence induced by 24-keV x-rays at the same concentration of dye.[12] The RCL lifetime after the electron pulse was in the order of some tens of the microseconds but could be made much longer by addition of some hydroxyl radical scavengers such as halide ions. At pH 10 the absolute quantum yield for the reaction

$$RhB^{\cdot}{}_{ox} + e_{aq}^{-} \rightarrow RhB^{*} \qquad (4.1)$$

was determined to be 0.018.[13]

It has been proposed that hot electrons are injected into the conduction band of water during a high-amplitude pulse polarization of thin insulating film-covered silicon and aluminum electrodes.[14,15] Upon contact with an electrolyte solution, the injected hot electrons are thermalized and solvated, which leads to the generation of hydrated electrons. These electrons are capable of generating highly oxidizing species from suitable precursors, such as peroxidisulfate ions, hydrogen peroxide, or molecular oxygen.[15,16] Thus, species with very different redox properties can be reduced simultaneously.

Controlled immobilization of oligonucleotides requires the addition of an anchoring functional group during synthesis, typically amino or thiol groups. The most common approach for the oligonucleotide immobilization is introduction of an amino functionality onto a solid support. Self-assembled aminosilane films have been deposited on a wide variety of hydroxylated surfaces, including glass,[17–19] silicon dioxide,[20–22] silicon nitride,[23] indium tin oxide,[24] and aluminum oxide.[25,26] The requirement for silane deposition is the presence of OH-groups on the surface, which allows the formation of Si-O bond between the surface oxygen and silicon in the silanization reagent.

4.2   Experimental

4.2.1   Chemicals and materials

Sodium tetraborate decahydrate, sodium azide, sodium nitrate, sodium nitrite, hydrogen peroxide, sodium iodine, sodium bromide, potassium phosphate buffer (pH 7.5), ethanol ($\leq$0.2% H_2O), and methanol (hypergrade for liquid chromatography) were obtained from Merck. Rhodamine B, pyridine, aminopropyltriethoxysilane (APTES), N-(2-aminoethyl)-3-aminopropyltrimethoxysilane (EDA), 1,4-phenylene diisothiocyanate (PDC), L-glycine, sodium dodecyl sulfate (SDS), N,N-dimethylformamide (DMF) and dimethylsulfoxide (DMSO) were acquired from Sigma-Aldrich. Succinimidyl ester of 5-(and 6-)-carboxytetramethylrhodamine (TAMRA) was a product of Molecular Probes. The same sequences of amino-modified oligonucleotides were used as described in Chapter 3, but additionally a noncomplementary sequence 5'-NH_2-AAAAAAAAAAAAAAA-3' was used. The abbreviations used for the labeled oligonucleotides in the present chapter are CT-TAMRA (CT complementary target), MT-TAMRA (MT mismatched target) and NT-TAMRA (NT noncomplementary target). For HECL measurements, boron-doped p-Si (100) with resistivity of 0.01-0.02 Ωcm (Okmetic Oy, Finland) and aluminum electrodes made from 99.9% pure aluminum band, 0.3 mm thick (Merck Art. 1057, batch 720 K22720857), were used.

4.2.2   TAMRA labeling of oligonucleotides

Oligonucleotides were labeled at their amino-modified 5'-terminal according to the procedure published by Molecular Probes, slightly modified.[27] Briefly, prior to labeling, oligonucleotides were purified by chloroform extraction and precipitated with ethanol. Then, amino-modified oligonucleotides were dissolved in 0.1 M tetraborate buffer, pH 8.5, to obtain a concentration of 250 μM. This solution was added to a small amount of TAMRA-DMSO solution so that the dye concentration was approximately 30-fold of the concentration of the oligonucleotide.

The mixture was left to react in the dark and was gently shaken during six hours. Labeled oligonucleotides were precipitated twice by addition of 3 M NaCl and cold absolute ethanol, 0.1:2.5 v/v with respect to the labeling solution. The mixture was kept 30 min at -20 ℃ and then centrifuged 30 min at 12 000 rpm. The supernatant was removed and the pellet was rinsed twice with cold 70% ethanol. Labeled oligonucleotides were allowed to dry in air during 10 min, and were stored at -20 ℃ until use.

4.2.3   Instrumentation and methods

UV-Vis absorbance spectra were measured with a Hewlett-Packard 8453 spectrophotometer using a 1-cm optical pathlength quartz cuvette. HECL measurements were carried out by using single photon counting with an instrumentation that consisted of a Perkin-Elmer MP 1993 photon counting module with yellow sensitive cathode and Nucleus MCS-II scaler card. The HECL signal was filtered with an optical filter of bandwidth 550 $\pm$ 40 nm or 600 $\pm$ 40 nm. The cell consisted of a sample holder made of Teflon, a Pt-wire counter electrode and a disposable silicon or aluminum working electrode. The effective area of the electrode in the cell was 63.6 mm^2. A laboratory-made coulostatic pulse generator[28] was applied to generate cathodic pulses, and a pulse generator was adjusted to yield cathodic pulses with 40 μC of charge and -40 V of voltage with frequency of 20 Hz. Contact angles were measured with a Drop shape analysis system (Kruss).

Aluminum electrodes were coated with 2-3 nm thick natural oxide film, while silicon electrodes were thermally oxidized in cleanroom according to a previously published procedure[29] to yield a 4-nm thick oxide layer. Thickness of the oxide film was determined by an ellipsometer operated at 632.8 nm (He–Ne laser). Ultra-thin silicon dioxide films are known to give an erroneous refractive index during measurement, and thus the refractive index of the SiO_2 was fixed at 1.465, a value known from thicker films. If the wafers were measured immediately after oxidation, and later the next day, the thickness increased by about 0.05 nm due

to adsorption of gases onto the surface. Silicon electrodes were diced to 9 x 9 mm and aluminum electrodes cut to 10 x 10 mm pieces. HECL measurement were performed in 0.05 M sodium tetraborate buffer at pH 9.2 or 7.8 (pH adjusted with 1 M sulfuric acid) in the case of hybridization assay. This buffer is known to be fairly unreactive with hydrated electrons and hydroxyl radicals, as well as with sulfate radicals.[30] Absorbance measurements were performed in 0.05 mol/L sodium tetraborate buffer at pH 7.8 which was adjusted with 1 M sulfuric acid.

4.2.4   Preparation of oligonucleotide-modified electrodes

Before silanization, aluminum and silicon electrodes were cleaned with methanol and water and dried in a nitrogen stream. Liquid phase aminosilanization was performed under ambient conditions using freshly made APTES-EDA solution (mixing ratio 1:1) at 5% total silane concentration (v/v) in methanol/water solution (99.5:0.5 v/v) for one hour. Substrates were then sequentially washed with methanol and water, dried in a nitrogen stream and cured in an oven at 115 ℃ for one hour. The surface was activated in a freshly prepared solution of distilled DMF and pyridine (9:1 v/v) containing 1 mM PDC for two hours at room temperature. The oligonucleotides were then immobilized by placing a droplet of 20 μL of amino-modified oligonucleotides in 40 mM phosphate buffer, pH 7.0, containing 0.150 M sodium nitrate (sodium nitrate was used instead of sodium chloride because chloride ions can have detrimental effect on very thin oxide films) on the surface and left overnight in a humid chamber. The substrates were subsequently sequentially washed with methanol and water, soaked in 0.01 M glycine solution prepared in 40 mM phosphate buffer, pH 7.0, for 30 min to deactivate surface isothiocyanate groups, and dried in a nitrogen stream.

4.2.5   Hybridization

Labeled targets were dissolved in the same buffer as used for immobilization; 30 μL of this solution was carefully pipetted to the center of an electrode and left

to incubate three hours at ambient temperature. After that the electrodes were washed with sodium tetraborate buffer, pH 7.8, to which 0.2% SDS has been added, heated to 35 ℃, dried in a nitrogen stream, and stored in dessicator until HECL measurement.

4.3   Results and discussion

The HECL spectrum of RhB induced on oxide-coated aluminum electrodes and fluorescence spectrum are presented in Figure 4.1. The profile of the HECL spectrum of RhB is very similar to that of the fluorescence emission spectrum; in both cases the emission maximum is at 575 nm.
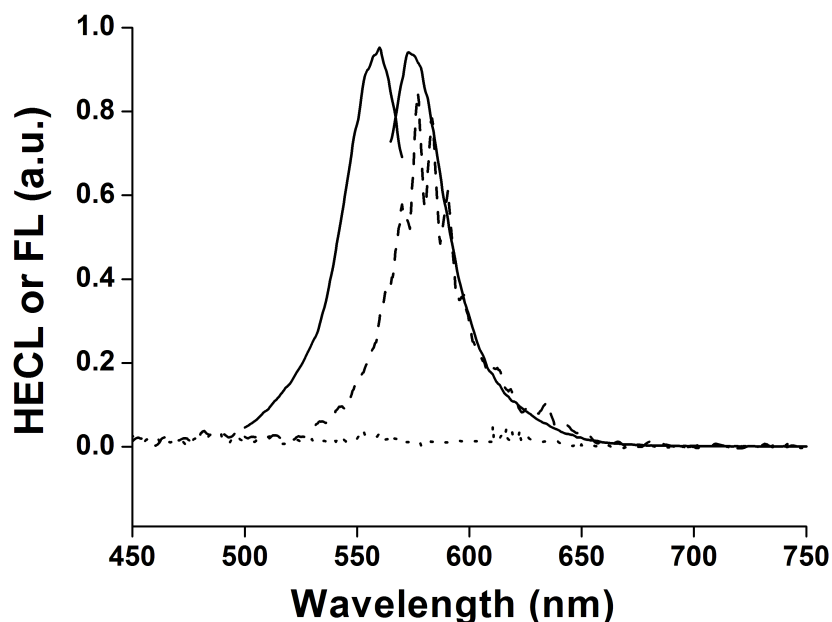

Figure 4.1: HECL (dashed line) and fluorescence (solid line) excitation and emission spectra of rhodamine B. The ECL blank is shown as a dotted line. Conditions: scanning speed 240 nm/min, Perkin-Elmer LS-50B spectrometer, slit widths 10 nm; coulostatic pulse generator: voltage -45 V, pulse frequency 80 Hz, pulse charge 120 μC; aluminum strip cathode, platinum wire anode.

68

The similarity makes it reasonable to assume that the emission is generated by the same luminescent species in both cases. Figure 4.2 shows the pH dependence of HECL of RhB in air-saturated tetraborate buffer solution. The HECL intensity of RhB is relatively stable in pH range from 3 to 9. Below pH 3 and above pH 10 the HECL intensity decreases steeply. The probable explanation for the decrease at low pH is a rapid conversion of hydrated electron into its conjugated acid, a hydrogen atom $(k(e_{aq}^- + H^+) = 2.3 \times 10^{10}$ Lmol^{-1}s^{-1}).[30] This would hinder reaction 4.1, which is proposed to be the initial reaction of HECL generation.
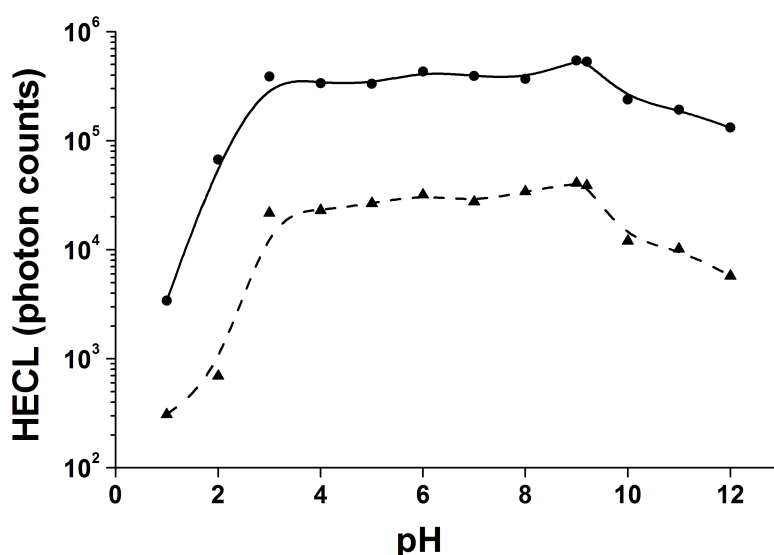

Figure 4.2: Effect of pH on HECL of RhB: cathodic HECL during the pulse (solid line); time-resolved HECL (dashed line). Conditions: 1 μM RhB in 0.1 M Na$_2$SO$_4$ and 0.03 M Na$_2$B$_4$O$_7$ supporting electrolyte solution, 0.01 M NaN$_3$. Solutions were adjusted to the desired pH with sulfuric acid or sodium hydroxide. Pulse voltage -45 V, pulse charge 120 μC, pulse frequency 20 Hz. TR-HECL signals were measured by delay 0 μs, gate time 200 μs. HECL and TR-HECL intensities were integrated over 1000 excitation cycles. All signals were measured through an interference filter of 600 $\pm$ 40 nm.

However, a more important reason for the rapid decrease in HECL intensity

in both highly acidic and alkaline conditions is dissolution and damage of the aluminum oxide film.[31] The anodically grown oxide film on aluminum can be made thicker than natural oxide.[32] Anodic oxide films are usually regarded as a mixture of amorphous and crystalline Al_2O_3.[31]

The effect of oxide film thickness on HECL intensity of RhB is shown in Figure 4.3. The HECL intensity decreases rapidly when the oxide film thickness exceeds 3 nm because electrons tunnel without loss of energy only through ultra-thin oxide films ($<ca.$ 4 nm).
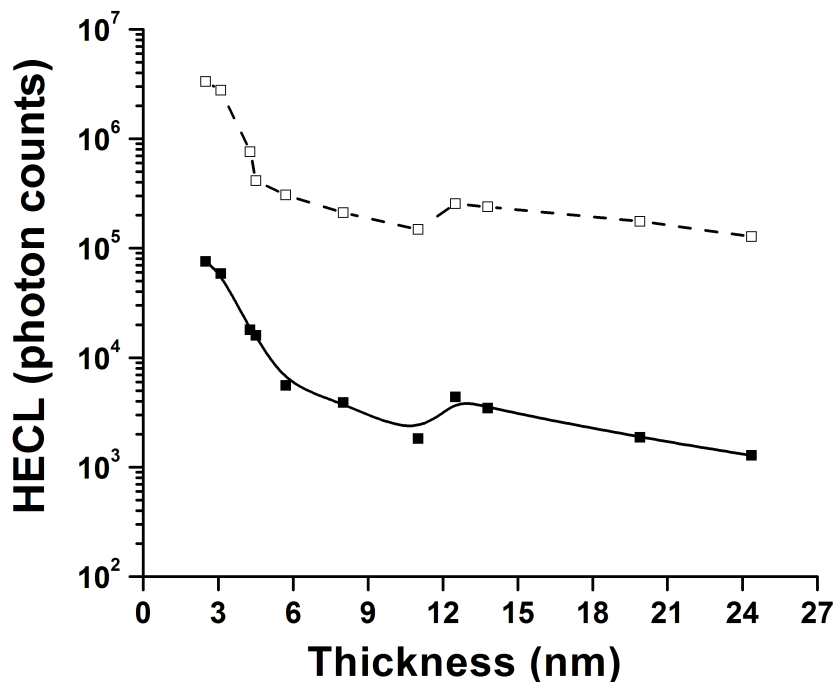

Figure 4.3: Dependence of HECL of RhB on the oxide layer thickness: cathodic HECL during the pulse (solid line); time-resolved HECL (dashed line). Measurements performed in 0.05 M $Na_2B_4O_7$ buffer in the presence of 0.01 M NaN_3, pH 9.2, other experimental conditions as described in Figure 4.2.

Upon increase of the oxide film thickness, Fowler-Nordheim (F-N) tunneling be-

comes the predominant electron transport mechanism. Under this regime, the electrons are first tunneled into the conduction band of the oxide and then heterogeneously transferred to the electrolyte solution from the bottom of the conduction band or from slightly above it at the oxide/electrolyte interface. Under these conditions the electrons lose part of their energy during tunneling through thicker oxide film, but also gain it from the electric field. Thus, thicker the oxide film is, the less probable is the generation of hydrated electrons becomes and the HECL intensity decreases with increase of the oxide film thickness.

4.3.1 Effect of free radical scavengers on HECL

If generation of HECL of RhB is mainly caused by the excitation pathways initiated by hydrated electrons as proposed above, hydrated electron scavengers should have striking effect on the HECL intensity. A group of hydrated electron scavengers was tested to explore this possibility. It can be seen from Figure 4.4 that $Co(NH_3)_6^{3+}$ is the strongest HECL quencher, and it is an approximately 10-fold stronger quencher than nitrate and nitrite ions at the same concentration. This is understandable in light of the second order reaction rate constants of these scavengers with hydrated electron. $k(e_{aq}^- + Co(NH_3)_6^{3+}) = 8.7 \times 10^{10}$ $Lmol^{-1}s^{-1}$ is about 10 times higher than $k(e_{aq}^- + NO_3^-) = 9.7 \times 10^9$ $Lmol^{-1}s^{-1}$ or $k(e_{aq}^- + NO_2^-)$ = 4.1 x 10^9 $Lmol^{-1}s^{-1}$).[30] Although the rate constants of $k(e_{aq}^- + NO_3^-)$ and $k(e_{aq}^- + NO_2^-)$[30] are a bit smaller than $k(RhB + e_{aq}^-) = 3 \times 10^{10}$ $Lmol^{-1}s^{-1}$, reactions between scavengers and hydrated electrons will predominate when concentrations of scavengers are higher than concentration of RhB in the system. HECL of RhB is quenched when concentrations of nitrate and nitrite ions exceed 10^{-4} M. Nitrite ions have a slightly stronger quenching effect on HECL than nitrate ions do. Perhaps because nitrite scavenges hydroxyl radical $[E°(NO_2^./NO_2^-) = 1.02$ V,[33] $k(OH^. + NO_2^-) = 1.0 \times 10^{l0}$ $Lmol^{-1}s^{-1}$,[30]] as well as hydrated electron.

Significant quenching of HECL by $Co(NH_3)_6^{3+}$ and nitrate ion supports the hypothesis of hydrated electron being the primary species of the HECL excitation
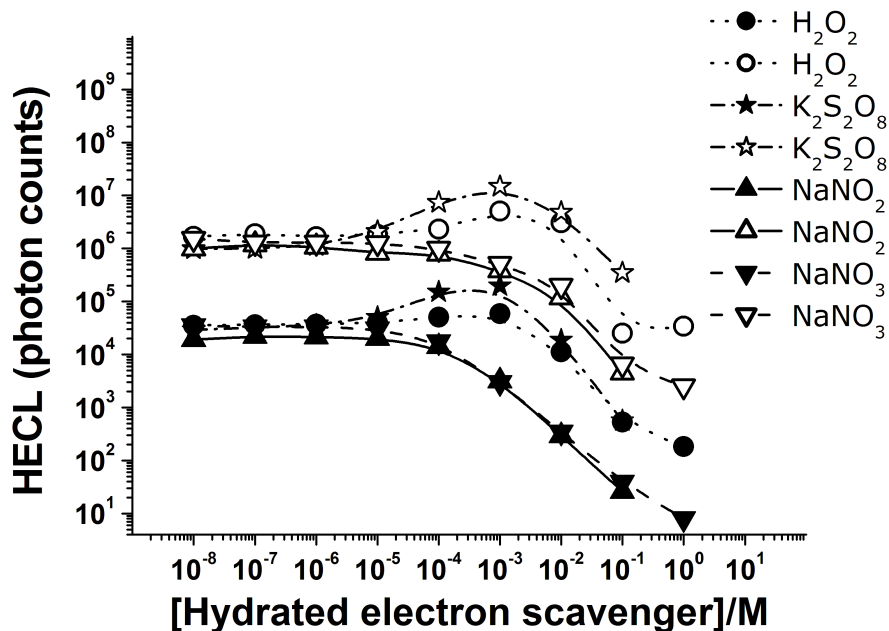
Figure 4.4: Effect of electron scavengers on the HECL of RhB (1 μM); filled symbols indicate cathodic HECL, hollow symbols TR-HECL. Measurements performed in 0.05 M $Na_2B_4O_7$ buffer, pH 9.2, other experimental conditions as in Figure 4.2.

route. Peroxydisulfate ions and hydrogen peroxide enhance the HECL intensity of RhB at concentration levels from 10^{-6} M up to 10^{-3} M, while further increase in concentration leads to quenching of the HECL. The rate constant $k(e^-_{aq} + S_2O_8^{2-})$ = 2.3 x 10^{10} Lmol^{-1}s^{-1}[30] is lower than $k(e^-_{aq} + RhB)$ = 3 x 10^{10} Lmol^{-1}s^{-1}. Upon reaction with hydrated electron, peroxydisulfate ions produce sulfate radical (SO_4^-), which is a strong one-electron oxidant (E°= 3.4 V *vs.* SHE)[34] capable of oxidizing a number of aromatic compounds but still reacting sluggishly with water. However, it also generates high background electroluminescence on thin aluminum oxide films. Hydrogen peroxide does not enhance background electroluminescence under the same conditions.[35] Excess concentration of $S_2O_8^{2-}$ ions (> 10^{-3} M) quenched the HECL due to the too efficient removal of hydrated electrons and through the recombination reaction of SO_4^- radical $(k(SO_4^- + SO_4^-)$ = 5.1 x 10^8 Lmol^{-1}s^{-1}) at elevated concentration.[36] Thus, the overall effect is the de-

crease in both sulfate radical concentration and hydrated electron concentration. Up to a concentration of 1 x 10^{-3} M hydrogen peroxide enhances HECL intensity of RhB in analogous way as peroxydisulfate ion, while above this concentration it quenches HECL intensity due to rapid reaction with hydrated electrons [k(e_{aq}^- + H_2O_2)= 1.2 x 10^{10} Lmol^{-1}s^{-1}].[30]

Previous studies[35,37] have suggested that electron centers present in an oxide film can act as primary oxidants capable of oxidizing hydroxide ions to hydroxyl radicals in alkaline aqueous solution. In addition, the presence of dissolved oxygen in an aqueous solution can produce hydroxyl radicals [E°(OH$^.$/OH$^-$)=2.2 V]. As oxidizing radicals, hydroxyl radicals might directly oxidize RhB to RhB$^{.+}$ in the present system [k(OH$^.$ + RhB) = 9 x 10^9 L mol^{-1}s^{-1}]. If the scheme described above is valid in the present system as well, hydroxyl radical scavengers would also strongly affect the HECL intensity of RhB. This assumption was tested by adding hydroxyl radical scavengers, such as ethanol and halide ions into the RhB solution and measuring their influence on the HECL intensity. The results are shown in Figure 4.5.

We observed that bromide and azide ions weakly enhanced HECL of RHB in the concentration range 10^{-5} M to 10^{-2} M, while iodide ions and ethanol quenched the HECL at concentrations above 10^{-5} M. The effect of halides on the HECL intensity could be explained by the following reactions:

$$OH^. + X^- \rightarrow OH^- + X^. \tag{4.2}$$

$$X^. + X^- \rightarrow X_2^{.-} \tag{4.3}$$

$$X^. + X^. \rightarrow X_2 \tag{4.4}$$

These hydroxyl radical scavengers, with the exception of ethanol, produce a series of secondary oxidizing radicals by one-electron oxidation [E°(Br$^.$/Br$^-$) = 1.92 V,
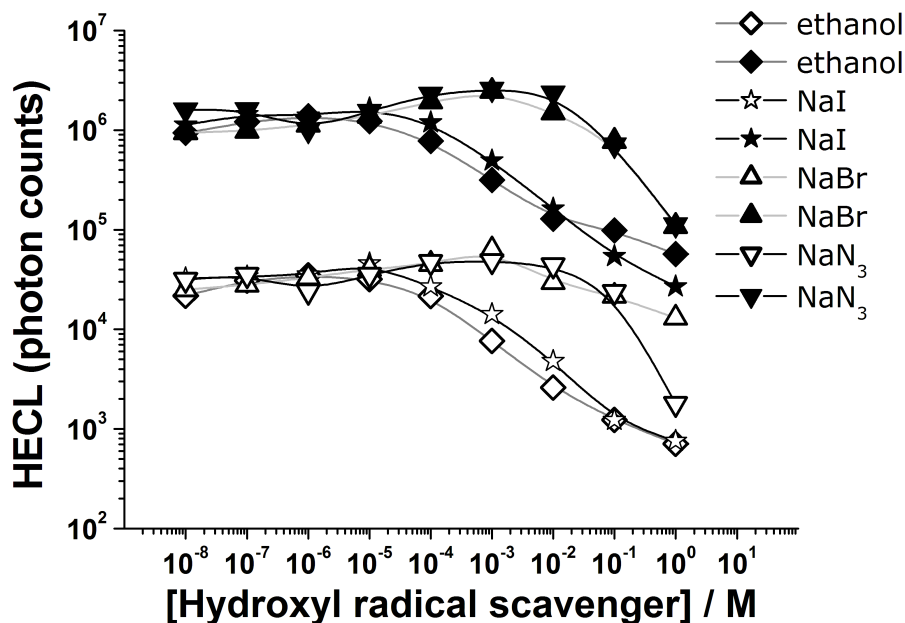
Figure 4.5: Effect of different hole scavengers on the HECL; full symbols cathodic HECL, hollow symbols to time-resolved HECL. Measurements performed in 0.05 M $Na_2B_4O_7$ buffer, pH 9.2, other experimental conditions as in Figure 4.2.

$E°(I^{.}/I^{-}) = 1.33$ V, $E°(N_3^{.}/N_3^{-}) = 1.33$ V].[33] Ethanol converts hydroxyl radical to reducing equivalents by hydrogen abstraction $[E°(C_2H_5OH/C_2H_4O^{.-}) = -1.2$ V]. The rate constants for hydroxyl radical reacting with bromide, iodide, azide and ethanol are 1 x 10^{10}, 1.1 x 10^{10}, 1.2 x 10^{10} and 1.9 x 10^9 L $mol^{-1}s^{-1}$, respectively.[30]

Ethanol quenches the HECL due to its reaction with hydroxyl radical and the subsequent production of strongly reducing secondary radicals ($C_2H_4O^{.-}$) by hydrogen abstraction as main secondary radicals (84.3%).[30] The reducing secondary radicals cannot act as oxidants and quench HECL.

Bromide enhances HECL of RhB in the present system similarly to azide. Increase in concentration of bromide ions or azide ions result in the formation of $Br_2^{.-}$ $[E°(Br_2^{.-}/2Br^{-}) = 1.62$ V] or $N_3^{.}$ $[E°(N_3^{.}/N_3^{-}) = 1.3$ V] through reaction with

hydroxyl radicals.[33] Both $Br_2^{\cdot-}$ and $N_3^{\cdot}$ are sufficiently oxidizing species to induce Ox-Red excitation route. However, continuous increase in the concentration of bromide or azide results in the formation of Br_3^- [$E°(Br_2/Br_2^{\cdot-}) = 0.58$ V versus SHE][33] and self-combination of azide radicals [$k(N_3^{\cdot}+N_3^{\cdot}) = 4.4$ x 10^9 L mol^{-1} s^{-1}].[36] Br_3^- is not as sufficiently strong oxidant to induce HECL of RhB as hydroxyl radical is, and a rapid quenching of HECL was observed at concentrations above 0.01 M.

In addition, a previous pulse radiolysis study revealed that both $N_3^{\cdot}$ and $Br_2^{\cdot-}$ react rapidly with RhB in aqueous solution.[38] $k(N_3^{\cdot}+ RhB)$ is about 5.0 x 10^9 Lmol^{-1} s^{-1} in an aqueous solution.[38] Although the value of $k(Br_2^{\cdot-} + RhB)$ is unknown, it can reasonably assumed to be similar to that of $k(N_3^{\cdot} + RhB)$. That would explane slight enhancement of the present HECL by both $N_3^{\cdot}$ and $Br_2^{\cdot-}$ in the appropriate concentration range.
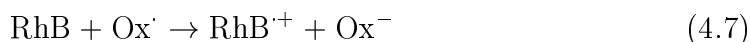
Although $I^{\cdot}$[$E°(I^{\cdot}/I^-)= 1.3$ V] is sufficiently strong oxidant to oxidize RhB and generate HECL, $I_2^{\cdot-}$ [$E°(I_2/I_2^{\cdot-})= 0.21$ V][33] is too weak oxidant for the generation of RhB HECL, except at high iodide ion concentrations. Thus, a clear quenching occurs when the concentration of iodide ion is increased.

In short, the effects of hydroxyl radical and hydrated electron scavengers on HECL of the RhB system suggest that the hydrated electrons and oxidizing species with properties similar to those of hydroxyl radical play an important role in the HECL excitation pathway.

4.3.2   Mechanism of HECL

In principle, the HECL excitation route of aromatic luminophores can be reduction-initiated oxidative excitation (red-ox) pathway (reactions 4.5 and 4.6) or oxidation-initiated reductive excitation (ox-red) pathway (reactions 4.7 and 4.8). The mech-

anisms can be written as follows:

$$\text{RhB} + \text{e}_{aq}^- \rightarrow \text{RhB}^{\cdot-} \tag{4.5}$$

$$\text{RhB}^{\cdot-} + \text{Ox}^{\cdot} \rightarrow \text{RhB}^* + \text{Ox}^- \tag{4.6}$$

$$\text{RhB} + \text{Ox}^{\cdot} \rightarrow \text{RhB}^{\cdot+} + \text{Ox}^- \tag{4.7}$$

$$\text{RhB}^{\cdot+} + \text{e}_{aq}^- \rightarrow \text{RhB}^* \tag{4.8}$$

$$\text{RhB}^* \rightarrow \text{RhB} + h\nu \tag{4.9}$$

where $\text{Ox}^{\cdot}$ is a one-electron oxidant, such as hydroxyl radical or azide radical, which is produced by scavenging the hydroxyl radical. In the reduction-initiated pathway, RhB undergoes one-electron reduction to a radical intermediate followed by one-electron oxidation, while in the oxidation initiated pathway the process is reversed. The light is emitted by radiative relaxation of the excited RhB^* molecule (reaction 4.9).

4.3.3 Applicability of HECL for bioanalysis

As discussed above, both peroxodisulfate and azide ions enhance HECL intensity of RhB. However, better analytical results are obtained with azide ions as coreactants. Figure 4.6 shows calibration curves of RhB obtained on aluminum electrode in the presence of azide ions.

As can be seen from Figure 4.6, the HECL response is linear from 1 x 10^{-10} to 1 x 10^{-5} M. A particularly interesting finding is the relatively long HECL lifetime of RhB, about 19 μs in the presence of azide ions and 12 μs in the presence of peroxodisulfate ions. The time-resolved signal of RhB was recorded for 200 μs immediately after each excitation pulse, and cathodic HECL was recorded during the excitation pulses.
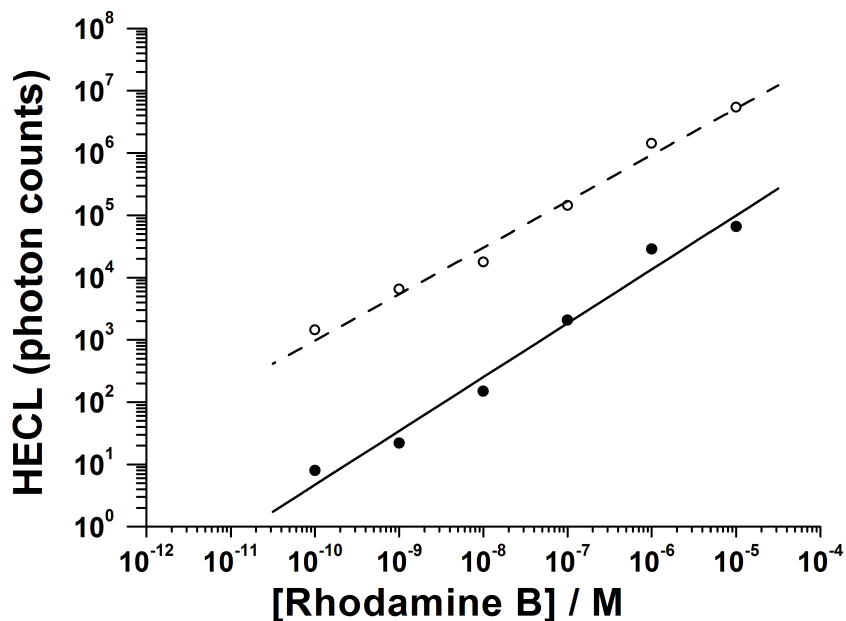
Figure 4.6: Calibration curve of RhB on oxide-coated aluminum electrodes: open symbols cathodic HECL, filled symbols time resolved HECL. All measurement were performed in 0.05 M $Na_2B_4O_7$ at pH 9.2 buffer solution containing 0.01 mol/L NaN_3, other experimental conditions as in Figure 4.2.

4.3.4   Characteristics of HECL-based hybridization assay

Figure 4.7 shows the scheme of a heterogeneous hybridization assay on thin oxide film-coated Al or Si electrodes. The electrode surfaces were modified with aminosilane in order to produce amino-terminating layer (Section 4.2.4), which allowed immobilization of amino-modified oligonucleotides via PDC cross-linking. After hybridization with a labeled target, a strong cathodic pulse was applied to the electrode, which caused hot electron injection into an electrolyte solution and subsequent excitation of the HECL luminophore, in this case TAMRA.

One of the features that make silicon the most useful material in microelectronics is its ability to grow a thin layer of silicon dioxide. At ambient environment, silicon surface is covered with a thin, less than 2-nm thick natural oxide layer,
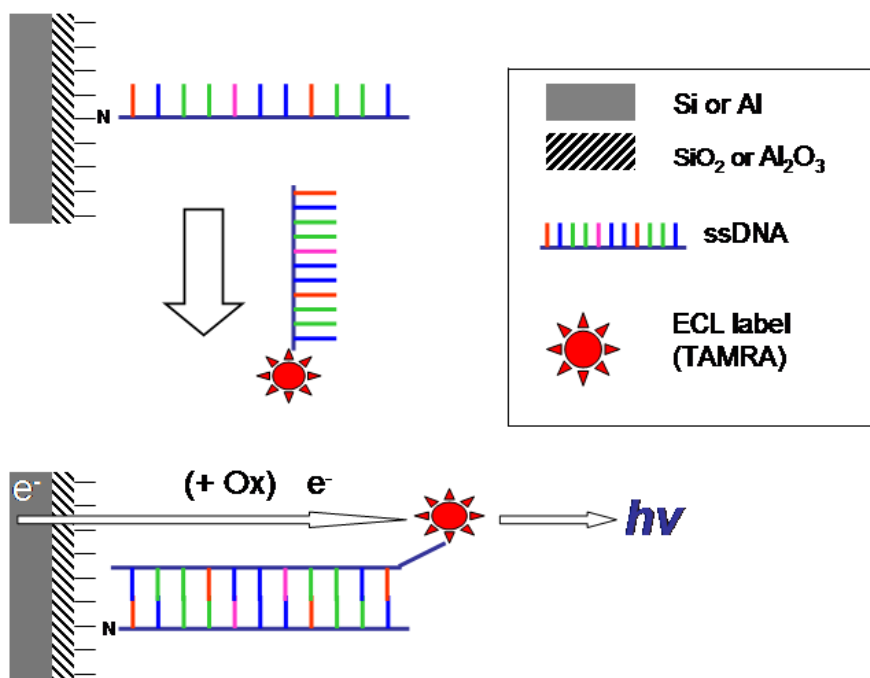
Figure 4.7: The scheme representing a heterogeneous hybridization assay on amino-modified electrode surface and hybridization detection with HECL. Figure not to scale.

which is inhomogeneous and contains impurities. This native silicon dioxide does not provide a sufficiently high barrier for the effective hot electron tunneling necessary for an intense HECL signal. On the other hand, the HECL intensity decreases exponentially when oxide thickness exceeds about 6 nm.[29] Silicon electrodes coated with a 4-nm thick thermally grown oxide layer have been used for the hybridization assay. As shown above, natural aluminum oxide which is 2-3 nm thick provides sufficiently high energy barrier to allow electron tunneling, and thus, aluminum electrodes coated with natural oxide were used.

4.3.5 UV-VIS properties of labeled compounds

The concentration of the oligonucleotides and labeling efficiency were determined by UV-VIS spectroscopy. Figure 4.8 shows the UV-Vis spectra of rhodamine B solution (a), unlabeled 15-base oligonucleotide (b) and TAMRA-labeled 15-mer oligonucleotide (c) measured in 0.05 M tetraborate buffer, pH 7.8.
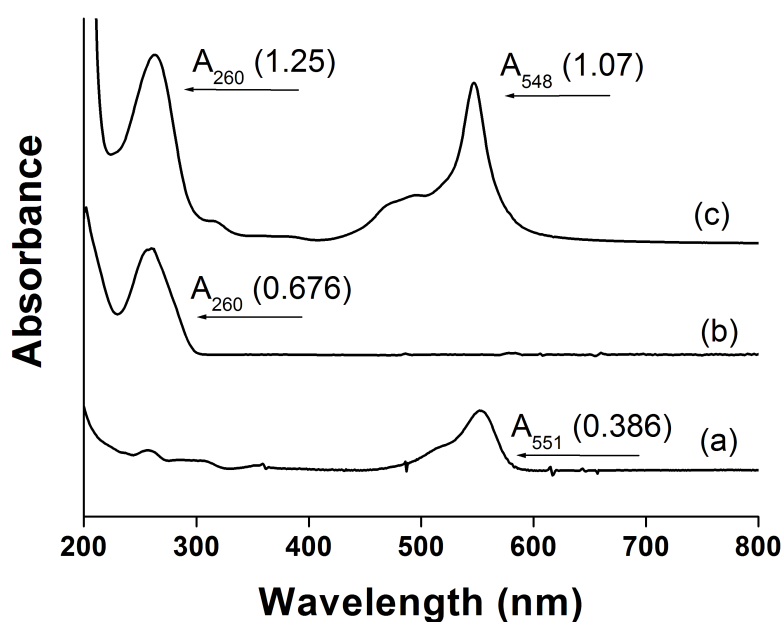
Figure 4.8: Absorbance spectra of rhodamine B (a), unlabeled probe (b) and TAMRA-labeled target (c).

The ratio of TAMRA to oligonucleotide, calculated from the absorbance peaks at 260 and 548 nm using absorption coefficient of 95 000 $cm^{-1}L^{-1}mol$ for TAMRA[39] and 155 000 $cm^{-1}L^{-1}mol$ for 15-base oligonucleotide (given by provider) is 1.4. No effort was made to further separate labeled oligonucleotides from nonspecifically adsorbed dye.

4.3.6 HECL of TAMRA-labeled DNA

Before the hybridization experiments, the HECL intensity of TAMRA-labeled DNA was investigated. Figure 4.9 shows the calibration curves obtained on oxide-film coated aluminum and silicon electrodes in the presence of 0.01 M NaN$_3$ as coreactant.[1]
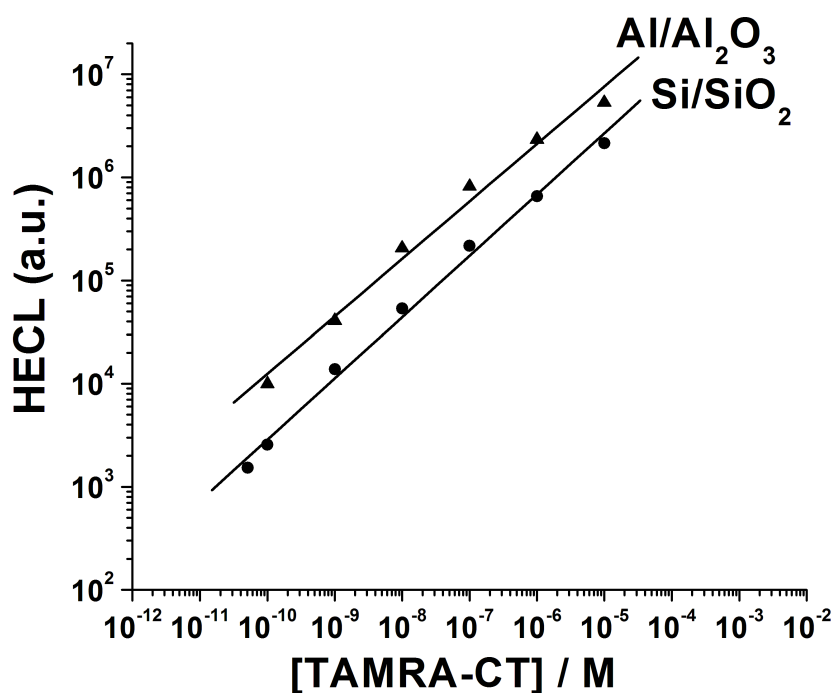
Figure 4.9: Calibration curve of TAMRA-labeled DNA on aluminum and silicon electrodes. Measurement conditions: 0.05 M tetraborate buffer containing 0.01 M sodium azide, pH 7.8. Experimental conditions: pulse voltage -40 V, pulse charge 40 μC, pulse frequency 20 Hz. The HECL intensities were integrated over 1000 excitation cycles and the signal was recorded through an emission filter of bandwidth 550 $\pm$ 40 nm.

Azide ions were used as coreactants, as the results presented above showed that azide ions quench background electroluminescence while slightly enhancing HECL intensity of RhB. Upon cathodic pulse polarization of oxide-coated aluminum or

silicon electrode, hot electrons tunnel through the oxide film into the electrolyte solution generating background electroluminescence. Several parallel mechanisms contribute to generation of this background, but it can mostly be explained by electron-center luminescence at the oxide/electrolyte interface and solid state high-field electroluminescence inside the oxide film.[14,16,40] Background electroluminescence was lower on silicon compared to aluminum electrodes, in agreement with previous results.[29] This is the probable reason that the detection limits were better on silicon electrodes than on aluminum, and TAMRA-labeled DNA could be detected down to concentration of 5 x 10^{-11} mol L^{-1}.

4.3.7 Characterization of modified surfaces

To investigate deposition of the aminosilane layer, the contact angle of water was measured on silicon and aluminum after each step of the surface treatment. The contact angle is the angle at the interface of a drop of pure water and a planar surface, and it provides a measure of hydrophobicity: greater the angle, the greater is hydrophobicity. A contact angle of 49°± 1 was measured at aminosilanized Si electrode and 48°±3 at the corresponding Al electrode. PDC treatment led to increase of the contact angle to 63°±2 at silicon and 64°±3 at aluminum. This was expected, as PDC treatment introduces a hydrophobic phenyl ring to the surface.[18,19] The increase of contact angle by 14° upon PDC treatment indicates successful surface modification.

4.3.8 HECL on monolayer-coated electrodes

HECL intensity of RhB is more or less constant over a wide pH range (Figure 4.2), but it diminishes as the oxide thickness increases (Figure 4.3). Thus, a thick silane layer might quench the signal. The thickness of the aminosilane layer was not measured, but published reports on similar modification conditions suggest it could be about 1 nm on silicon dioxide[18,20] and about 2 nm[25] on aluminum oxide. The deposited silane layer could also influence the background electro-

luminescence. If hot electrons react by luminescent pathways with a deposited monolayer or phenyl groups introduced on the surface, background electroluminescence would increase. To investigate the pathways, HECL and background electroluminescence were recorded on modified and unmodified electrodes (Figure 4.10).
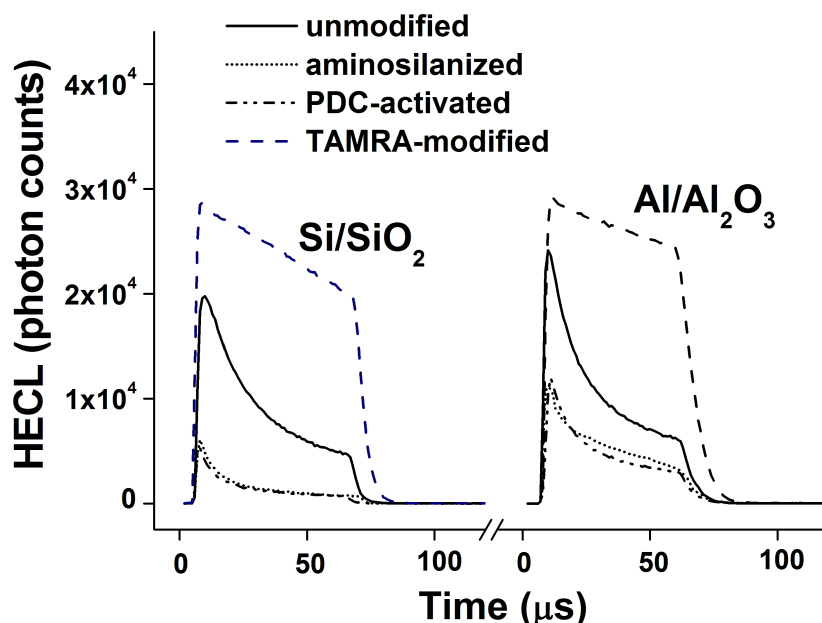

Figure 4.10: Electrochemiluminograms obtained on oxide-coated silicon (left) and aluminum (right) electrodes, on unmodified electrode (solid curve), aminosilane modified electrode (short dotted curve), PDC activated electrode (dash-dotted dot curve) and incubated with 1 μM solution of TAMRA-label (dashed curve). Conditions: 0.05 M tetraborate buffer containing 0.01 M sodium azide, pH 7.8. Experimental conditions as in Figure 4.9.

We also wished to know weather we had managed to generate an amino-terminated surface suitable for the oligonucleotide immobilization. Contact angle measurements revealed the formation of silane layer and introduction of phenyl group upon PDC treatment, which indicates an amino-terminated surface. To confirm the nature of the surface, aminosilanized electrodes were incubated with 1 μM solution of TAMRA labeling reagent dissolved in 0.05 M tetraborate buffer, pH

7.8, for three hours. Results shown in Figure 4.10 (i) confirm a successful surface treatment, (ii) demonstrate that the reagents used do not react with hot electrons too efficiently and do not generate significant background electroluminescence in the present measurement conditions, (iii) demonstrate that the deposited aminosilane layer does not quench the analytical signal. Both HECL intensity and background electroluminescence measured are higher on aluminum electrodes than on silicon, in agreement with previous HECL-related investigations.[29] It should also be noted that after surface treatment, background electroluminescence decreased considerably more on silicon electrodes than on aluminum electrodes, and was also highly reproducible.

4.3.9   HECL on DNA-modified electrodes

The validity of the method was next evaluated by hybridization experiments. Figure 4.11 shows electrochemiluminograms obtained on silicon and aluminum electrodes modified with 500 nM of probe and incubated with 1 μM solution of labeled complementary strand (TAMRA-CT), labeled mismatched strand (TAMRA-MT) and labeled noncomplementary strand (TAMRA-NT). To verify that no observable background luminescence is generated upon reaction of hot electrons with nucleic acids, control experiments were performed, in which DNA-modified electrodes were incubated with solutions of unlabeled complementary strand. The signals were comparable to the background electroluminescence, and it can be concluded that nucleic acids do not generate any detectable HECL upon reaction with hot electrons in the present measurement conditions. One of the major challenges in DNA-analytics is nonspecific adsorption.

Figure 4.11 shows that the incubation with noncomplementary labeled strand generates a signal comparable to the background electroluminescence, which is significantly weaker on silicon than on aluminum electrode. This result indicates low nonspecific adsorption and confirms that the analytical signal is due to hybridization. While at present we can not explain the reasons for higher
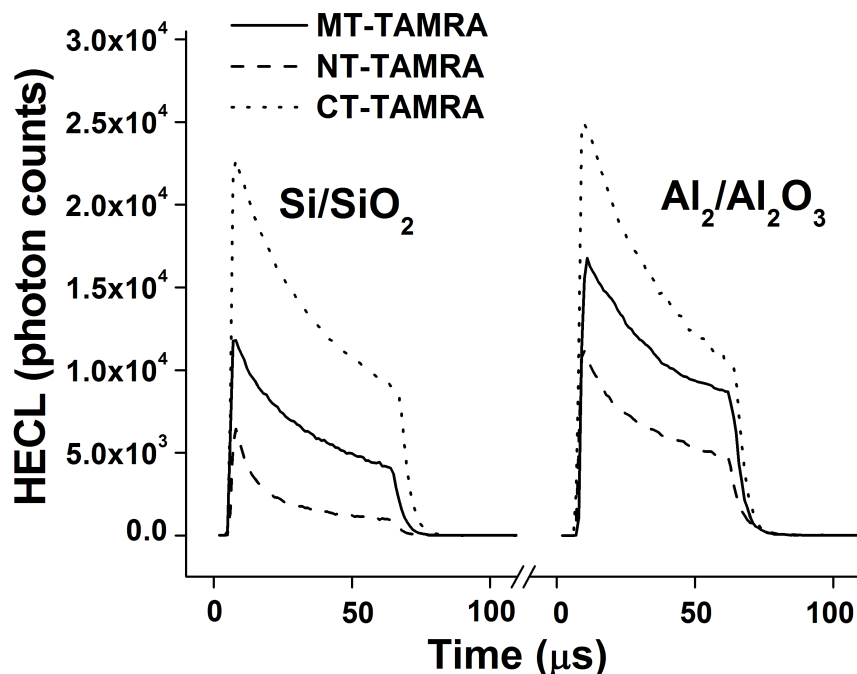
Figure 4.11: Electrochemiluminograms obtained on silicon (left) and aluminum (right) electrodes derivatized with 500 nM probe solution and incubated with 1 μM solution of: TAMRA-CT (dotted curve), TAMRA-MT (solid curve) and TAMRA-NT (dashed curve). Immobilization and hybridization were performed in 40 mM phosphate buffer containing 0.150 M $NaNO_3$, pH 7.0. HECL measurement conditions as in Figure 4.9.

background and nonspecific adsorption on aluminum than on silicon electrodes, a probable explanation is different adsorption properties of alumina and silica.

To further evaluate the validity of the presented method for detection of DNA hybridization, hybridization was performed with a DNA strand containing two mismatched nucleotides (TAMRA-MT). Efficient discrimination of mismatched strands is one of the most powerful proofs of the validity of a method. The mismatched strand with two noncomplementary and 13 complementary bases was efficiently discriminated; the signal was significantly lower than upon hybridization with the complementary strand. For some reason, the signal rise time was

different on the Al and Si electrodes, 10 and 8 μs, respectively. The mismatched strand having two noncomplementary bases was efficiently discriminated; however, again the signal was weaker on silicon than on aluminum. Thus, the results are considerably better on silicon than on aluminum.
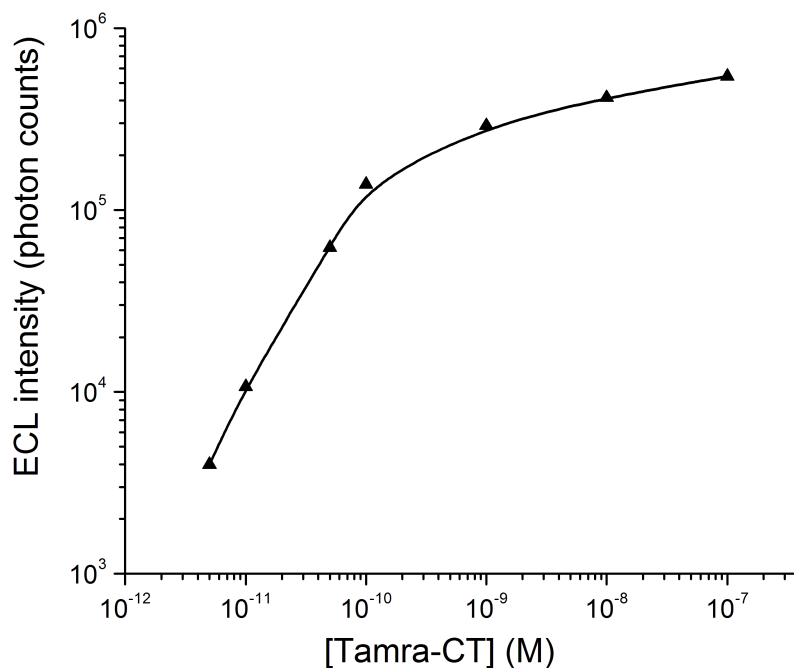
Figure 4.12: Calibration plot of TAMRA-CT on silicon electrodes derivatized with 500 nM probe solution. Immobilization and hybridization conditions as in Figure 4.11, HECL measurement conditions as in Figure 4.9.

Finally, the sensitivity of the system was investigated by hybridizing probe-derivatized silicon electrodes with increasing concentration of TAMRA-labeled complementary strand. Figure 4.12 presents the results. Comparison of Figures 4.9 and 4.12 shows that the sensitivity of the HECL detection of TAMRA-CT is higher in the heterogeneous assay format than in the solution. There are two explanations: (i) background electroluminescence is decreased upon surface modification; (ii) in heterogeneous assay format the whole sample is concentrated at the surface of the electrode, where the detection occurs.

Two slopes appear in the calibration curve: steeper up to a target concentration of 1×10^{-10} M and less steep up to concentration 1×10^{-7} M. It should be noted that the HECL intensity did not increase upon further increase of the target concentration, which indicates saturation of the binding sites. The results demonstrate the potential of HECL for DNA-hybridization detection. A strong appeal of this method is the possibility to carry out multiplexing analysis using wavelength and lifetime discrimination. In addition, microfabrication technology for silicon is well developed, and large-scale production of silicon based sensors can be readily envisaged. The method thus has good potential for the development of disposable DNA biosensors.

4.4   Conclusions

The mechanism and suitability of HECL of rhodamine B for heterogeneous hybridization assay were investigated using short oligonucleotides labeled with rhodamine derivative. RhB showed high HECL intensity on oxide-coated aluminum and silicon electrodes and its derivative TAMRA was therefore chosen for oligonucleotide labeling. An amino-terminated silane layer was deposited on oxide-coated Al and Si electrodes in liquid phase, and short 15-base amino-modified oligonucleotides were immobilized on the modified electrodes *via* diisothiocyanate coupling. Modified surfaces were characterized with contact angle measurements and the immobilization of a reactive fluorophore.

It was demonstrated that surface treatment decreases the background electroluminescence caused by the injection of hot electrons into the electrolyte solution and increases the S/N ratio. Nonspecific adsorption was low and two base pair mismatches were successfully discriminated. Thus, HECL appears to be potentially useful for the detection of DNA hybridization. A possible application is disposable silicon-based DNA biosensor. The targets were detected down to subnanomolar concentration and surface treatment led to increased sensitivity due to the lower background electroluminescence. Thus, HECL appears to offer a

highly useful method of detection for hybridization assays on silicon-based microsystems. Multiplexing analysis could easily be adapted into the method. The capability for simultaneous excitation of different luminophores means that the method could easily be adapted for multiplexing analysis.

References

1. Jiang, Q., Spehar, A.-M., Hakansson, M., Suomi, J., Ala-Kleme, T., Kulmala, S., Hot electron-induced cathodic electrochemiluminescence of rhodamine B at disposable oxide-coated aluminium electrodes, *Electrochim. Acta* **51** (2006) 2706–2714.

2. Spehar-Deleze, A.-M., Suomi, J., Jiang, Q., de Rooij, N., Koudelka-Hep, M., Kulmala, S., Heterogeneous oligonucleotide-hybridization assay based on hot electron-induced electrochemiluminescence of a rhodamine label at oxide-coated aluminum and silicon electrodes, *Electrochim. Acta* **51** (2006) 5438–5444.

3. Hinckley, D. A., Seybold, P. G., Borris, D. P., Solvatochromism and thermochromism of rhodamine solutions, *Surface Interface Analysis* **42A** (1986) 747–754.

4. Mandal, K., Pearson, T. D. L., Demas, J. N., Luminescent quantum counters based on organic dyes in polymer matrixes, *Anal. Chem.* **52** (1980) 2184–2189.

5. Ma, Y., Zhou, M., Jin, X., Zhang, B., Chen, H., Guo, N., Flow-injection chemiluminescence determination of ascorbic acid by use of the cerium(IV)-rhodamine B system, *Anal. Chim. Acta* **464** (2002) 289–293.

6. Chen, H., Zhou, M., Jin, X., Song, Y., Zhang, Z., Ma, Y., Chemiluminescence determination of ultramicro DNA with a flow-injection method, *Anal. Chim. Acta* **478** (2003) 31–36.

7. Townshend, A., Wheatley, R. A., Oxidative chemiluminescence of some nitrogen nucleophiles in the presence of formic acid as an ancillary reductant, *Analyst* **123** (1998) 267–272.

8. Hemmila, I. A., *Applications of fluorescence in immunoassays*, Wiley-Interscience 1991.

9. Wang, L., Gaigalas, A. K., Blasic, J., Holden, M. J., Gallagher, D., Pires, R., Fluorescence resonance energy transfer between donor–acceptor pair on two oligonucleotides hybridized adjacently to DNA template, *Biopolymers* **72** (2003) 401–412.

10. Sommermeyer, K., Birkwald, V. B., Pruetz, W., On the fluorescence of aqueous solutions of aromatic compounds following excitation by roentgen rays, *Strahlentherapie* **116** (1961) 354–363.

11. Sommermeyer, K., Pruetz, W., Excitation of fluorescence in aqueous dye solutions with x-rays and its dependence on linear energy transfer, *Naturforschung A* **21** (1966) 1081–1084.

12. Pruetz, W., Sommermeyer, K., Land, E. J., Light emission after pulse radiolysis of aqueous solutions of dyes, *Nature* **212** (1966) 1043–1044.

13. Pruetz, W. A., Land, E. J., Chemiluminescent reaction after pulse radiolysis of aqueous dye solutions, *J. Phys. Chem.* **78** (1974) 1251–1253.

14. Ala-Kleme, T., Kulmala, S., Latva, M., Generation of free radicals and electrochemiluminescence at pulse-polarized oxide-covered silicon electrodes in aqueous solutions, *Acta Chim. Scandinavica* **51** (1997) 541–546.

15. Kulmala, S., Haapakka, K., Mechanism of electrogenerated luminescence of terbium(III)-2,6-bis[N,N-bis(carboxymethyl)aminomethyl]-4-4benzoylphenol chelate at an oxide-covered aluminium electrode, *J. Alloys and Compounds* **225** (1995) 502–506.

16. Kulmala, S., Ala-Kleme, T., Heikkila, L., Vare, L., Energetic electrochemiluminescence of (9-fluorenyl)methanol induced by injection of hot electrons into aqueous electrolyte solution, *J. Chem. Soc. Faraday Transactions* **93** (1997) 3107–3113.

17. Manning, M., Galvin, P., Redmond, G., A robust procedure for DNA microarray fabrication and screening in the molecular biotechnology laboratory, *Am. Biotech. Lab.* **20** (2002) 16–17.

18. Oh, S. J., Cho, S. J., Kim, C. O., Park, J. W., Characteristics of DNA microarrays fabricated on various aminosilane layers, *Langmuir* **18** (2002) 1764–1769.

19. Charles, P. T., Vora, G. J., Andreadis, J. D., Fortney, A. J., Meador, C. E., Dulcey, C. S., Stenger, D. A., Fabrication and surface characterization of DNA microarrays using amine- and thiol-terminated oligonucleotide probes, *Langmuir* **19** (2003) 1586–1591.

20. Chrisey, L. A., Lee, G. U., O'Ferrall, C. E., Covalent attachment of synthetic DNA to self-assembled monolayer films, *Nucleic Acids Research* **24** (1996) 3031–3039.

21. Souteyrand, E., Cloarec, J. P., Martin, J. R., Wilson, C., Lawrence, I., Mikkelsen, S., Lawrence, M. F., Direct detection of the hybridization of synthetic homo-oligomer DNA sequences by field effect, *J. Phys. Chem. B* **101** (1997) 2980–2985.

22. Zhang, F., Srinivasan, M. P., Self-assembled molecular films of aminosilane immobilization capacities, *Langmuir* **20** (2004) 2309–2314.

23. Manning, M., Redmond, G., Formation and characterization of DNA microarrays at silicon nitride substrates, *Langmuir* **21** (2005) 395–402.

24. Su, H.-J., Surrey, S., McKenzie, S. E., Fortina, P., Graves, D. J., Kinetics of heterogeneous hybridization on indium tin oxide surfaces with and without an applied potential, *Electrophoresis* **23** (2002) 1551–1557.

25. Kurth, D. G., Bein, T., Thin films of (3-aminopropy1)triethoxysilane on aluminum oxide and gold substrates, *Langmuir* **11** (1995) 3061–3067.

26. Saprigin, A. V., Thomas, C. W., Dulcey, C. S., Jr, C. H. P., Spector, M. S., Spectroscopic quantification of covalently immobilized oligonucleotides, *Surface Interface Analysis* **36** (2004) 24–32.

27. Molecular probes, Eugene, USA, *Amine-reactive probes* (2003), mP00143.

28. Kulmala, S., Hakansson, M., Spehar, A.-M., Nyman, A., Kankare, J., Loikas, K., Ala-Kleme, T., Eskola, J., Homogeneous and heterogeneous electrochemiluminoimmunoassays of hTSH at disposable oxide-covered aluminum electrodes, *Anal. Chim. Acta* **458** (2002) 271–280.

29. Jiang, Q., Suomi, J., Hakansson, M., Niskanen, A. J., Kotiranta, M., Kulmala, S., Cathodic electrogenerated chemiluminescence of $Ru(bpy)_3^{2+}$ chelate at oxide-coated silicon electrodes, *Anal. Chim. Acta* **541** (2005) 157–163.

30. Buxton, G. V., Greenstock, C. L., Helman, W. P., Ross, A. B., Critical review of rate constants for reactions hydrated electrons, hydrogen atoms and hydroxyl radicals in aqueous solution, *J. Phys. Chem. Reference Data* **17** (1988) 513–886, and references cited herein.

31. Despic, A., Modern aspects of electrochemistry, Plenum press, New York, Vol. 20 1989, pp. 400–503.

32. Diggle, J. W., Downie, T. C., Goulding, C. W., Anodic oxide films on aluminum, *Chem. Rev.* **69** (1969) 365–405.

33. Stanbury, D., Reduction potentials involving inorganic free radicals in aqueous solution, *Advance Inorg. Chem. Radiochem.* **33** (1989) 69–138.

34. Memming, R., Mechanism of the electrochemical reduction of persulfates and hydrogen peroxide, *J. Electrochem. Soc.* **116** (1969) 785–90.

35. Kulmala, S., Ala-Kleme, T., Hakanen, A., Haapakka, K., F-centre luminescence from oxide-covered aluminum cathode induced by two-step reduction of peroxydisulfate anions, *J. Chem. Soc. Faraday Transactions* **93** (1997) 165–168.

36. Neta, P., Huie, R. E., Ross, A. B., Rate constants for reactions of inorganic radicals in aqueous solutions, *J. Phys. Chem. Reference Data* **17** (1988) 1027–1284, and references cited herein.

37. Kulmala, S., *Electrogenerated lanthanide(III)luminescence at oxide-covered aluminum electrodes in aqueous solutions and closely related studies*, Ph.D. thesis, University of Turku (1995).

38. Beaumont, P. C., Johnson, D. G., Parson, B. J., Excited state and free radical properties of rhodamine dyes in aqueous solution: A laser flash photolysis and pulse radiolysis study, *J. Photochem. Photobiol A* **107** (1997) 175–183.

39. Molecular probes, Eugene, USA, *Long-Wavelength Rhodamines, Texas Red Dyes and QSY Quenchers* (27.10. 2005), http://probes.invitrogen.com/servlets/datatable?item=6105&id=38090.

40. Kulmala, S., Ala-Kleme, T., Vare, L., Helin, M., Lehtinen, T., Hot electron-induced electrogenerated luminescence of Tl(I) at disposable oxide-covered aluminum electrodes, *Anal. Chim. Acta* **398** (1999) 41–47.

5. Hybridization assay on oxide-coated silicon electrodes

An oligonucleotide hybridization assay utilizing a synthesized Ru(II) label (Section 3.2.2) as HECL luminophore is described. Silicon electrodes coated with thin oxide film were used as the immobilization and detection platform.

5.1 Introduction

$Ru(bpy)_3^{2+}$ is the most widely used luminophore in anodic ECL, but also other Ru(II)complexes in which some or all bipyridine ligands have been changed to phenanthrolines generate anodic ECL signal (Chapter 3).[1,2] Previous investigations[3,4] have shown that $Ru(bpy)_3^{2+}$ generates HECL on oxide-coated aluminum and silicon electrodes in the presence of a suitable coreactant, such as $S_2O_8^{2-}$. The HECL generation of $Ru(bpy)_3^{2+}$ follows the reactions presented in equations 2.5-2.9 (Section 2.1.3). Detection limits are reportedly better on oxide-coated silicon compared to oxide-coated aluminum electrodes due to higher background electroluminescence on Al/Al_2O_3 electrodes.[4] HECL of Ru(II)complexes with other ligands than bipyridine has not been reported. An application of $Ru(bpy)_3^{2+}$ derivative as a HECL label in an immunoassay on oxide-coated aluminum electrodes has been reported.[3] In that work, oxide-coated silicon electrodes were physically coated with antibodies and immunoreaction was detected by HECL of analytes labeled with $Ru(bpy)_3^{2+}$-derivative.

5.2 Experimental

All chemicals, materials, oligonucleotides, and surface derivatization processes were as described in Chapter 4. The oligonucleotide was labeled as described in Chapter 3, with the synthesized bis(2,2'-bipyridine)-5-isothiocyanato-1,10-phenanthroline ruthenium label Ru(II)-**2**. All HECL measurements were performed in 0.05 M tetraborate buffer, pH 7.8. Peroxydisulfate solution was added to mea-

surement buffer in concentration of 1 mM immediately before HECL recording. Light was recorded through an optical filter of bandwidth 600 ± 40 nm.

5.3 Results and discussion

5.3.1 HECL of Ru(II)-1

Figure 5.1 shows the calibration curve of the Ru(II)-**1** complex measured on silicon electrodes coated with 4-nm-thick oxide film in tetraborate buffer in the presence of peroxodisulfate ions as coreactants. Although $Ru(bpy)_3^{2+}$ is the most widely used Ru(II) complex in ECL analysis, other Ru(II) complexes such as $Ru(phen)_3^{2+}$ reportedly generate comparable anodic ECL. However, the ligand type influences the hydrophobicity of the complex and the ECL properties. In the case of HECL,there are no reports of other Ru(II) complexes than $Ru(bpy)_3^{2+}$ possessing this property.

As can be seen, Ru(II)-**1** could be detected down to subnanomolar concentration, similarly to $Ru(bpy)_3^{2+}$.[4] HECL obtained in the absence of peroxydisulfate ions, or in the presence of azide ions as corectants, was comparable to background electroluminescence, as in the case of $Ru(bpy)_3^{2+}$.[3] Thus it is reasonable to assume that the HECL generation also occurs according to the reaction 2.5-2.9. The hot or hydrated electrons react with peroxydisulfate ions forming highly reactive sulfate radicals, which in turn react with a Ru(II) complex.

5.3.2 Background luminescence on surface-modified electrodes

Figure 5.2 shows background electroluminescence decay curves recorded on unmodified and modified electrode surfaces. Since HECL intensity is highly dependent on insulating barrier thickness, it was important to investigate the effect of surface modification on background electroluminescence. As discussed in Chapter

4, background electroluminescence can mainly be explained in terms of electron - center luminescence at the oxide/electrolyte interface solid state high-field electroluminescence inside the oxide film.[5]

As can be seen from Figure 5.2, surface treatment caused a decrease of the background electroluminescence relative to the unmodified electrode. However, the difference in the background on unmodified and modified electrodes was considerably less with Ru(II)-**1** than with TAMRA (Figure 4.10). A probable reason for this is the coreactant. The azide ions used to enhance HECL of TAMRA also decrease the background. In the case of Ru(II) complexes, the generation of HECL requires presence of more strongly oxidizing radicals, and peroxydisulfate
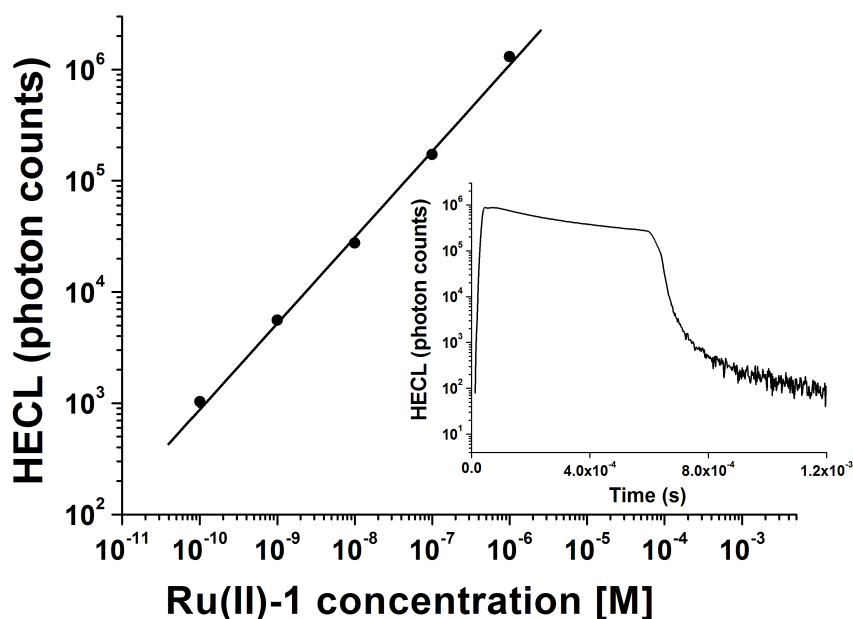

Figure 5.1: Calibration curve of Ru(II)-**1** obtained on p-Si electrodes covered with 4 nm thick thermal oxide layer, data points present the average of two measurements. Experimental conditions: electrode area 63.6 mm^2, tetraborate buffer containing 1 mM $K_2S_2O_8$, pH 7.8, pulse charge 200 μC, pulse lengths ca. 600 μs, pulse voltage -45 V, frequency 50 Hz. HECL intensity was integrated over 1000 excitation pulses. Inset: Decay curve of 1 μM Ru-**1** solution.

95

ions were found to be the best coreactants for generation of HECL of Ru(II)-complexes. A disadvantage of peroxydisulfate ions is that they enhance the background electroluminescence.

5.3.3 HECL on DNA-modified electrodes

From Figure 5.3 it can be seen that complementary strands generated the highest HECL signal, while noncomplementary strands generated HECL comparable to background. The HECL signal generated from the mismatched strand containing two base mismatches was clearly lower than upon hybridization with a complementary strand.
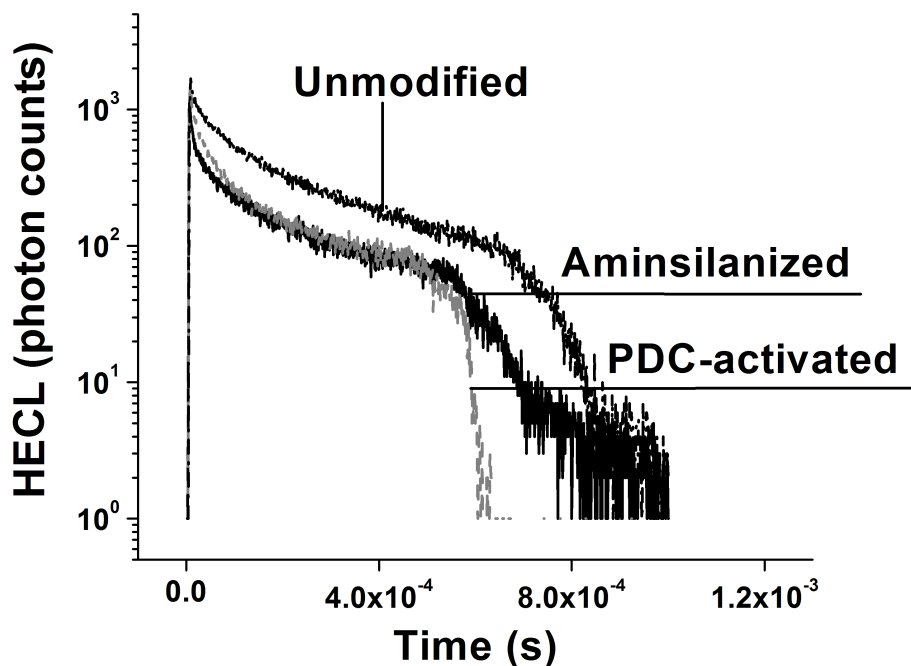

Figure 5.2: Decay curves of background electroluminescence measured in 0.05 M tetraborate buffer, 1 mM $K_2S_2O_8$, pH 7.8, on unmodified, aminosilanized, and PDC-activated Si/SiO$_2$-electrode. HECL measurement conditions as in Figure 5.1.

These results are similar to those obtained for TAMRA and confirm previous observations that nonspecific adsorption is low and that the HECL signal is due to hybridization. To investigate the sensitivity of the assay, a set of aminosilanized and PDC-activated silicon electrodes were modified with probe solutions of different concentration (0, 1, 10, 100 pM, 1, 10, 100, 500, and 1000 nM) and derivatized with a constant concentration (1 μM) of Ru(II)-**2**- labeled complementary strand. The obtained calibration curve is shown in Figure 5.4.

From Figure 5.4 it can be seen that the lowest probe concentration to yield a clearly detectable HECL signal was 10^{-10} M. HECL intensity reached a plateau
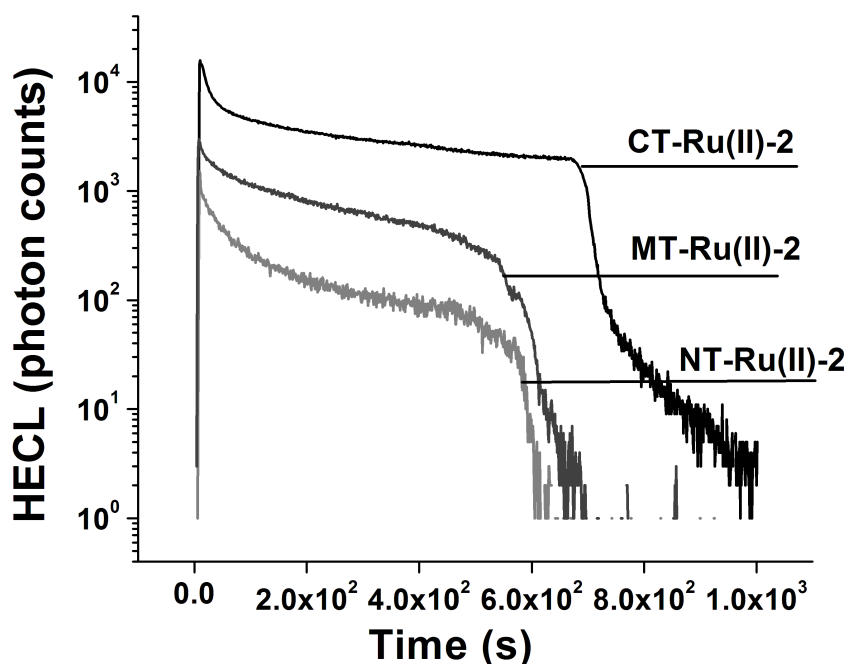

Figure 5.3: HECL on Si/SiO$_2$ electrodes derivatized with 500 nM probe solution and incubated with 1 μM solution of complementary strand (CT-Ru(II)-**2**), 2-base mismatched strand (MT-Ru(II)-**2**), and noncomplementary strand (NT-Ru(II)-**2**), measured in 0.05 M tetraborate buffer containing 1 mM K$_2$S$_2$O$_8$, pH 7.8. HECL measurement conditions as in Figure 5.1.

at probe concentration of 5 x 10^{-7} M. It seems reasonable to conclude that at this probe concentration the maximum surface probe density is achieved. Although the surface density was not actually measured, it was reasonable to conclude that all probes pipetted on the modified electrode got immobilized at the plateau probe concentration (5 x 10^{-7} M, V=20 μL). Taking into account the surface of the detection area (63 mm^2), the maximum surface density was then calculated as 9.6 x 10^{12} molecules/cm^2. This result is close to the reported theoretical surface probe density.[6,7]
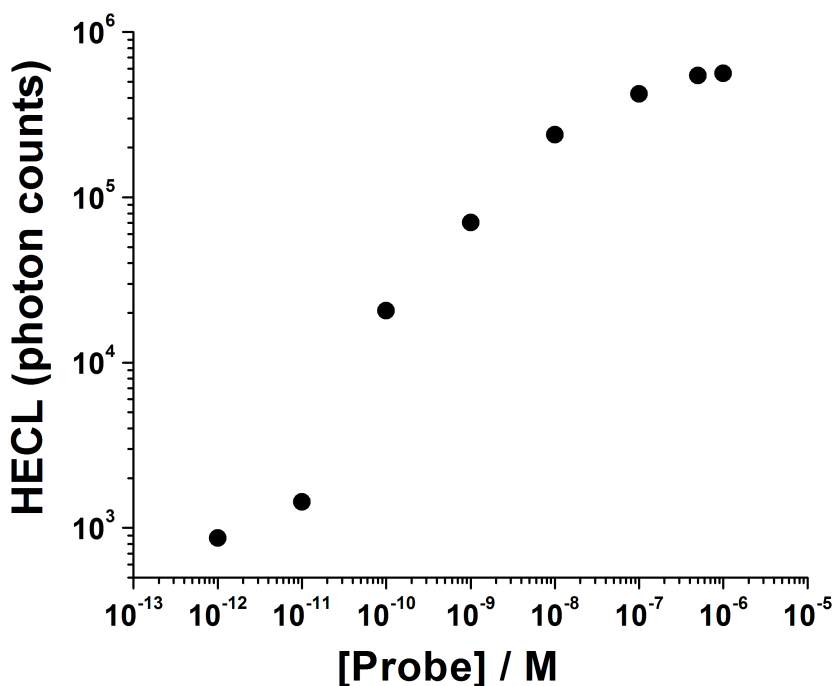

Figure 5.4: Calibration curve obtained on aminosilane/PDC-modified silicon electrodes modified with probe solution of different concentrations and a constant concentration (1 μM) of Ru(II)-**2**-labeled complementary strand. HECL measurement conditions as in Figure 5.1.

5.4 Conclusions

The Ru(II)-**2** complex, composed of two bipyridine and one phenanthroline ligand exhibited HECL comparable to the more commonly used $Ru(bpy)_3^{2+}$ complex. It could be detected down to subnanomolar concentration on oxide-coated silicon electrodes. Aminosilane modification of the oxide-coated silicon electrodes allowed immobilization of oligonucleotides with high surface probe density. Surface modification slightly decreased the background electroluminescence without affecting the strong analytical signal. Ru(II)-labeled oligonucleotide targets could be detected down to subnanomolar level. The results show that other Ru(II)-complexes than $Ru(bpy)_3^{2+}$ can be used as HECL labels. The sensitivity and detection limits of HECL hybridization assays could be improved by using labels with long luminescence lifetimes. The results presented are useful for the construction of DNA biosensor with HECL detection.

References

1. Richter, M., Electrochemiluminescence ECL, *Chem. Rev.* **104** (2004) 3003–3036.

2. Spehar-Deleze, A.-M., Schmidt, L., Neier, R., Kulmala, S., de Rooij, N., Koudelka-Hep, M., Electrochemiluminescent hybridization chip with electric field aided mismatch discrimination, *Biosens. Bioelectron. doi:10.1016/J.bios.2006.02.013* .

3. Ala-Kleme, T., Kulmala, S., Vare, L., Juhala, P., Helin, M., Hot electron-induced electrogenerated chemiluminescence of Ru(bpy)$_3^{2+}$ chelate at oxide-covered aluminum electrodes, *Anal. Chem.* **71** (1999) 5538–5543.

4. Jiang, Q., Suomi, J., Hakansson, M., Niskanen, A. J., Kotiranta, M., Kulmala, S., Cathodic electrogenerated chemiluminescence of Ru(bpy)$_3^{2+}$ chelate at oxide-coated silicon electrodes, *Anal. Chim. Acta* **541** (2005) 157–163.

5. Kulmala, S., Ala-Kleme, T., Vare, L., Helin, M., Lehtinen, T., Hot electron-induced electrogenerated luminescence of Tl(I) at disposable oxide-covered aluminum electrodes, *Anal. Chim. Acta* **398** (1999) 41–47.

6. Gooding, J. J., Electrochemical DNA hybridization biosensors, *Electroanalysis* **14** (2002) 1149–1156.

7. Steel, A. B., Herne, T. M., Tarlov, M. J., Electrochemical quantification of DNA immobilized on gold, *Anal. Chem.* **70** (1998) 4670–4677.

6. HECL of terbium(III) chelate labels

A heterogeneous immunoassay of human thyroid stimulating hormone (hTSH) as model analyte is described in this chapter. Double barrier aluminum/aluminum oxide electrodes were used as solid supports for the antibody immobilization. Immunoassay was performed in a sandwich format and Tb(III) chelates were used as HECL luminophores for the detection of immunoreaction.

6.1   Introduction

Terbium chelates are labels suitable for photoluminescence bioassays[1–3] due to their narrow-line emission, with strongest line at 545 nm, and long luminescence lifetimes, on the order of milliseconds. Detectable ECL of these compounds cannot be generated in fully aqueous solutions by means of traditional electrochemistry.

Previous investigations have shown that Tb(III) chelates generate high intensity HECL at oxide-coated aluminum electrodes upon cathodic pulse polarization and subsequent injection of hot electrons into an aqueous electrolyte solution.[4–6] Chemiluminescence of Tb(III) ions and chelates can also be generated by DC polarization of aluminum electrodes, but this ECL cannot be classified as HECL.[7]

HECL has been used for biorecognition detection in immunoassays.[6,8–10] Capturing antibodies were physically adsorbed on oxide-coated aluminum[6,8,9] and silicon[10] electrodes, and the biorecognition reaction was detected using antibodies labeled with electrochemiluminescent dyes. Antibodies are relatively large molecules (MW $\approx$ 160 kDa) containing numerous amino and carboxylic acid groups, which means that they can be readily physically adsorbed on unmodified oxide surfaces through a combination of electrostatic and hydrophobic interactions. HECL detection has been reported for both homogeneous and heterogeneous

immunoassays.[9] In both cases, nonlabeled capturing antibodies were physically immobilized on the detection electrode. Antibodies are incubated with a sample containing antibody-specific antigens (analytes) and labeled secondary antibodies, and an immunorecognition reaction is allowed to take place. In a homogeneous assay format, measurement is taken without washing away the unbound analytes. This format is possible with HECL because of the high spatial control of the method. Only labels at close proximity to the electrode are excited, while labels at a few tens of nanometers away are not excited. In a heterogeneous assay format, a washing step is performed and a different measurement buffer can be used. An advantage of homogeneous assays is the simpler set up, as there is no need for liquid handling and contamination risks are reduced. Heterogeneous assays are usually more sensitive, however, due to the quenching effects of human serum.

Our group has earlier shown that double barrier $Al/Al_2O_3/Al/Al_2O_3$ electrodes where a thin layer of oxidized high-purity aluminum is vacuum-evaporated on the top of the less pure original Al/Al_2O_3 electrode perform better that single barrier oxide-coated aluminum electrodes.[11] A considerably lower detection limit was achieved with double barrier electrodes than with Al/Al_2O_3 electrodes.[9]

6.2 Experimental

6.2.1 Materials

Monoclonal anti-TSH primary antibodies (cathing antibodies) specific to the α-chain of hTSH (MOAB, lot: M-21310, catalogue number MIT0406, concentration 6.87 mg/ml) were purchased from Medix Inc., USA, and a secondary monoclonal anti-TSH specific to the β-chain of hTSH (clone 5404, lot SPC099, concentration 5.5 mg/ml) was obtained from Medix Biochemica Oy Ab, Finland. Tris(hydrosymethyl)aminomethane (Tris), sodium tetraborate decahydrate, sulfuric acid, bovine serum albumine, sodium azide, and D-sorbitol were all from

Sigma-Aldrich. The chelating ligands for terbium were Tb(III)-**1**, $2, 6-bis[N, N-bis(carboxymethyl)aminomethyl]-4-benzoylphenol$ (inset in Figure 6.1), and Tb(III)-**2**, the isothiocyanate-containing derivative of Tb(III)-**1**. Chelates were obtained from Orion Diagnostics Oyj, Turku, and Wallac Oy, Turku, Finland. Aluminum electrodes from usually 99.9% pure aluminum band, 0.3-mm thick (Merck Art. 1057, batch 720 K22720857), were covered with a 2-3-nm-thick natural oxide film and cut into 15 mm x 15 mm pieces. The double barrier aluminum electrodes were fabricated as described elsewhere.[11]

6.2.2   Instrumentation and methods

All HECL measurements were made in 0.05 mol/L sodium tetraborate buffer, pH 9.2 or 7.8 (pH adjusted with 1 M sulfuric acid). The excitation was carried out either with our coulostatic pulse generator[9] or with a home-made pulse generator and Pine Instruments RD-4 potentiostat, which also allowed the use of bipolar pulses. The HECL measurements were carried out with single photon counting with instrumentation consisting of a Hamamatsu R 1527 photomultiplier, Stanford Research Systems SR-440 preamplifier, SR-400 gated photon counter, and Nucleus MCS-II scaler card. The immunoassay measurements were performed in the wells of microtiter strips as described earlier.[11]

6.2.3   Immunoassay of hTSH

Double barrier $Al/Al_2O_3/Al/Al_2O_3$ electrodes were used as a solid phase for the hTSH immunoassay. Primary antibodies were dissolved in 0.05 M Tris-H_2SO_4, pH 7.8, 0.5% NaN_3, and 0.025% bovine gammaglobulin to obtain concentration of 30 μg/ml and were then physically adsorbed on the electrodes. The incubation was allowed to progress three hours in a humid chamber, after which the surface was washed with MES buffer. The surface was then allowed to be saturated during 3 h with 0.05 M Tris-H_2SO_4 buffer, pH 7.75, containing 0.1% bovine serum albumin, 0.1% NaN_3 and 5% D-sorbitol. The electrodes were rinsed with buffer

and water, dried, and stored in dry conditions. The secondary monoclonal antibodies were labeled with Tb(III)-**2** as described elsewhere.[11] The labeling ratio was determined to be 5-10 label molecules per antibody. The immunoassay was carried out in the wells of microtiter strips. First, 25 μL of standard and 175 μL assay buffer (0.05 M Tris-H_2SO_4, pH 7.8, 0.5% NaN_3, 0.05% bovine gammaglobulin and 0.01% Tween 20) containing labeled antibody were added. Then the coated electrodes were added and the immunoreaction was allowed to progress for 1 h on a shaker. Finally the electrode was washed with distilled water and time-resolved (TR)-HECL was measured.

6.3   Results and discussion

6.3.1   HECL properties of Tb(III)labels

Figure 6.1 shows HECL emission spectra of Tb(III)-**1** chelate measured on aluminum cathode coated with native oxide film. It can be seen that it has four narrow emission peaks with the present photomultiplier, the highest centered at 545 nm. HECL of Tb(III)chelates is based on excitation of the ligand by a redox reaction sequence initiated by hot electron injection, followed by intramolecular excitation transfer from ligand to the central atom. The resulting HECL spectra are similar to the photoluminescence spectra of Tb(III)chelates.

Figure 6.2 shows the decay curve of Tb(III)-**1** at n-silicon electrode, which is anodically oxidized *in situ* during the HECL measurement. The HECL of Tb(III) chelates decays slowly, and the emission lasts on the order of milliseconds. This enables application of time-resolved detection (TR), that is, measurement only after the background solid state electroluminescence of the cathodic pulse has decayed away. TR measurements thus tend to be more sensitive and to result in lower detection limits, as the analytical signal can be completely separated from the background noise.
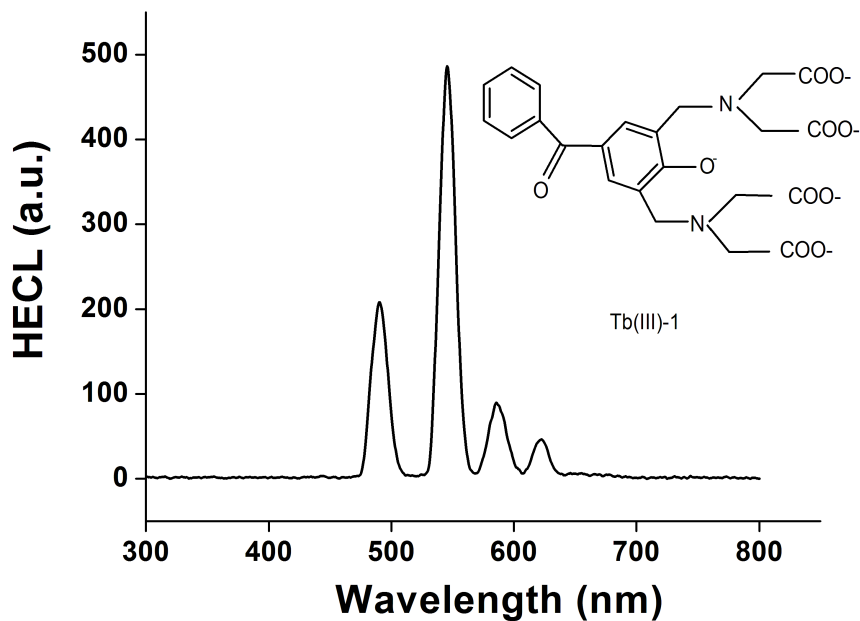
Figure 6.1: HECL emission spectra of 10 μM Tb-chelate measured in 0.05 M tetraborate buffer, pH 9.2, with an LS-50 luminometer. Molecular structure of Tb(III)-**1** is shown as an inset.

Unlike aluminum electrodes, silicon electrodes coated with natural oxide film cannot be used for HECL detection because their native oxide film is too thin (see Chapter 4). The native oxide film is preferably first stripped off and then an oxide about 4 nm thick is thermally grown. As pointed out here, however, *in situ* anodic oxidation can also be applied for both aluminum and silicon electrodes. The emission spectra and decay times of Tb(III) chelates are identical at all thin insulating-film coated electrodes. A particular advantage of the use of *in situ* anodic pulse is the possibility to repair the oxide film after damage possibly induced by a cathodic pulse.
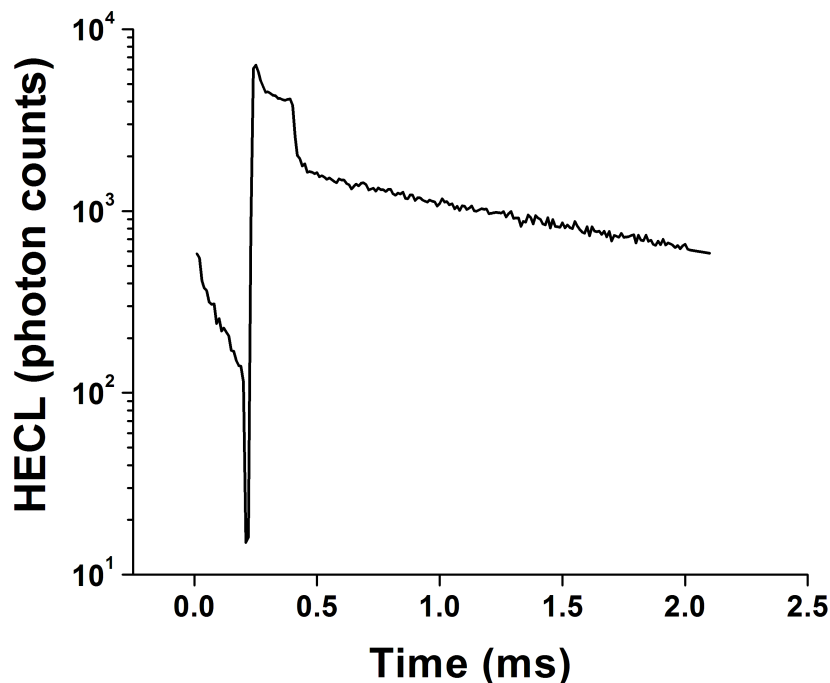
Figure 6.2: Decay curve of 1 μM Tb(III)-**1** at n-silicon electrodes. Experimental conditions: 0.05 M tetraborate buffer, pH 9.2 containing 1.0 M Na$_2$SO$_4$, pulse lengths 200 μs, anodic pulse amplitude 5 V, cathodic pulse amplitude -10 V, Pine Instruments RD4 potentiostat.

6.3.2   hTSH immunoassay

The sensitivity of the method utilizing the double barrier electrodes was investigated by incubating the modified electrodes with 100 μL of increasing concentration of Tb(III)-**2**-labeled hTHS antibody solution (0, 0.1, 0.5, 2, 10, and 50 μU/ml) during 30 min. Figure 6.3 displays the calibration curve of hTSH at double barrier Al/Al$_2$O$_3$/Al/Al$_2$O$_3$ electrodes.

Azide ions were used as coreactant instead of peroxydisulfate ions because they not only slightly enhance HECL of Tb(III)-labels, but they also decrease the background electroluminescence. In addition, they prevent bacterial growth on
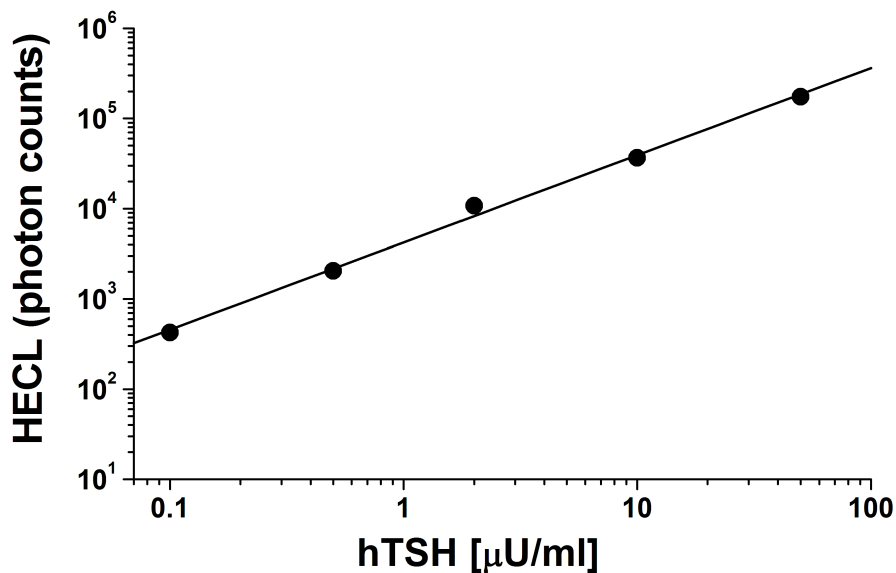
Figure 6.3: hTHS immunoassay on double barrier aluminum electrodes measured on Arcus intrument described in detail elsewhere.[12] Incubation time was 30 min. Experimental conditions: 0.05 M $Na_2B_4O_7$ adjusted to pH 7.8 with sulfuric acid, 0.03% Tween 20, 0.1% NaN_3, delay time 10 μs, gate time 2.4 ms, pulse voltage -10 V.

protein-modified electrodes during storage. As Figure 6.3 indicates, the calibration range is wide and the sensitivity excellent. Compared with previous hTHS immunoassays based on HECL of Tb(III) chelate label, the results are better.[9,10] This is due to lower background electroluminescence on double than on single barrier electrodes. The obtained straight line follows equation y=0.9669x + 3.62662. R is 0.998 and SD 7.4% for five samples.

6.4   Conclusions

Tb(III) chelates are the best HECL labels so far. With their long luminescence lifetimes and high intensity, under the present conditions, they can be

detected down to subpicomolar levels. The long lifetimes make it possible to use time-resolved detection, which allows effective discrimination of analytes from background luminescence. Background luminescence generated at the electrode/electrolyte interphase upon injection of hot electrons compromises the HECL sensitivity of short-lifetime HECL luminophores. Owing to the numerous charged and hydrophobic groups present in antibodies, it is fairly easy to produce antibody-modified electrodes. The set up needed for HECL generation is relatively simple: only excitation electronics, a cell containing a counter electrode, and a luminescence measurement module are required. As the antibody-coated electrodes can be stored several months, this method is highly promising for point-of-care applications and disposable biosensors.

References

1. Blomberg, K., Hurskainen, P., Hemmila, I., Terbium and rhodamine as labels in a homogeneous time-resolved fluorometric energy transfer assay of the β subunit of a human chorionic gonadotropin in serum, *Clin. Chem.* **45:6** (1999) 855–861.

2. Nurmi, J., Wikman, T., Karp, M., Lovgren, T., High-performance real-time quantitative RT-PCR using lanthanide probes and a dual-temperature hybridization assay, *Anal. Chem.* **74** (2002) 3525–3532.

3. Sueda, S., Yuan, J., Matsumoto, K., A homogeneous DNA hybridization system by using a new luminescence terbium chelate, *Bioconjugate Chem.* **13** (2002) 200–205.

4. Kulmala, S., Kankare, J., Haapakka, K., Electrogenerated luminescence of terbium(III) in aqueous solutions, *Anal. Chim. Acta* **252** (1991) 65–76.

5. Kulmala, S., Haapakka, K., Mechanism of electrogenerated luminescence of terbium(III)-2,6-bis[N,N-bis(carboxymethyl)aminomethyl]-4-4benzoylphenol chelate at an oxide-covered aluminium electrode, *J. Alloys and Compounds* **225** (1995) 502–506.

6. Kankare, J., Haapakka, K., Kulmala, S., Nanto, V., Eskola, J., Takalo, H., Immunoassay by time-resolved electrogenerated luminescence, *Anal. Chim. Acta* **266** (1992) 205–212.

7. Hakansson, M., Jiang, Q., Spehar, A.-M., Suomi, J., Kotiranta, M., Kulmala, S., Direct current-induced electrogenerated chemiluminescence of hydrated and chelated Tb(III) at oxide-coated aluminum cathodes, *Anal. Chim. Acta* **541** (2005) 171–177.

8. Ala-Kleme, T., Kulmala, S., Vare, L., Juhala, P., Helin, M., Hot electron-induced electrogenerated chemiluminescence of Ru(bpy)$_3^{2+}$ chelate at oxide-covered aluminum electrodes, *Anal. Chem.* **71** (1999) 5538–5543.

9. Kulmala, S., Hakansson, M., Spehar, A.-M., Nyman, A., Kankare, J., Loikas, K., Ala-Kleme, T., Eskola, J., Homogeneous and heterogeneous electrochemiluminoimmunoassays of hTSH at disposable oxide-covered aluminum electrodes, *Anal. Chim. Acta* **458** (2002) 271–280.

10. Helin, M., Vare, L., Hakansson, M., Canty, P., Hedman, H. P., Heikkila, L., Ala-Kleme, T., Kankare, J., Kulmala, S., Electrochemiluminoimmunoassay of hTSH at disposable oxide-coated n-silicon electrodes, *J. Electroanal. Chem.* **524** (2002) 176–183.

11. Hakansson, M., Jiang, Q., Suomi, J., Loikas, K., Nauma, M., Ala-Kleme, T., Kankare, J., Juhala, P., Eskola, J. U., Kulmala, S., Cathodic electrochemiluminescence at double barrier $Al/Al_2O_3/Al/Al_2O_3$ tunnel emission electrodes, *Anal. Chim. Acta* **556** (2006) 450–454.

12. Eskola, J., Makinen, P., Oksa, L., Loikas, K., Nauma, M., Jiang, Q., Hakansson, M., Suomi, J., Kulmala, S., Competitive immunoassay by hot electron-induced electrochemiluminescence detection and using a semiautomatic electrochemiluminometer, *J. Luminescence* **118** (2006) 238–244.

7. Homogeneous hybridization assay

A homogeneous hybridization assay utilizing 15- and 30-base oligonucleotide probes labeled with $Ru(bpy)_3^{2+}$-moiety and hybridized with Cy5-labeled targets is described.[1] Hybridization was detected by quenching of anodic ECL of the $Ru(bpy)_3^{2+}$ label by Cy5 label. The ECL results are compared with photoluminescence results.

7.1 Introduction

Homogeneous hybridization assays are more attractive detection formats than heterogeneous assays. There is no need to carry out time-consuming washing steps, which reduce the contamination risk, and they are more amenable to automation. $Ru(bpy)_3^{2+}$ and other Ru(II)-complexes having bipyridine and phenanthroline ligands have been extensively studied as sensitizers of photochemical electron[2-5] and energy transfer[6-10] processes. Their long luminescence lifetimes make them useful tools for studying the mechanism of electronic energy transfer via quenching of their luminescence. Energy transfer can be described by the following expression, where M can be either an electron donor and an electron acceptor:

$$Ru(bpy)_3^{2+*} + M \rightarrow Ru(bpy)_3^{3+\cdot/+\cdot} + M^{-\cdot/+\cdot} \qquad (7.1)$$
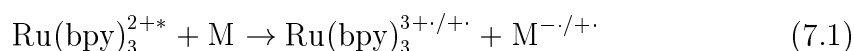
Electron transfer can occur at distances where the orbitals of an electron donor and an electron acceptor overlap, or at longer distances if the donor and the acceptor are connected through a bridging ligand that enhances electronic coupling. Electron and energy transfer processes between Ru complexes and other chromophores have been studied with use of various bridge molecules including polyphenylene groups,[4] amino acids,[5,9] and DNA strands.[10]

$Ru(bpy)_3^{2+}$ and its derivatives have been used as energy donors in several lu-

minescence resonance energy transfer (LRET) based bioassays.[11–14] The long lifetime of the excited state of Ru(II) complexes makes it possible to do time-resolved luminescence intensity measurements. A time-resolved immunoassay where $Ru(bpy)_3^{2+}$ -labeled human serum albumin was used as an energy donor and a squaranine type cyanine label as an acceptor has been described.[12] The wide emission spectrum of the ruthenium complex has been utilized for multiplex bioassays where different dyes with absorbance spectra overlapping with the emission spectrum of $Ru(bpy)_3^{2+}$ were used as energy acceptors in LRET based assays.[13] An LRET-based oligonucleotide hybridization assay, where the resonance energy was transferred from the laser-excited $Ru(bpy)_3^{2+}$ donor to a near-infrared RB 631 acceptor has also been described.[14]

LRET occurs through a coulombic interaction and does not require physical contact between a donor and an acceptor.[7] LRET results in a decrease of the donor emission, and an increase of the acceptor emission when it is a luminophore. LRET can be described by the following expression, where M is an energy acceptor:

$$Ru(bpy)_3^{2+*} + M \rightarrow Ru(bpy)_3^{2+} + M^* \tag{7.2}$$
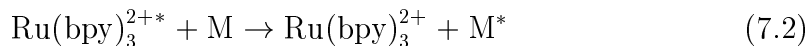
Upon photoexcitation, $Ru(bpy)_3^{2+}$ undergoes transition to the ^{1}MLCT state. This is followed by intersystem crossing with subsequent formation of the triplet state, ^{3}MLCT, from which luminescence occurs. The $Ru(bpy)_3^{2+}$ spectra generated by ECL are closely similar to those generated by the photoluminescence excitation. Thus, the same orbitals are presumed to be involved in the emission independently of whether the triplet is formed photochemically or electrochemically. The same phenomena should occur, therefore, regardless of the origin of the excited state.

The interaction between electrochemically excited $Ru(bpy)_3^{2+}$ and other chromophores has been widely investigated. Richter *et al.*[15] have studied ECL of dimetallic $Ru(bpy)_3^{2+}$ complexes connected through bridging bipyridyl ligands. The ECL quantum yield of a dicentered $Ru(bpy)_3^{2+}$ complex was doubled, rela-

tive to that of a single-centered $Ru(bpy)_3^{2+}$ because the bipyridyl bridges provided weak electronic coupling between the metal centers, thus preventing electron transfer and consequent quenching of the ECL signal. Several other attempts to increase ECL efficiency through the use of polynuclear $Ru(bpy)_3^{2+}$ complexes have been reported. Di- and tricentered $Ru(bpy)_3^{2+}$ complexes, where metal centers were connected with an amino acid lysine and the dipeptide (lysine–lysine) were synthesized.[16] Although the spectral and electrochemical measurements of these complexes showed no electrochemical or spectral interaction between metal centers, the efficiency of the ECL per unit of $Ru(bpy)_3^{2+}$ was observed to decrease when the number of the $Ru(bpy)_3^{2+}$ units was increased. The decrease was attributed to slow diffusion of the multimetallic compound on the electrode. Progesterone immunoassays relying on multicentered $Ru(bpy)_3^{2+}$ compounds were also tested. Dendrimeric compounds containing two, four, and eight $Ru(bpy)_3^{2+}$ units were attached to the paramagnetic nanoparticles and subsequently preconcentrated on the electrode surface with a magnet. In this case, ECL was observed to be the sum of the emissions from individual $Ru(bpy)_3^{2+}$ units since the diffusion limitations were overcome. However, high background caused by non-specific binding of the multiruthenium complexes to the streptavidin-coated beads limited the sensitivity. Zhou *et al.* reported a trinuclear dendritic $Ru(bpy)_3^{2+}$ label that produced ECL signals two to three times as strong as monomeric $Ru(bpy)_3^{2+}$.[17] This molecule was tested for protein labeling in an immunoassay. Recently, a dual-labeled molecular beacon, using ECL excited $Ru(bpy)_3^{2+}$ at one end as a donor and a Black Hole Quencher-2 (BHQ-2) at the other end as an acceptor, was described.[18] A quenching efficiency of 95% was reported.

7.2 Materials and methods

7.2.1 Chemicals and materials

The synthetic oligonucleotides were purchased from Microsynth (Balgach, Switzerland) (see Table 7.1). Strands Cy5-A2 and Cy5-A3 were purchased labeled,

whereas strand A1 was labeled in the laboratory. Bis(2,2'-bipyridine)-4'-methyl-4-carboxy-bipyridine-ruthenium N-succinimidyl ester-bis(hexafluorophosphate) ($Ru(bpy)_3^{2+}$ label), Tris(2,2'- bipyridyl)ruthenium(II) dichloride hexahydrate ($Ru(bpy)_3^{2+}$ x 6 H_2O), tri-n-propylamine (TPA, 98%), dimethylsulfoxide (DMSO), sodium dodecyl sulfate (SDS) and boric acid were purchased from Fluka (Buchs, Switzerland). Sodium dihydrogen phosphate monohydrate, disodium hydrogen phosphate dihydrate, sodium tetraborate decahydrate and ethanol (0.2% H_2O) were obtained from Merck (Darmstadt, Germany) and Cy5-dye was from Amersham Bioscience (Freiburg, Germany). The ECL buffer was prepared by dissolving TPA and SDS in 300 mM phosphate buffer to obtain concentrations of 100 mM TPA and 0.1 w-% SDS. Final pH of the ECL buffer was 7.8.

Table 7.1: Name and sequence of the used oligonucleotides

Name	Sequence
Ru-A1	5'-ACATTTTGCTGCCGG-C_6-NH_2-$Ru(bpy)_3^{2+}$-3'
Cy5-A2	5'-Cy5-CCGGCAGCAAAATGT-3'
A2	5'-CCGGCAGCAAAATGT-3'
Cy5-A3	5'-Cy5-AAAAAAAAAAAAAAA-3'
Ru-B1	5'-GATTACGAATCCGATTTGCTAAGGATCATT-$Ru(bpy)_3^{2+}$-3'
Cy5-B2	5'-Cy5-ATCCTTAGCAAATCGGATTCGATTCGTAATC-3'
Cy5-B3	5'-Cy5-TAGCAAATCGGATTCGATTCGTAATC-3'
Cy5-B4	5'-Cy5-AAATCGGATTCGATTCGTAATC-3'

7.2.2 Instrumentation and methods

The electrochemical cell consisted of carbon interdigitated (C-IDA) working and counter electrodes with a spacing of 2 μm and total area of 1 mm^2, as described in detail previously.[19] An Ag pseudoreference electrode was integrated on a chip. Potential was applied with a potentiostat (PAR EG&G 273), and the ECL-generated light signal was collected with a photomultiplier tube (model Hamamatsu H5701-50, Schuepfen, Switzerland), installed close to the electrochemical cell. A voltage of -950 V was supplied to the PMT using a laboratory-built high-voltage power supply. Two different optical filters (600 $\pm$ 80 nm and 670$\pm$ 40 nm) were used to filter ECL generated light. The ECL signal was collected by a 10x microscope

objective, filtered by a band-pass filter and measured by PMT and recorded with a PC using a lab-written Labview program, which collected 8 points per second. Cyclic voltammetry of Cy5 was performed with an IBM voltammetric analyzer (EC/225) using a standard Ag/AgCl reference electrode. All potentials are reported against an Ag/AgCl reference electrode. All measurements were performed at room temperature. The UV/VIS absorption spectra of labeled oligonucleotides and free dyes were measured with an UV/VIS spectrophotometer (Hewlett-Packard 8452A).

7.2.3 Oligonucleotide labeling procedure

The oligonucleotide strands A1 and A2 were labeled with Ru(bpy)$_3^{2+}$ *via* a C$_6$ linker to their amino modified 3'-end. One milligram of Ru(bpy)$_3^{2+}$ dye was dissolved in 50 μL of DMSO, and the oligonucleotides were dissolved in 0.1 M tetraborate buffer, pH 8.5, mixed and added to the dye solution. The solution was gently shaken in a shaker and left to react at room temperature in the dark overnight. Labeled oligonucleotides were precipitated twice by addition of 1/10 of volume of 3 M NaCl and 2.5 fold volume of cold, absolute ethanol. The mixture was kept 30 min at -20 ℃ and centrifuged for 30 min at 12000 RPM. The supernatant was carefully removed and the pellet was rinsed twice with cold 70% ethanol. Labeled oligonucleotides were allowed to dry in air during 10 min, and then were stored at -20 ℃. Before the hybridization experiment, the pellet was redissolved in deionized water.

7.2.4 Hybridization assay

For the hybridization step a constant concentration of Ru-A1 strand was combined with various concentrations of the labeled complementary Cy5-A2 strand. The same was performed with the nonlabeled complementary strand A2 and labeled noncomplementary strand Cy5-A3, respectively. The hybridization was performed in 50 mM phosphate buffer containing 150 mM NaCl, pH 7.0. The

samples were heated to 65 ℃ for 1 hour and allowed slowly to cool to room temperature in a water bath. Before the ECL measurement, 500 μL of the ECL buffer was added to the samples. Measurement volume was 500 μL.

7.2.5 Determination of the labeling efficiency

The labeling efficiency of the 3'-amino group of the A1 strand with $Ru(bpy)_3^{2+}$ label was determined by absorbance measurements of free $Ru(bpy)_3^{2+}$ and Ru-labeled oligo. Based on the Lambert-Beer law the labeling efficiency was calculated to be 50%. The unlabeled oligonucleotides were not separated from the solution. The degree of labeling of the other oligonucleotides was reported by the supplier to be 100%. The absorption and emission spectra of $Ru(bpy)_3^{2+}$ were red-shifted upon hybridization, which is in agreement with previous reports.[8] No shift was observed in the absorption spectra of free and conjugated Cy5.

7.3 Results and discussion

7.3.1 Electrochemical and spectral properties

LRET requires an overlap of the donors emission and the acceptors excitation spectra. From Figure 7.1 it can be seen that the photoluminescence emission spectrum of $Ru(bpy)_3^{2+}$ overlaps with the excitation spectrum of Cy5.

Before the hybridization experiments, the electrochemical and spectral properties of the system were characterized. The CV of $Ru(bpy)_3^{2+}$ in an aqueous solution has previously been reported on C-IDAs.[20] From the cyclic voltammogram of Cy5 recorded in aqueous solution, it was visible that an irreversible oxidation of Cy5 occurred at approximately 0.70 V and a reduction at approximately -0.65 V *vs.* an Ag/AgCl reference electrode.[1]
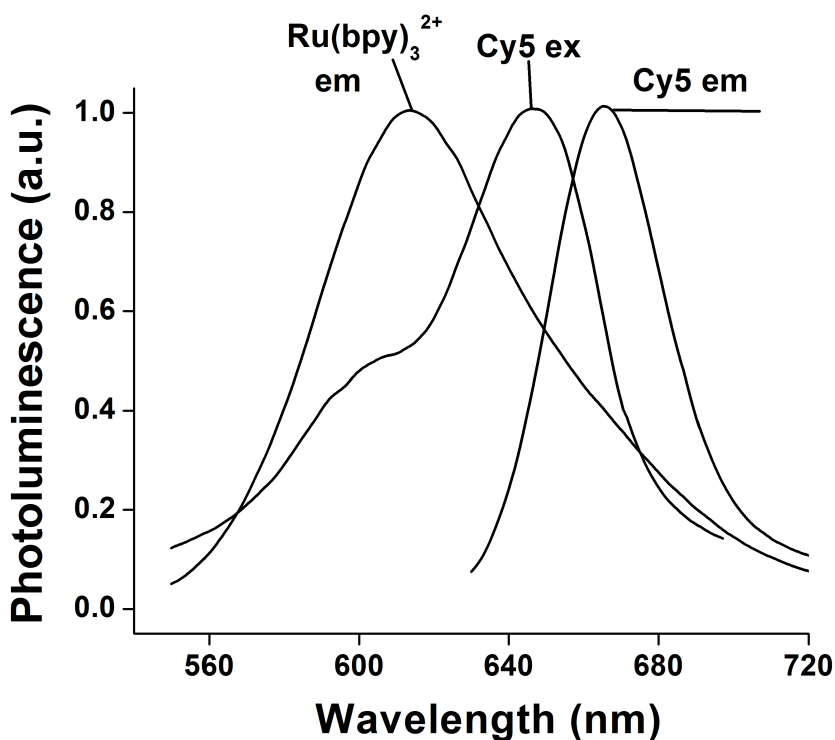
Figure 7.1: Normalized photoluminescence emission spectrum of 2 μM Ru(bpy)$_3^{2+}$ oligonucleotide, fluorescence excitation and emission spectra of 1 μM Cy5, measured in 0.05 M phosphate buffer, pH 7.0.

The spectral and electrochemical properties of the labeled oligonucleotides used in this work are listed in Table 7.2,

Table 7.2: Electrochemical and spectral data of the Ru(bpy)$_3^{2+}$ and Cy5-labeled oligonucleotides

Sample	λ_{ex} (nm)	λ_{em}	E$_{ox}$ (V)	E$_{red}$ (V)	E$_{0-0}$ (eV)
Ru(bpy)$_3^{2+}$	450	610	1.1	-1.3	2.08
Ru-A1	460	620	1.1	-1.3	2.06
Cy5-A2	650	670	0.70	-0.65	1.88

where E$_{ox}$ and E$_{red}$ are the first one-electron oxidation and reduction potentials of the electron donor and acceptor, respectively, and E$_{0-0}$ the 0-0 transition energy of the dye. This 0-0 transition energy is obtained from the equation 7.3[21]

$$E_{0,0} = hcv_{0-0} \tag{7.3}$$

where h is the Planck's constant, c is speed of light and v_{0-0} is the wavenumber for the 0-0 transition of the dye. This 0-0 wavenumber can be obtained from[21]

$$v_{0-0} = \frac{(v_{max,abs} + v_{max,em})}{2} \tag{7.4}$$

where $v_{max,abs}$ and $v_{max,em}$ correspond to maxima of absorption and emission of the appropriated dye. This equation is not valid for $Ru(bpy)_3^{2+}$, however, because its emission occurs from triplet state, which has energy of 2.12 eV.[22]

7.3.2   ECL of hybridized samples

In the case of LRET, when Ru-A1 is excited through ECL, the emission of $Ru(bpy)_3^{2+}$ centered at 620 nm should be quenched, while the emission of Cy5 at 670 nm should be induced. To investigate this, a constant concentration of 0.75 μM Ru-A1 was hybridized with 0-1.9 μM of its complementary Cy5-A2 strand and the ECL signal was generated by scanning the voltage from -0.1 V to 1.3 V at a scan rate of 100 mV/s. The signal was measured at two different wavelengths, using bandpass filters of 600 ± 80 nm to monitor the emission of $Ru(bpy)_3^{2+}$ and 670 ± 40 nm to monitor the emission of Cy5. Figure 7.3 shows the normalized ECL as a function of the molar ratio of Cy5-A2 and the Ru-A1 strands. It also includes results of control experiments performed with the nonlabeled complementary strand A2 and the labeled noncomplementary strand Cy5-A3. It can be seen that at both measured wavelengths, the ECL intensity of Ru-A1 strongly decreased upon hybridization with increasing concentrations of Cy5-A2. The decrease of the signal indicates that the fluorescence emission of Cy5 has not been induced even though the ECL was quenched. It should be noted that Cy5 itself

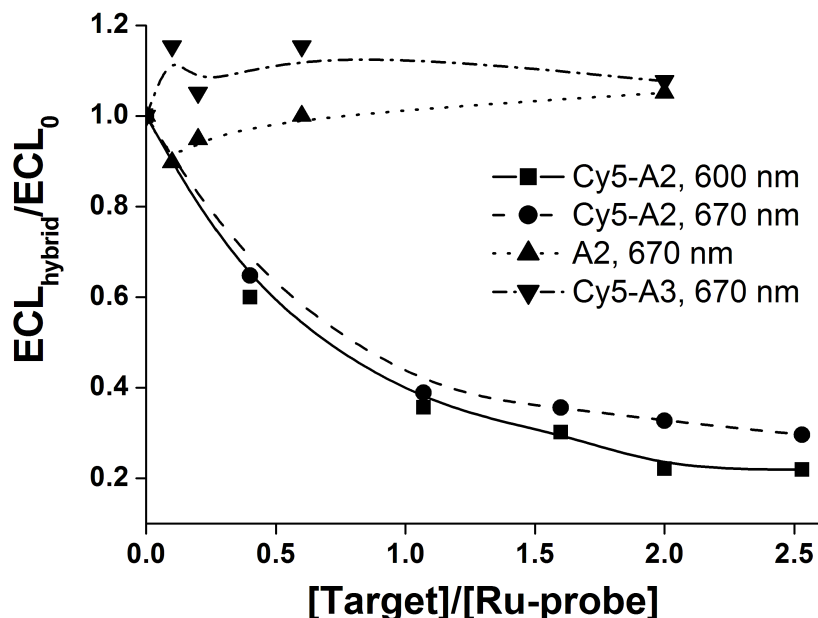does not have any detectable ECL under the conditions employed.

Figure 7.2: ECL after hybridization of Ru-A1 with nonlabeled target (A2), Cy5-labeled complementary target (Cy5-A2), and Cy5-labeled noncomplementary target (Cy5-A3).

All nucleotides are known to quench the emission of certain luminophores to some extent,[23,24] which raises the question whether the ECL quenching is due to the hybridization with the complementary strand. This was investigated in a control experiment where a constant concentration of 0.50 μM Ru-A1 strand was hybridized with different concentrations (0-1.0 μM) of the unlabeled A2 strand. The ECL signal remained constant, indicating that quenching was due to the interaction with Cy5 and not with the complementary strand. This study confirmed previously published results which have indicated that the luminescence of the photoexcited Ru(bpy)$_3^{2+}$ does not change upon hybridization with nonlabeled complementary strand.[14] Direct generation of ECL by a redox reaction sequence between guanines in a DNA strand and Ru(bpy)$_3^{2+}$ has been reported by Dennany *et al.*.[25] The group made 10-nm thin films composed of alternative layers of [Ru(bpy)2(PVP)$_{10}$] and DNA, PVP standing for poly(4-vinylpyridine).

They observed direct ECL emission with guanines and $Ru(bpy)_3^{2+}$ as reagents, while the other nucleotides did not generate any noticeable ECL signal. As our control experiment with the nonlabeled complementary strand showed, however, there was no interaction between the $Ru(bpy)_3^{2+}$ label and the complementary strand in our system. To determine whether the ECL of the Ru-A1 strand is dynamically quenched by the free Cy5 dye, up to 30-fold excess of Cy5 was added to the 0.030 μM Ru-A1 solution. No change in the signal was observed. This result was confirmed by a hybridization experiment where a constant concentration of 0.50 μM Ru-A1 strand was hybridized with 0-1.0 μM labeled, noncomplementary Cy5-A3 strand.

7.3.3 Photoluminescence measurements

The same samples were measured with a luminescence spectrometer. With excitation wavelength of 450 nm, $Ru(bpy)_3^{2+}$ is efficiently excited, while the direct excitation of Cy5 is very low. Figure 7.4 shows the intensity of the hybridized sample composed of 0.75 μM Ru-A1 and 1.5 μM Cy5-A2 (dashed line) and the emission of 0.75 μM Ru-A1 alone (dashed dotted line). While the emission of Ru-oligo decreased that of Cy5 remained constant. Figure 7.4 includes the combined emission spectra of the individual labeled oligonucleotides, scaled to the size of the hybrid emission, to facilitate comparison. As can be seen, the emission peaks of the hybridized oligonucleotides are shifted and deformed with respect to the free parent strands.

These results lead to two important conclusions: (i) the quenching of the $Ru(bpy)_3^{2+}$-label emission occurs regardless of the excitation mode and (ii) the quenching of the ECL occurs only when the Cy5 and $Ru(bpy)_3^{2+}$ moieties are in close proximity. Two quenching mechanisms are known to take place at small intermolecular distances: electron transfer and static quenching. These mechanisms are discussed below.
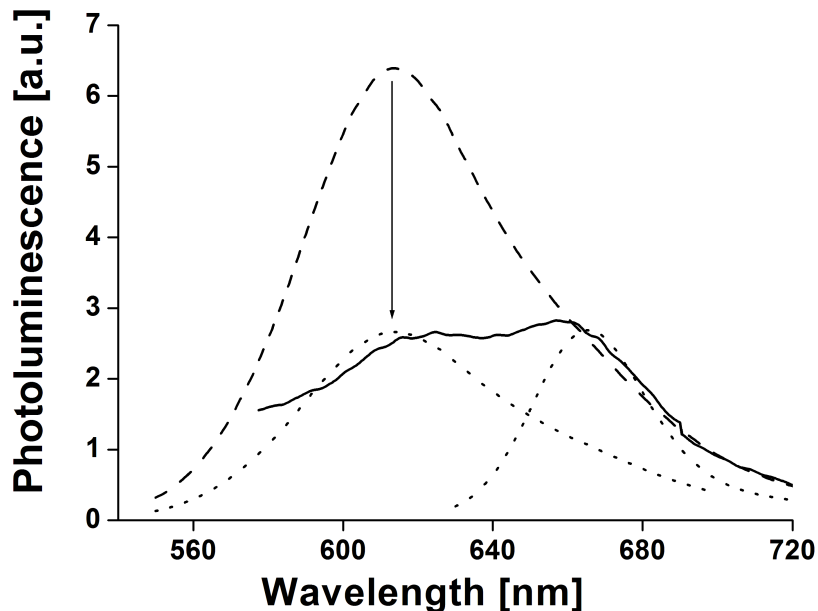
Figure 7.3: Photoluminescence of 750 nM 15-mer Ru-A1 strand alone (dashed line) and hybridized with 1.5 μM of complementary Cy5-A2 strand (solid line) in phosphate buffer containing 300 mM TPA. Individually measured emission spectra of Ru-A1 and Cy5-A2 strand are shown in dotted line, scaled to size of the duplex for purposes of comparison. Excitation wavelength was 450 nm, slit width of excitation and emission monochromators 5 nm.

7.3.4 Electron transfer

For quenching by electron transfer to be observed, the reaction must be thermo-dynamically allowed. The free energy change of the electron transfer reaction can be estimated using the Rehm-Weller equation:[21]

$$\Delta G = E_{ox} - E_{red} - E_{0-0} + C \tag{7.5}$$

where E_{ox} is the first one-electron oxidation potential of the electron donor and E_{red} is the first one-electron reduction potential of the acceptor in the solvent

under consideration. C is a coulombic term related to the energy of the separated ions. In polar solvents like water it is sufficiently small that it can be neglected.[23,24] As Cy5 has a lower oxidation potential than $Ru(bpy)_3^{2+}$ it is clearly a better electron donor. The free energy change of electron transfer from Cy5 to $Ru(bpy)_3^{2+}$ is -0.06 eV when $Ru(bpy)_3^{2+}$ is excited through ECL, and +0.12 eV when Cy5 becomes excited by LRET, calculated using equation 7.3 and the values from Table 7.2. The calculated negative Gibbs free energy indicates that the electron transfer from Cy5 to $Ru(bpy)_3^{2+}$ is possible and might cause quenching. The free energy change for photo-induced electron transfer from guanine to Cy5 is +0.25 eV,[23] which means that guanine cannot quench the emission of Cy5 by electron transfer.

7.3.5 Static quenching

Static quenching occurs when two luminophores are in very close proximity, and it implies either the existence of a sphere of effective quenching or the formation of a ground state nonluminescent complex.[21] In static quenching, the emissions of both donor and acceptor are decreased. However, the quenching efficiency depends on the hydrophobic and electrostatic interactions between the luminophores. Although the major force that brings luminophores together in a hybridization assay is the binding affinity of the complementary strands, the possibility exists that the two labeled moieties have enough affinity to form a nonluminescent ground state complex. It is difficult to estimate the extent of the interaction between the luminophores. However, since the $Ru(bpy)_3^{2+}$-label is positively charged and the Cy5 negatively, there is electrostatic attraction between them. The spectral properties of dyes in a ground state complex are known to differ from their parent dyes. From Figure 7.4 it can be seen that the emission of the hybrid is not a sum of the emissions of its two parent dyes, but rather the emission peaks are significantly shifted and are degenerated. In the case of LRET, the luminophores are known to retain their intrinsic spectral properties.[26] Thus, the spectral changes would seem to suggest the formation of a complex. The formation of a nonluminescent ground state complex can be described by the expression[21]

$$I_0/I = 1 + K_C * [Q] \tag{7.6}$$

where K_C is the formation constant of a nonluminescent complex, I_0 the emission intensity in the absence of a quencher, I the intensity in the presence of a quencher and [Q] the concentration of a quencher, in this case Cy5-A2 strand. The relationship between the ratio of the ECL signal of Ru-A1 in the absence and presence of Cy5-A2 as a function of the concentration of Cy5 target was found to be linear at low concentrations (R^2=0.978, K_C= 2.9 μM^{-1}), supporting the hypothesis that the ECL quenching might be due to the formation of a ground state nonluminescent complex. It should be noted that the electron transfer quenching and static quenching mechanisms are not mutually exclusive and can occur simultaneously.

7.3.6 Determination of quenching efficiency

To determine the quenching efficiency, we hybridized 0.75 μM Ru-A1 with increasing concentrations of Cy5-A2. The resulting ECL graphs versus applied potential are shown in Figure 7.5. As can be seen, the ECL signal decreased considerably upon hybridization with a rather low concentration, μM of Cy5-A2.

Figure 7.6 shows the ratio of the ECL of the signal in the presence (ECL_{hybrid}) and absence (ECL_0) of Cy5-A2 strand plotted as a function of the molar ratio of the hybridized sample to the pure Ru-A1 sample. The curve shows the sensitivity of the system for nanomolar concentrations of Cy5-A2. To investigate the potential of our system for a homogeneous hybridization assay, 1 μM of the Ru-A1 was hybridized with 0.170 μM of Cy5-A2 in the presence and absence of 0.300 μM Cy5-A3. This excess of the noncomplementary Cy5-A3 did not influence the result.
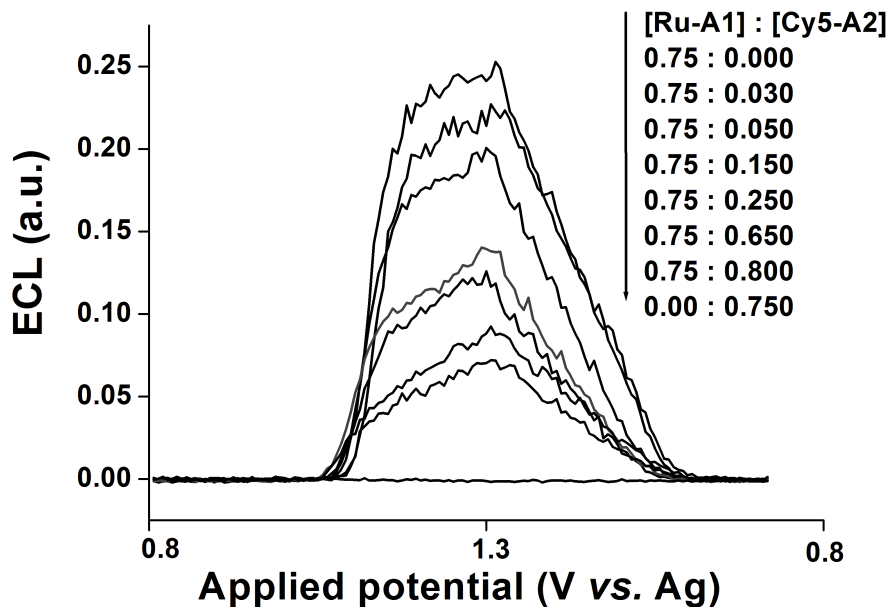
Figure 7.4: ECL signal upon hybridization of Ru-A1 strand of constant concentration 0.75 μM with increasing concentrations of complementary Cy5-A2 strand. Scan rate was 100 mV/s up to 1.3 V *vs.* Ag and back to starting potential. The ECL signal was filtered at 670 $\pm$ 40 nm.

The quenching efficiency can be calculated from the decrease of the donor emission using the following expression:[21]

$$E_Q = \left(1 - \frac{I_{DA}}{I_D}\right) \tag{7.7}$$

where I_{DA} is the intensity of the D-A pair and I_D that of the donor alone. The quenching efficiency was found to be 78% at both 600 nm and 670 nm. This is lower than values reported for contact quenching with non-fluorescent quenchers, but compares well with values of LRET-mediated quenching.[26] Better quenching efficiencies have been reported where a dark dye was used as an acceptor.[18]
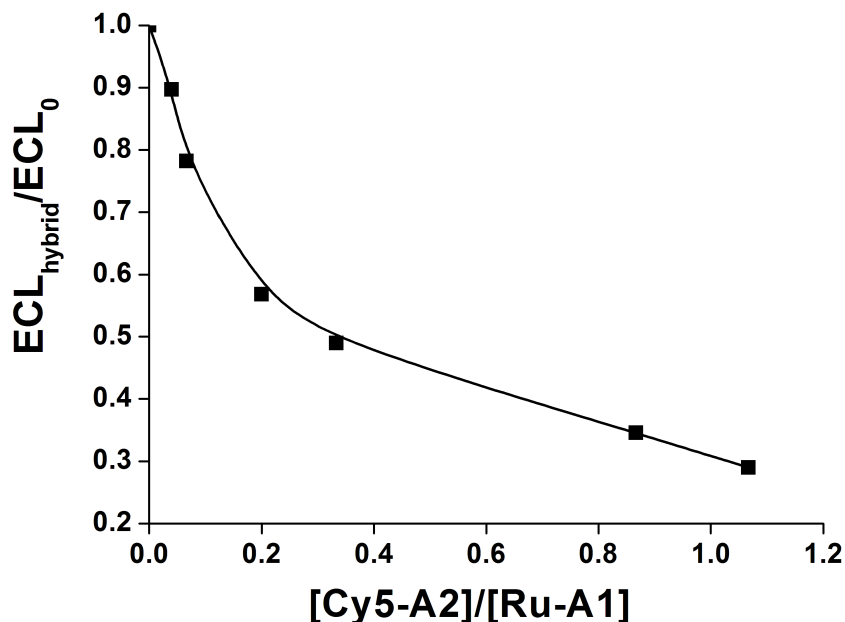
124

Figure 7.5: Quenching efficiency calculated using data presented in the Figure 7.5.

7.3.7 Quenching as a function of distance between label moieties

To further investigate the nature of the quenching mechanism, 1 μM of Ru-B1 was hybridized with equimolar concentrations of Cy5-B2, Cy5-B3, and Cy5-B4. ECL emission of Ru-B1 did not change upon hybridization with Cy5-B2 but increased slightly upon hybridization with Cy5-B3 and Cy5-B4. The ECL spectra of the hybridized samples showed that this increase in emission occurred at 620 nm, and thus was not due to LRET.

Photoluminescence spectra changed considerably upon hybridization of Ru-B1 with Cy5-labeled strands (see Figure 7.7). The photoluminescence of Ru-B1 is strongly quenched upon hybridization with Cy5-B2, and the Cy5 emission peak, though weak, is clearly observed. The highest LRET occurs with hybrid Ru-B1 Cy5-B3. The hybridization of Ru-B1 with Cy5-B4 results in less intense Cy5

emission compared to Cy5-B3, while the emission of Ru-B1 is in intensity equal to the original intensity.
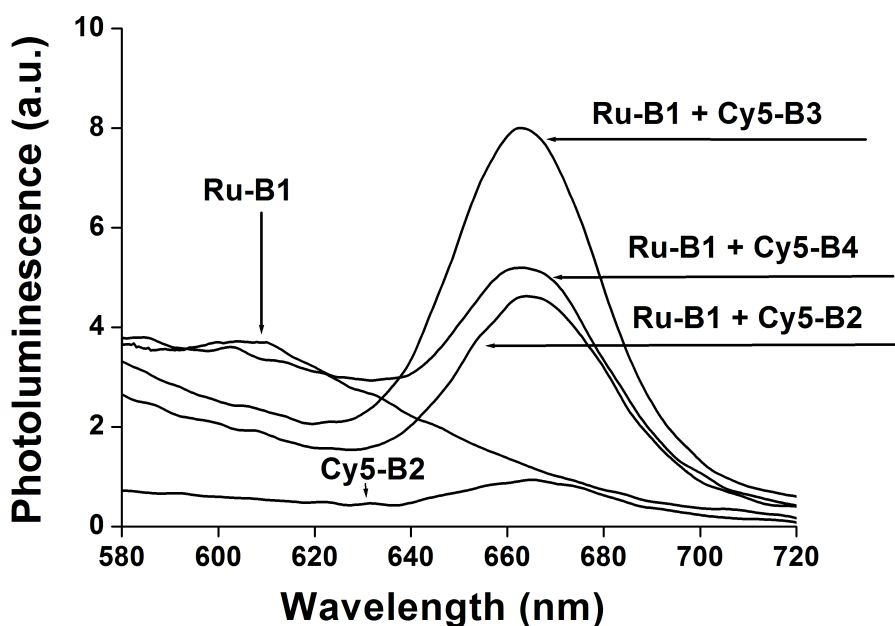
Figure 7.6: Photoluminescence spectra and LRET from $Ru(bpy)_3^{2+}$-label to Cy5 as a function of distance between label moieties, measured in 0.3 M phosphate buffer, 0.1 M TPA, 0.01 % SDS, pH 7.8. Experimental conditions: excitation wavelength 450 nm, excitation and emission slit widths 10 nm.

In the case of ECL, when there is only a short distance between the label moieties, the ECL emission of the Ru-label is quenched. However, when the distance between labels is increased to five nucleotides, the presence of Cy5 label has little effect on the ECL efficiency. This finding further confirms that the quenching of ECL of $Ru(bpy)_3^{2+}$ requires close proximity of the two labels.

126

7.4   Conclusions

In this chapter it has been demonstrated that, upon hybridization, the ECL signal of the $Ru(bpy)_3^{2+}$-labeled oligonucleotide is strongly quenched by the Cy5-labeled complementary strand. The hybridization with a nonlabeled complementary or a labeled noncomplementary strand did not change the intensity of the ECL signal. These results suggest that static quenching and/or electron transfer are the most likely quenching mechanisms. Since these two mechanisms are not mutually exclusive and can occur simultaneously, it is not possible, at present, to distinguish between them. From differences in photoluminescence and ECL spectra of the hybridized samples it is clear that LRET did not occur from the ECL-excited $Ru(bpy)_3^{2+}$ label to the Cy5 label in the present system.

References

1. Spehar, A.-M., Koster, S., Kulmala, S., Verpoorte, E., de Rooij, N., Koudelka-Hep, M., The quenching of electrochemiluminescence upon oligonucleotide hybridization, *Luminescence* **19** (2004) 287–295.

2. Cooley, L. F., Headford, C. E. L., Elliott, C. M., Kelley, D. F., Intramolecular electron transfer in linked tris(2,2-bipyridine)ruthenium(II)diquat complexes, *J. Am. Chem. Soc.* **110** (1988) 6673–6682.

3. Ryu, C., Wang, R., Schmehl, R. H., Ferrere, S., Ludwikow, M., Merkert, J. W., Headford, C. E. L., Elliot, C. M., Photoinduced electron transfer in linked ruthenium(II) diimine-diquat complexes: linkage dependence, *J. Am. Chem. Soc.* **114** (1992) 430–438.

4. Barigelletti, F., Flamigni, L., Balzani, V., Colling, J.-P., Sauvage, J.-P., Sour, A., Constable, E. C., Thompson, A. M. W., Intramolecular energy transfer through phenyl bridges in rod-like dinuclear Ru(II)Os(II) terpyridine-type complexes, *J. Am. Chem. Soc.* **116** (1994) 7692–7699.

5. Mecklenburg, S., Peek, B. M., W., B., Meyer, T. J., Photoinduced electron transfer in redox-active lysines, *J. Am. Chem. Soc.* **113** (1991) 8540–8542.

6. Ward, M., Barigelletti, F., Control of photoinduced energy transfer between metal-polypyridyl luminopores across rigid covalent, flexible covalent, or hydrogen-bonded bridges, *Coord. Chem. Rev.* **216-217** (2001) 127–154.

7. Cola, L. D., Belser, P., Photoinduced energy and electron transfer processes in rigidly bridged dinuclear Ru/Os complexes, *Coord. Chem. Rev.* **177** (1998) 301–346.

8. Wilson, G. J., Sasse, W. H. F., Mau, A. W.-H., Singlet and triplet energy transfer processes in ruthenium(II)bipyridine complexes containing covalently bound arenes, *Chem. Phys. Letters* **250** (1996) 583–588.

9. Maliwal, B., Grynzynski, Z., Lakowitz, J. R., Long-wavelength long lifetime luminophors, *Anal. Chem.* **73** (2001) 4277–4285.

10. Lakowicz, J. R., Piszczek, G., Kang, J. S., On the possibility of long-wavelength long-lifetime high-quantum-yield luminophores, *Anal. Biochem.* **288** (2001) 62–75.

11. Youn, H., Terpetschnig, E., Szmacinski, H., Lakowitz, J. R., Fluorescence energy transfer immunoassay based on a long-lifetime luminescent metal-ligand complex, *Anal. Biochem.* **232** (1995) 24–30.

12. Augustin, C. M., Oswald, B., Wolfbeis, O. S., Time resolved luminescence energy transfer immunobinding study using a ruthenium-ligand complex as a donor label, *Anal. Biochem.* **305** (2002) 166–172.

13. Kurner, J. M., Klimant, I., Krause, C., Pringsheim, E., Wolfbeis, O. S., A new type of phosphorencent nanospheres for use in advanced time-resolved multiplexed bioassays, *Anal. Biochem.* **297** (2001) 32–41.

14. Augustin, C., *Ruthenium-ligand complexes as luminescent probes for polarisation and energy transfer systems*, Ph.D. thesis, University of Regensburg (2001).

15. Richter, M., Bard, A. J., Kim, W., Schmehl, R. H., Electrogenerated chemiluminescence. 62. Enhanced ECL in bimetallic assemblies with ligands that bridge isolated chromophores, *Anal. Chem.* **70** (1998) 310–318.

16. Staffilani, M., Hoss, E., Giesen, U., Schneider, E., Hartl, F., Josel, H.-P., Cola, L. D., Multimetallic ruthenium(II) complexes as electrocemiluminescent labels, *Inorg. Chem.* **42** (2003) 7789–7798.

17. Zhou, M., Roovers, J., Robertson, G. P., Grover, C. P., Multilabeling biomolecules at a single site. 1. Synthesis and characterization of a dendritic label for electrochemiluminescence assays, *Anal. Chem.* **75** (2003) 6708–6717.

18. Wilson, R., Johannsson, M. K., Photoluminescence and electrochemilumines-cence of a Ru(II)(bpy)$_3$-quencher dual-labeled oligonucleotide probe, *Chem. Communications* **21** (2003) 2710–2711.

19. Fiaccabrino, G. C., de Rooij, N. F., Koudelka-Hep, M., On-chip generation and detection of electrochemiluminescence, *Anal. Chim. Acta* **359** (1998) 263–267.

20. Fiaccabrino, G. C., Koudelka-Hep, M., Hsueh, Y. T., Collins, S. D., Smith, R. L., Electrochemiluminescence of tris(2,2'-bipyridine)ruthenium in water at carbon microelectrodes, *Anal. Chem.* **70** (1998) 4157–4161.

21. B.Valeur, *Molecular fluorescence: principles and application*, Wiley-VCH Verlag 2001.

22. Juris, A., Balzani, V., Barigelletti, F., Campagna, S., Belser, P., von Zelewsky, A., Ru(II) polypyridine complexes: photophysics, photochemistry, electrochemistry and chemiluminescence, *Coord. Chem. Rev.* **84** (1988) 85–277.

23. Dietrich, A., Buschmann, V., Mueller, C., Sauer, M., Fluorescence resonance energy transfer FRET and completing processes in donor-acceptor substi-tuted DNA strands: a comparative study of ensemble and single-molecule data, *Rev. Molecular Biotech.* **82** (2002) 211–231.

24. Torimura, M., Kurata, S., Yamada, K., Yokomaku, T., Kamagata, Y., Kana-gawa, T., Kurane, R., Fluorescence-quenching phenomenon by photoinduced electron transfer between a fluorescent dye and a nucleotide base, *Anal. Sci.* **17** (2001) 155–160.

25. Dennany, L., Foster, J., Rusling, J., Simultaneous direct electrochemilumines-cence and catalytic direct voltammetry detection of DNA in ultrathin films, *J. Am. Chem. Soc.* **125** (2003) 5123–5128.

26. Marras, S. A. E., Kramer, F. R., Tyagi, S., Efficiencies of fluorescence res-onance energy transfer and contact-mediated quenching in oligonucleotide probes, *Nucleic Acids Res.* **30** (2002) 1–8.

8. ECL applications in PDMS-based analytical microsystems

The fabrication of a microfluidic chip of PDMS and glass for electrochemical or ECL detection is described. A carbon fiber working electrode was integrated with a Pt counter and pseudoreference electrodes into a microfluidic chip. Guanosine was used as model analyte. The electrokinetic properties of PDMS microchannels were determination.[1]

8.1 Introduction

PDMS is gaining popularity as a material for fabrication of chemical microsystems due to its transparency, flexibility, electrical isolation, and easy bonding to a number of materials such as another PDMS slide, glass, silicon, silicon dioxide and silicon nitride.[2] An almost unlimited number of PDMS devices can be replicated from a single master. Because of their flexibility, PDMS slides can easily adapt to the conformational structures of electrodes, thus allowing easy integration of metal electrodes fabricated on a glass or silicon wafer with a microfluidic system fabricated in PDMS. The main disadvantage of PDMS is its hydrophobicity, which is caused by its repeating groups, -O-Si(CH$_3$)$_2$. Hydrophobicity makes it difficult to fill PDMS microchannels with aqueous solutions and leads to adsorption and absorption of biomolecules on the channel walls and into the bulk of PDMS. These problems can be overcome by performing suitable surface modifications.[3] Gas permeability of PDMS has been utilized for power-free pumping in PDMS microchannels.[4]

As described in Chapter 2, anodic ECL of Ru(bpy)$_3^{2+}$ can be used in two detection modes: (i) direct ECL detection where the analyte is a coreactant and Ru(bpy)$_3^{2+}$ is present in excess (typically in mM concentration range), (ii) labeling of an analyte with a Ru(II)-label and using TPA as a coreactant (typically 50-100 mM

range). The former detection mode has been used to detect amino acids, codeine, lidocaine, guanine, and oxalic acid, among others. The interest in this method stems from the fact that it does not require a time-consuming and costly labeling procedure, but the disadvantage is lack of selectivity. The selectivity problem can be solved by coupling ECL detection with a separation technique, such as capillary electrophoresis (CE). The movement of fluid in CE is due to the electroosmotic flow, which is inherently dependent on the surface properties of the separation channel.

The most common detection method in microchip CE is laser induced fluorescence (LIF), which requires an external excitation source and labeling of the analytes with a photoluminescent luminophore. The advantage of ECL over fluorescence is that there is no need for an external excitation source. In addition, direct ECL circumvent the need for analyte labeling. As the sample volumes in microchip CE systems are very low, in the order of hundreds of picoliters, the detection method has to be very efficient. A few μCE-ECL systems based on direct ECL have been reported.[5–7] In a typical case, the analytes (coreactants) are separated due to their different mobility in a separation buffer, and $Ru(bpy)_3^{2+}$ is added in excess (typically in mM concentration range) in a detection reservoir. Addition of a relatively large and charged molecule to a separation buffer is difficult, due to its influence on EOF and adsorption on channel walls.

Electrokinetic pumping is based on a surface-driven phenomenon which makes it very suitable for microsystems. Electrokinetic pumping takes advantage of the surface charge of the microchannel for sample moving and separation of analytes. Silica-based surfaces become negatively charged at pH values above their pK_a values. Thus, materials like silica, glass, and PDMS can support EOF, but the magnitude of EOF depends of the density of the surface charge. Rapid bioassays can be performed in microfludic systems. Standard DNA-hybridization assays and immunoassays rely on diffusion to achieve hybridization or immunoreaction. Owing to the very small diffusion coefficients of these molecules, long reaction times, in order of several hours to overnight, are needed. Miniaturization has

132

beneficial influence on the hybridization rate due to the reduced mass transfer distances and proportional increase of initial concentration.[8] For these reasons, it was of interest to investigate the magnitude of EOF in PDMS microchannels.

8.2 Experimental section

All chemicals employed were of analytical grade and obtained from Sigma-Aldrich, Switzerland.

8.2.1 Fabrication of an ECL microsystem

PDMS structures were manufactured by replica molding, channels in Pyrex were etched in 10% HF (Section 2.3.6), and Pt electrodes were fabricated by lift-off process (Section 2.3.5). Due to nonplanar structures on wafer, the photoresist (AZ 1518) was deposited in thickness of 15 μm. Channel width at the wider section was 200 μm and at the thinner section 50 μm, while the depth was 15 μm (Figure 8.1). Upon fabrication of PDMS slab for carbon fiber electrodes, the width and height of the master and depth of the PDMS groove were measured with an Alpha-Step profilometer (KLA-Tencor, San Jose, CA, USA). It was observed that the PDMS stucture were smaller than the master. The shrinkage of the structures in lateral direction is up to 20%, and 25-30% in height(based on measurement of three different structures).

8.2.2 EOF measurement

PDMS/PDMS devices were made by reversibly sealing two PDMS slabs, and hybrid PDMS/glass devices by reversibly sealing a PDMS slab with Corning Pyrex 7740 wafer of 100 mm diameter. PDMS channels were formed by replica molding using a silicon master (Section 2.3.8), and the channel widths were estimated by scanning electron microscopy. The depths and widths of the master and the chan-

nels were measured with an Alpha-Step profilometer. Cross-sections of PDMS microchannels were trapezoidal, with a cross-sectional area of 1035.5 μm^2 (68 μm wide across the top, 41 μm across the bottom and 19 μm deep). The channel lengths of the PDMS/PDMS devices were 6.1 cm and for the PDMS/glass structures, 5.9 cm. Prior to the measurements, the channels were conditioned with 0.1 M NaOH for at least 60 min, washed with deionized water for 3 min, and flushed for 10 min with buffer. The treatment with 0.1 M NaOH was found not to decrease the hydrophobicity of native PDMS. The introduction of aqueous solutions into the PDMS/PDMS channel was facilitated by first filling it with a polar organic solvent (isopropanol or ethanol).[9,10] All the solutions were filtered with a disposable 0.45 μm syringe filter (Semadeni, Switzerland). Data for 50-μm-ID fused silica capillaries of 70 cm total length that are those taken from a previous publication.[11] A PC-controlled, laboratory built high-voltage power supply and a program written in LabVIEW (National Instruments, Austin, Texas, USA) was employed for current monitoring.

8.3   Results and discussion

8.3.1   ECL in a microchannel

One of the distinct advantages of microtechnology is the possibility to fabricate electrodes from different materials and geometries. Carbon is a particularly interesting material for the detection of bioanalytes because it is less prone to fouling and has a relatively large potential window. The microfabrication technology for thin film carbon is still at a relatively early development stage, however. Figure 8.1 shows an electrode chip containing a Pyrex channel and Pt electrodes, and, in the lower part, a bonded device where carbon fiber electrode is positioned in a PDMS slab (Section 8.2.1).

The flexibility of PDMS allows coupling of carbon fiber electrodes with noble metals. Different electrode materials are suitable for different purposes, and for

some applications it may be beneficial to combine several materials. While noble metal electrodes or thin film carbon can be deposited on silicon or glass wafers, technological limitations do not allow their combination on a single wafer. Noble metal electrodes can be fabricated on non-planar surfaces by using two-step lithography, one step to define the channel, and the second to define the electrodes. Because of its flexibility, PDMS can reversibly bond to wafers that are nonplanar (at least on the order of 100 nm). Use of a master allows fabrication of PDMS microchannels of different geometry, whereas microchannels in glass are always semicircular due to the isotropic wet etching of glass. The system shown
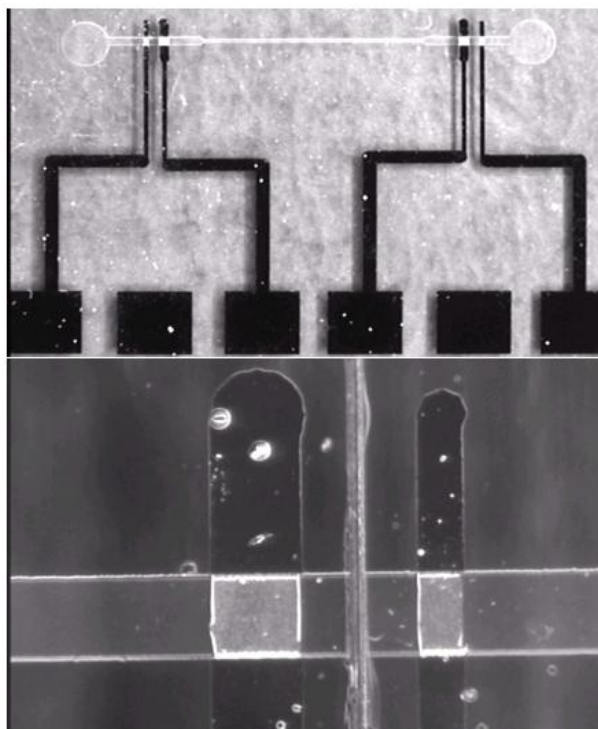

Figure 8.1: Microfluidic chip with channels fabricated in Pyrex and platinum electrodes (100 and 200 μm) fabricated in the channel. Carbon fiber (diameter 30 μm) is placed in a groove fabricated in PDMS slab and reversible bonded with Pyrex. The distance between two platinum electrodes is fixed lithographically to 200 μm, while the exact position of carbon fiber electrode depends of the alignment of two slides, however, it is placed between two platinum electrodes.

in Figure 8.1 was tested for ECL measurement of guanosine because it is known to generate ECL from $Ru(bpy)_3^{2+}$ [12] and is very important analyte (e.g. GMP, GDP, and GTP).
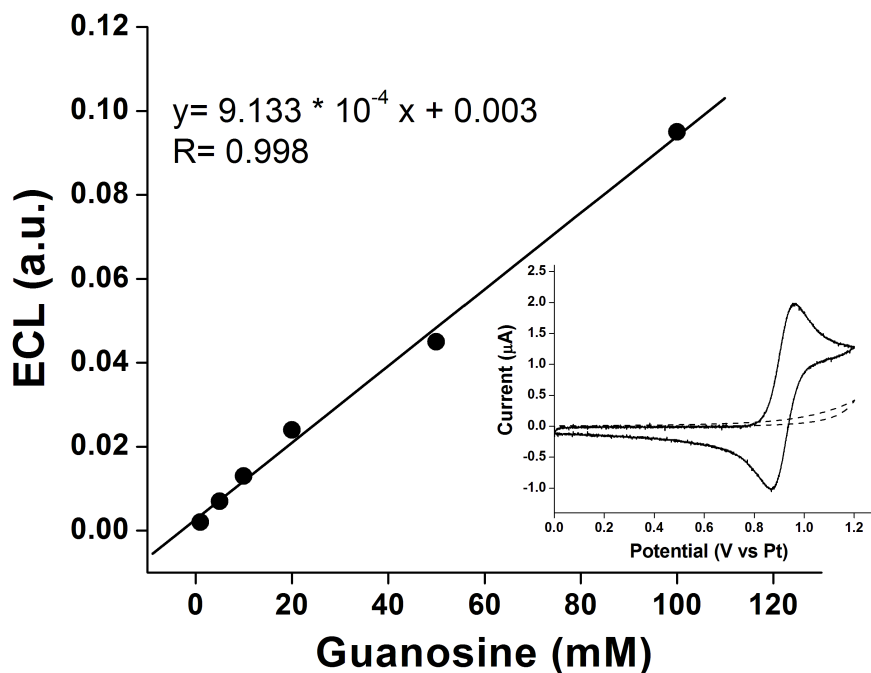

Figure 8.2: ECL as a function of guanosine concentration. Conditions: 1 mM $Ru(bpy)_3^{2+}$ solution in 50 mM phosphate buffer, pH 7.5. Inset: Cyclic voltammogram of 1 mM $Ru(bpy)_3^{2+}$ solution in 50 mM phosphate buffer, pH 7.5 (solid line) and measured on a 30 μm carbon fiber using platinum counter and pseudoreference electrodes integrated into the microfluidic channel. Scan speed was 100 mV/s. Background is shown as a dashed line.

The inset in the Figure 8.2 shows the cyclic voltammogram of $Ru(bpy)_3^{2+}$ recorded on a carbon fiber microelectrode integrated into a microchip with platinum counter and pseudoreference electrodes. Guanosine could be measured as ECL with linear range extending from 1 to 100 μM. It is important in microfluidic systems to place electrodes close to each other, to insure stable potential. A long distance between the electrodes in a microchannel is problematic, especially in the low ionic strength buffer solutions.

136

Both guanosine and guanine can induce ECL of $Ru(bpy)_3^{2+}$. Guanine is the most easily oxidized of therefore DNA bases, and many electrochemical DNA determination methods based on guanine oxidation have been reported.[13–17] Guanine has also been observed to generate ECL.[12] Immobilization of probes for oligonucleotide detection is very important. DNA can be immobilized on many different types of carbon, although carbon fiber is not suitable material for direct immobilization of DNA.[18] This becomes feasible, however, through application of a suitable coating.[19] A highly sensitive method for electrochemical DNA detection was introduced by group of Thorp.[13–15] Electrochemical oxidation of $Ru(bpy)_3^{2+}$ catalyses the oxidation of guanine in a DNA chain, and thus considerably higher guanine oxidation peaks can be achieved by addition of $Ru(bpy)_3^{2+}$. The general problem with direct electrochemical as well as ECL for DNA measurement is that it is mainly suitable for long ssDNA chains because guanine in a hybridized DNA strand is protected by the double helix.

8.3.2 Determination of EOF in PDMS microchannels

The magnitude of electroosmotic mobility in PDMS microchannels was determined by the current monitoring method.[20] The cathodic reservoir and the channel were filled with a buffer of concentration C, while the anodic reservoir was filled with a buffer of concentration 0.95 C. Upon application of voltage, the more dilute buffer penetrates into the channel due to EOF, and a current decrease is monitored until the channel is completely filled. The electroosmotic mobility EO was calculated according to equation:

$$EO = \frac{L}{tE} \tag{8.1}$$

where L is the channel length (m), E is the applied electric field strength (V/m) and t is the time (s) required to reach a constant current. Measurements were performed at three different voltages, namely 2000, 3000, and 4000 V. Except for

the buffers with a high ionic strength (Figure 8.4), these voltages are considered to provide currents that follow Ohm's law. EOF was measured as a function of ionic strength at constant pH, and as a function of pH at constant ionic strength. Figure 8.3 shows EOF as a function of pH, determined between pH 4 and 9.2 using buffers with ionic strength of 32.81 mM. The buffers employed were composed of 200 mM acetate (pH 4.0), 48.97 mM acetate (pH 5.0), 29.93 mM phosphate (pH 5.8), 24.60 mM phosphate (pH 6.4), 17.52 mM phosphate (pH 7.0), ACES/NaOH (pH 7.8, c(NaOH)= 32.8 mM) and 17.84 mM tetraborate (pH 9.2). The values presented are mean values calculated for 4 to 13 determinations.

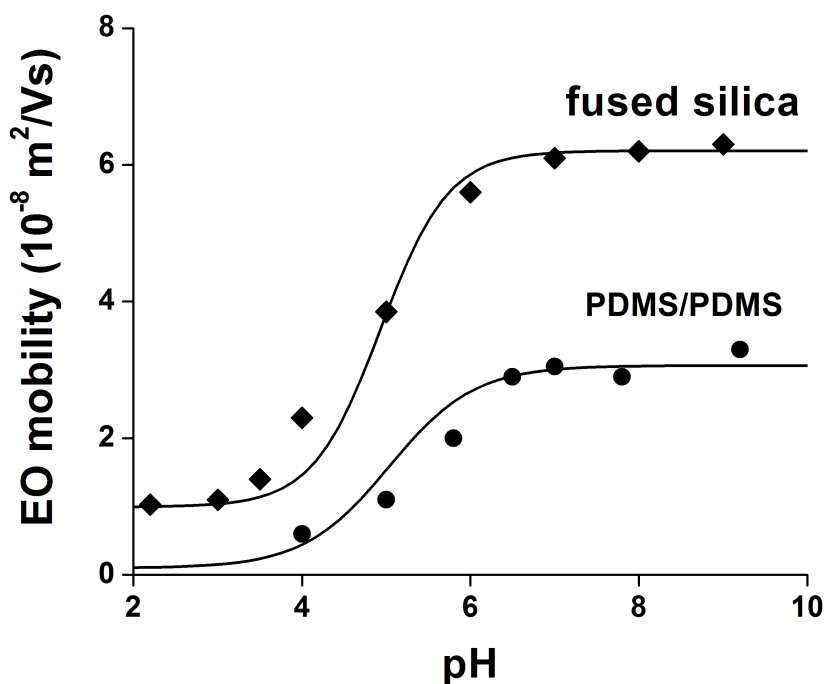**Figure 8.3:** Electroosmotic mobility data determined in PDMS/PDMS microchannel using buffers with an ionic strength of 32.81 mM, and similar data obtained in a FS capillary of 50 μm ID[11] using 40 mM phosphate buffers. Solid lines represent μ_{EO} calculated with the silanol dissociation model with a pK$_a$ value of 5.0, a wall mobility value at full ionization and a correction for adsorption of anions at low pH.

Values given for pH 4 and 5 are only estimates because measurements were difficult to perform due to extensive air bubble formation. The data obtained was compared with data presented in the literature for fused silica.[11]. Solid lines represent values calculated with the equation

$$\mu_{EO} = \mu_0 \alpha + \mu_c \left(1 - \alpha\right) \tag{8.2}$$

where μ_0 is the electroosmotic mobility at full dissociation of silanol, μc is a corrected mobility for surface charge contributions not originating from the dissociation of the silanol groups, and α is given by the relationship

$$\alpha = 10^{(pH - pK_a)} / \left[1 + 10^{(pH - pK_a)}\right] \tag{8.3}$$

In this equation, α is the degree of ionization of the wall, which varies from 0 to 1, pK_a refers to the ionization constant of silanol, and pH is the pH value of the solution in the channel.[11,21] The sigmoidal curve for FS shown in Figure 8.4 was obtained using a wall pK_a of 5 and μ_0 and μ_c values of 6.3 x 10^{-8} m^2/Vs and 1.0 x 10^{-8} m^2/Vs, respectively; it is the same as in the ref. 10.[11] For purposes of comparison, the same pK_a value was employed for the curve referring to the PDMS/PDMS microchannel. Corresponding mobilities were 3.0 x 10^{-8} m^2/Vs and 0.1 x 10^{-8} m^2/Vs, and they were chosen arbitrarily.

Electroosmotic mobilities are a function of the ionic strength of the buffer.[11,21–23] Electroosmotic mobility data determined in PDMS/PDMS and PDMS/glass microchannels as a function of ionic strength are shown in Figure 8.4. The data was determined using buffer containing 100 mM N-(2-acetamido)-2-aminoethanesulfonic Acid (ACES)/90 mM NaOH at pH 7.8 with an ionic strength of 90 mM and dilutions thereof. Multiple determinations were made ($9 \le n \le 11$), and RSD values were found to range between 2.6 and 9.1 %.

Compared with fused silica, electroosmotic mobility in PDMS/glass and PDMS/PDMS microchannels was considerably smaller. It is important to note that in plasma-oxidized PDMS microchannels electroosmotic mobilities similar to those in glass microchannels have been reported.[10] With 20 mM phosphate buffer at pH 7 (ionic strength of 35.25 mM) and PDMS/glass channels, EOF was determined via application of electric field strengths between 300 and 800 V/cm. The obtained value of about 4 x 10^{-8} m^2/Vs compares well with those given in Figure 8.3. For this configuration, RSD values for multiple runs performed in the same chip were <6% (n=4) and up to 10% for runs in three different chips.
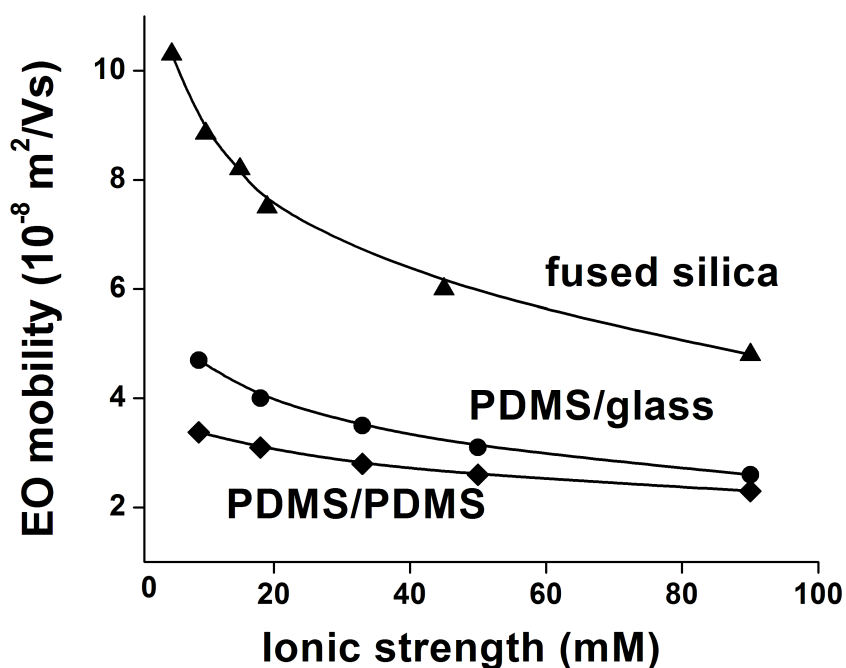

Figure 8.4: Electroosmotic mobility as a function of ionic strength monitored in ACES buffers. Values were obtained at 2-4 kV in the PDMS/PDMS and PDMS/glass microchannels and at 10 kV in the fused silica capillary of 50 μm ID.[11]

8.4 Feasibility of CE-ECL

To date, the most efficient coreactant for generation of ECL of $Ru(bpy)_3^{2+}$ is TPA,[24] which makes label-based ECL a far more sensitive detection method than direct ECL. The only amino acid known to generate sufficiently strong ECL for real-world analytical applications is proline. Of the four DNA bases, only guanine generates ECL, though owing to its electrochemical activity it can also be detected by electrochemical methods. The most useful applications of direct ECL are the detection of various drug molecules, such as codeine and lidocaine, which are not easily detected by other methods. It can be expected that other new applications will be found.

In ECL bioassays where $Ru(bpy)_3^{2+}$ derivatives are used as labels, TPA is used as a coreactant in a concentration range 0.1-0.3 M. Owing to the basic character of TPA, a buffer with strong buffering capacity, typically 0.2-0.3 M phosphate, is necessary for efficient ECL generation. This requirement is contrary to that for the EOF, whose magnitude is inversely proportional to the ionic strength. Thus, CE-ECL with $Ru(bpy)_3^{2+}$-labeled biomolecules cannot be readily envisaged.

8.5 Conclusions

PDMS is well suited for the fabrication of channel structures. Shrinkage of cured PDMS with respect to the master was observed, in lateral direction up to 20%, and in height 25-30%. The flexibility and easy bonding of PDMS with different materials allows realization of various kinds of chemical microsystems and the combination of different electrode materials otherwise difficult to combine.

Under all conditions examined in this study, PDMS/PDMS and PDMS/glass microchannels exhibited an EOF towards the cathode. Compared with fused silica, EOF in PDMS/PDMS and PDMS/glass microchannels is significantly (50-70%) lower, and the EOF in a PDMS/glass device is somewhat higher than in a

PDMS/PDMS channel. With respect to the ionic strength and pH dependence of the EOF, there is great similarity between the data obtained in native PDMS microchannels and FS capillaries. These data support the assumption that silica fillers in native PDMS are acting as source of surface charge and thus of EOF.[11] Air bubble formation was much more pronounced at acidic than at basic pH values, and channel conditioning was found to be very important for obtaining a stable current and to prevent bubble formation. Conditioning of new devices for several hours and chips that are not used for several days is strongly recommended. At pH 6.4, reproducibility of EOF was found to be satisfactory for chemical analysis; however, at pH values < 6.4, the EOF in PDMS/PDMS and PDMS/glass channels is rather weak and so unstable that it has to be controlled via application of a suitable coating.[25,26]

Coupling of ECL detection with CE separation appears challenging. Different separation and detection buffers would be required, adding an additional level of complexity to the system. However, the use of microfluidic systems to increase the speed of biorecognition reaction with separate ECL detection seems reasonable.

References

1. Spehar, A.-M., Koster, S., Linder, V., Kulmala, S., de Rooij, N., Verpoorte, E., Sigrist, H., Thormann, W., Electrokinetic characterisation of poly(dimethylsiloxane) microchannels, *Electrophoresis* **24** (2003) 3674–3678.

2. Sia, S. K., Whitesides, G. M., Microfluidic devices fabricated in poly(dimethylsiloxane) for biological studies, *Electrophoresis* **24** (2003) 3563–3576.

3. Makamba, H., Kim, J. H., Lim, K., Park, N., Hahn, J. H., Surface modification of poly(dimethylsiloxane) microchannels, *Electrophoresis* **24** (2003) 3607–3619.

4. Hosokawa, K., Sato, K., Ichikawa, N., Maeda, M., Power-free poly(dimethylsiloxane) microfluidic devices for gold nanoparticle-based DNA analysis, *Lab-on-a-Chip* **4** (2004) 181–185.

5. Arora, A., Eijkel, J. C. T., Morf, W. E., Manz, A., A wireless electrochemiluminescence detector applied to direct and indirect detection for electrophoresis on a microfabricated glass device, *Anal. Chem.* **73** (2001) 3282–3288.

6. Qiu, H., Yan, J., Sun, X., Liu, J., Cao, W., Yang, X., Wang, E., Microchip capillary electrophoresis with an integrated indium tin oxide electrode-based electrochemiluminescence detector., *Anal. Chem.* **75** (2003) 5435–5440.

7. Yan, J., Yang, X., Wang, E., Electrogenerated chemiluminescence on microfluidic chips, *Anal. Bioanal. Chem.* **381** (2005) 48–50.

8. Vanderhoeven, J., Pappart, K., Dutta, B., Vanhummelen, P., Baron, G. V., Desmet, G., Exploiting the benefits of miniaturization for the enhancement of DNA microarrays, *Electrophoresis* **25** (2004) 3677–3686.

9. Ocvirk, G., Munroe, M., Tang, T., Oleschuk, R., Westra, K., Harrison, J. D., Electrokinetic control of fluid flow in native poly(dimethylsiloxane) capillary electrophoresis devices, *Electrophoresis* **21** (2000) 107–115.

10. Ren, X., Bachman, M., Sims, C., Li, G. P., Allbritton, N. J., Electroosmotic properties of microfluidic channels composed of poly(dimethylsiloxane), *J. Chromatogr. B* **762** (2001) 117–125.

11. Caslavska, J., Thormann, W., Electrophoretic separation in PMMA capillaries with uniform and discontinuous buffers, *J. Microcolumn Separations* **13** (2001) 69–83.

12. Dennany, L., Foster, J., Rusling, J., Simultaneous direct electrochemiluminescence and catalytic direct voltammetry detection of DNA in ultrathin films, *J. Am. Chem. Soc.* **125** (2003) 5123–5128.

13. Yang, I. V., Thorp, H. H., Modification of indium tin oxide electrodes with repeat polynucleotides: electrochemical detection of trinucleotide repeat expansion, *Anal. Chem.* **73** (2001) 5316–5322.

14. Yang, I. V., Ropp, P. A., Thorp, H. H., Toward electrochemical resolution of two genes on one electrode: using 7-deaza analogs of guanine and adenine to prepare PCR product with differential redox activity, *Anal. Chem.* **74** (2002) 347–354.

15. Armistead, P. A., Thorp, H. H., Electrochemical detection of gene expression in tumor samples: overexpression of rak nuclear tyrosine kinase, *Bioconjug. Chem.* **13** (2002) 172–176.

16. Ferapontova, E., Dominguez, E., Direct electrochemical oxidation of DNA on polychrystalline gold electrodes, *Electroanalysis* **15** (2003) 629–634.

17. Oliveira-Brett, A., Piedade, J. A. P., da Silva, L. A., Diculescu, V. C., Voltammetric determination of all DNA nucleotides, *Anal. Biochem.* **332** (2004) 321–329.

18. Cai, X., Rivas, G., Farias, P. A. M., Shiraishi, H., Wang, J., Palecek, E., Evaluation of different carbon electrodes for adsorptive stripping analysis of nucleic acids, *Electroalalysis* **8** (1996) 753–758.

19. Caruana, D. J., Heller, A., Enzyme-amplified amperometric detection of hybridization and of a single base pair mutation in an 18-base oligonucleotide on a 7-μm-diameter microelectrode, *J. Am.Chem. Soc.* **121** (1999) 769–774.

20. Huang, X., Gordon, M. J., Zare, R. N., Current-monitoring method for measuring the electroosmotic flow rate in capillary zone electrophoresis, *Anal. Chem.* **60** (1988) 1837–1838.

21. Thormann, W., Zhang, C.-X., Caslavska, J., Gebauer, P., Mosher, R., Modeling of the impact of ionic strength on the electroosmotic flow in capillary electrophoresis with uniform and discontinuous buffer systems, *Anal. Chem.* **70** (1998) 549–562.

22. van Orman, B. B., Liversidge, G. G., McIntire, G. L., Olefirowicz, T. M., Ewing, A. G., Effect of buffer composition on electroosmotic flow in capillary electrophoresis, *J. Microcolon Separations* **2** (1990) 176–180.

23. Foret, F., Krivankova, L., Bocek, P., Capillary zone electrophoresis, VCH Weinheim 1993, pp. 41–48.

24. Leland, J. K., Powell, M. J., Electrogenerated chemiluminescence – an oxidative-reduction type ECL reaction sequence using tripropyl amine, *J. Electrochem. Society* **137** (1990) 3127–3131.

25. Belder, D., Ludwig, M., Surface modification in microchip electrophoresis, *Electrophoresis* **24** (2003) 3595–3606.

26. Dolnik, V., Wall coating for capillary electrophoresis on microchips, *Electrophoresis* **25** (2004) 3589–3601.

9. Summary and outlook

9.1   Anodic ECL *vs.* cathodic HECL

The two ECL methods studied in this work are very different: anodic ECL is based on traditional electrochemistry, while HECL is a novel physicochemical technique. The main advantage of anodic ECL of $Ru(bpy)_3^{2+}$ and its derivatives is that they undergo reversible redox reactions and the same label can be recycled many times. In addition, a large number of analytes, such as various amine-containing compounds, oxalic acid, and guanine, can be detected directly, thus circumventing the need for labeling. A drawback of anodic ECL is its strong dependence upon pH, ionic strength and the presence or absence of surfactants.[1]

HECL intensity is largely independent of pH, but depends on the thickness of the insulating film. A large number of luminophores having different redox and luminescence properties as well as different luminescence lifetimes can be excited using the HECL method, enabling both time and wavelength discrimination in detection. Many different luminescent molecules and chelates can be excited simultaneously using HECL. HECL luminophores are mainly used as labels, but some coreactants, such as hydrogen peroxide, peroxodisulfate and peroxodiphosphate can be determined using HECL.[2]

The results presented in this work demonstrate that both types of ECL are suitable for heterogeneous oligonucleotide hybridization assays. Efficient oligonucleotide assays require immobilization and subsequent suitable surface modification in order to achieve high surface density of immobilized probes, controlled orientation, and efficient hybridization. Amino-modified probes were used in all described assays. Immobilization on gold electrodes was achieved using carboxylic acid terminated SAM thiol, which allowed EDC/NHS coupling of probes. On oxide-coated aluminum and silicon electrodes immobilization was performed using a deposited aminoterminating silane layer, which allowed cross linking of

146

two amino groups with PDC cross-linker. Oligonucleotide-modified surfaces were characterized in all cases, and the results indicate that probe density on the order of 10^{12} molecules/cm^2 was achieved.

Oligonucleotides labeled with bis(2,2'-bipyridine)-5- isothiocyanato-1,10-phenanthroline ruthenium(II) complex were used as luminophores for hybridization detection by anodic ECL (Chapter 3) and cathodic HECL (Chapter 5). With anodic ECL, hybridization could be detected down to probe concentration of 1 x 10^{-9} M, and with cathodic HECL down to 1 x 10^{-10} M. These results are not directly comparable, however, due to the considerably different surface areas of the working electrodes, which were 0.20 mm^2 in anodic ECL measurement and 63 mm^2 in HECL measurement. Another difference in the results arises from the different measurement system and detector response: in anodic ECL a short pulse was applied and ECL peak intensity was taken, while in cathodic HECL over 1000 pulses were applied and the area of the HECL signal was integrated. Two base pair mismatch detection was achieved in both cases. Electric field- aided mismatch hybrid denaturing was performed in connection with anodic ECL, while traditional washing steps were performed in case of cathodic HECL detection.

In summary, the results in the present work show the great potential of ECL methods for bioaffinity assays. In anodic ECL, electrodes of micrometer size were microfabricated, whereas in cathodic HECL, the electrode were of millimeter size and microfabrication methods were used for the growth of ultrathin oxide films. Microfabrication technologies are promising for the large-scale production of low-cost devices for ECL-based point-of-care devices and biosensors, where disposable devices are needed to avoid contamination risk. The combination of silicon, glass, and polymeric materials allows cheap fabrication of large numbers of microdevices for bioanalytical applications based on ECL detection.

9.2 Outlook

As described in Chapter 3, the electrode potential can be controlled to increase selectivity toward mismatches. For the future, influence of the electric field on immobilization and hybridization rates and oligonucleotide orientation should be investigated as this could provide a powerful tool for the reduction of assay times. With the described HECL-based hybridization assays, interesting results in terms of detection limits and sensitivity were achieved with large electrodes. Future work should investigate the scalability of HECL detection on electrodes of considerably smaller size, with the goal of achieving high-throughput measurements. Another important issue to be investigated is the quantitative effect of an applied detection potential on immobilized strands and deposited silane layer. The disadvantages of traditional, passive bioaffinity reactions are the long incubation times needed due to the diffusion- limited reactions and large diffusion coefficients of biomolecules. A combination of microfluidic elements with a detection system in order to enhance mass transport can reduce reaction times from hours to minutes.

Both types of ECL can be applied for detection in various stages of flow separation analysis, especially in their miniaturized versions. Anodic ECL based on direct label-free detection has already been coupled to μCE separation systems. Microfabrication allows easy fabrication of micrometer-size electrodes for detection of separated analytes. Coupling of CE to label-based anodic ECL may be of interest due to the lower detection limits. In this case, high concentration of coreactant, TPA, could be placed into a detection reservoir since its addition to a separation buffer is challenging when the buffer must of high buffering capacity. Disposable HECL-based immunosensors with integrated detection electrode coupled to a PDMS microchannel can be envisaged. The electrode could be a relatively large oxide-coated piece of Si or Al. Other electrode materials could also be considered. Microfluidic connections could easily be fabricated in PDMS and bonded to the electrode. The surface of the microchannel would define the active area of the electrode, circumventing the need for an additional photolithographic step. Capturing biomolecules should be patterned at a predetermined

place by photopatterning or in a microfluidic side channel. A device prepared in this way could be stored several months in dry conditions. Upon sample injection, immunometric reaction would take place and an HECL-based response could be measured with a relatively simple photodetector equipped with suitable electronics and a counter electrode.

References

1. Richter, M., Electrochemiluminescence ECL, *Chem. Rev.* **104** (2004) 3003–3036.

2. Hakansson, M., Jiang, Q., Spehar, A.-M., Suomi, J., Kotiranta, M., Kulmala, S., Direct current-induced electrogenerated chemiluminescence of hydrated and chelated Tb(III) at oxide-coated aluminum cathodes, *Anal. Chim. Acta* **541** (2005) 171–177.